UNIVERSITÀ
DEGLI STUDI
DI PADOVA

UNIVERSITÀ DEGLI STUDI DI PADOVA

DIPARTIMENTO DI INGEGNERIA DELL'INFORMAZIONE

CORSO DI LAUREA MAGISTRALE IN BIOINGEGNERIA

TESI DI LAUREA MAGISTRALE

3D BIOCERAMIC SCAFFOLDS MANUFACTURING AND VALIDATION FOR CANCER TREATMENT

Relatore: Prof. essa ELISA CIMETTA
Correlatore: Ing. SARA MICHELI
Correlatore: Prof. ENRICO BERNARDO
Correlatore: Ing. ELSAYED HAMADA SAID ABDELWAHAB

Laureanda: MARILINA TAMARA TOTARO
Matricola: 2025870

ANNO ACCADEMICO 2022/2023

21/04/2023

Summary

Bone tissue engineering is a rapidly growing field that aims to regenerate and repair damaged or lost bone tissue using principles of engineering and biology. One of the key components of bone tissue engineering is the use of scaffolds, which provide a three-dimensional structure for cells to attach, grow, and differentiate. Scaffolds can be made from a variety of materials, including natural and synthetic polymers, ceramics, and composites. The use of scaffolds in bone tissue engineering allows for the creation of structures that mimic the natural bone extracellular matrix, providing mechanical support and promoting new bone formation. The development of effective scaffolds is critical for the success of bone tissue engineering, and ongoing research continues to explore new materials and fabrication techniques for scaffold design and fabrication.

This study utilized stereolithography 3D bioprinting to create scaffolds from bio-glass 70S30C with two different compositions. This material was chosen for its ability to release ions such as Ca^{2+} and $(SiO)^{4-}$, which can promote the formation of hydroxyapatite (HA) - a natural component of bone tissue - through interaction with the biological environment.

Various cell types were used to demonstrate the biocompatibility of 70S30C scaffolds, to determine whether a synthetic ceramic can provide a suitable cell-culture environment. Both cancer (SK-N-AS and SaOs-2) and not cancerous cells (hMSCs and BJ) were seeded on the scaffold to prove the biocompatibility and cytocompatibility of the scaffold and different biological tests were conducted to verify that. Specifically, Live&Dead assay and immunofluorescent staining were carried out to demonstrate cell adhesion and proliferation over time. Additionally, SEM microscopy revealed the protein network created by the cells after 14 days of culture and confirmed cells' morphology.

These scaffolds were also tested to prove their photothermal effect, a novel strategy that has shown promise in the treatment of tumors. When cancer cells are exposed to a surge of infrared (IR) waves, the temperature of the surrounding environment increases. This local increase in temperature can cause cancer cells to die. Samples seeded with cancer cells were irradiated with IR waves to confirm that a consistent number of cells were dead, due to the increase of temperature. Live&Dead and MTT assays were conducted on scaffolds seeded with cancer cells and treated with IR waves for different times.

Results demonstrate that bio-glass 70S30C has a photothermal effect, which could open up new possibilities for cancer treatment. This approach would likely be less invasive and have fewer effects than traditional chemotherapy.

Riassunto

La rigenerazione del tessuto osseo attraverso l'ingegneria tissutale è un campo in rapida crescita che mira a promuovere la riparazione e la rigenerazione del tessuto osseo danneggiato o perso, utilizzando principi di ingegneria e biologia. Gli *scaffold* sono uno dei componenti chiave dell'ingegneria tissutale, poiché forniscono un supporto tridimensionale per l'adesione, la crescita e il differenziamento delle cellule. Gli *scaffold*, il cui termine deriva dalla traduzione letterale del termine "impalcatura", possono essere realizzati con una varietà di materiali, tra cui polimeri naturali e sintetici, ceramiche e compositi. L'uso di *scaffold* nell'ingegneria del tessuto osseo consente di creare strutture che imitano la matrice extracellulare ossea naturale, fornendo supporto meccanico alle cellule e promuovendo la formazione di nuovo tessuto. Lo sviluppo di *scaffold* performanti è fondamentale per il successo dell'ingegneria del tessuto osseo e la ricerca continua a studiare e valutare nuovi materiali e tecniche di fabbricazione per la loro progettazione e produzione.

Nel progetto di ricerca descritto in questa tesi, la tecnica utilizzata per la realizzazione degli *scaffold* è la biostampa 3D in stereolitografia, al fine di creare *scaffold* in bio-vetro 70S30C con due diverse composizioni. Questo materiale è stato scelto per la sua capacità di rilasciare ioni come Ca^{2+} e $(SiO)^{4-}$, che possono promuovere la formazione di idrossiapatite (HA) - un componente naturale del tessuto osseo - grazie all'interazione di tali ioni con l'ambiente biologico.

Nel progetto di ricerca, sono state considerate diverse tipologie di linee cellulari per dimostrare la biocompatibilità degli *scaffold* 70S30C e determinare se un materiale ceramico sintetico possa fornire un adeguato supporto per la coltura cellulare. Sia cellule cancerogene (SK-N-AS e SaOs-2) che cellule non tumorali (hMSC e BJ) sono state seminate sullo *scaffold* per valutarne la biocompatibilità e la citocompatibilità, e sono stati eseguiti diversi test biologici per verificare tali proprietà. In particolare, tramite Live&Dead è stata valutata la vitalità cellulare sullo *scaffold* mentre tramite immunofluorescenza è stata dimostrata l'adesione cellulare e la proliferazione nel tempo. Inoltre, l'adesione cellulare è stata confermata mediante microscopia SEM, che ha permesso di osservare la deposizione di proteine da parte delle cellule dopo 14 giorni dalla semina e di confermarne la morfologia.

Gli *scaffold* seminati con cellule tumorali sono stati anche testati per valutarne l'effetto fototermico e i risultati hanno mostrato un'effettiva efficacia nel trattamento. Gli *scaffold* in seguito all'esposizione tramite onde infrarosse (IR) aumentano localmente la loro temperatura fino a raggiungere e superare i 50°C. L'aumento della temperatura induce la morte delle cellule tumorali, rappresentando un possibile approccio per il trattamento al cancro. Per verificare la mortalità delle cellule tumorali sullo *scaffold* in seguito all'irradiamento IR sono stati eseguiti test di Live&Dead e MTT.

Grazie ai test effettuati, è stato dimostrato che il biovetro 70S30C ha un effetto fototermico, il che potrebbe aprire nuove possibilità per il trattamento del cancro. Questo approccio potrebbe essere meno invasivo e avere meno effetti collaterali rispetto alla chemioterapia tradizionale.

Table of contents

List of Figures

List of Tables

Introduction

The term “Tissue Engineering” refers to the utilization of a combination of multidisciplinary approaches to repair or replace damaged or missing biological tissues. In recent years, with the rapid development of the Tissue Engineering, Bone Tissue Engineering (BTE) has become a completely innovative approach for repairing bone defects concerning both the cortical and the trabecular bone. Scaffolds play an essential role in BTE since they serve to mimic the structure, mechanical and physical functions of the natural bone extracellular matrix (ECM). They provide a three-dimensional (3D) environment that promotes cellular adhesion, proliferation, and differentiation. An ideal scaffold should be biodegradable, biocompatible, bioactive and osteoconductive. Different biomaterials can be used to create scaffolds, including natural or synthetic polymers, metals, composites but most importantly ceramics. This class of materials exhibits mechanical and structural properties that are similar to those of the natural bone. Scaffold fabrication is a crucial step in Bone Tissue Engineering, as the scaffold serves as a template for the growth of new bone tissue. Different techniques can be used to fabricate scaffolds, depending on the desired properties and characteristics of the final product. One common approach is to use additive manufacturing techniques, such as 3D bio-printing or stereolithography, which allow for precise control over the scaffold's geometry and porosity.

The work of this thesis was developed in the BIAMET (Biomedical Applications of Multiscale Engineering Technologies) laboratory, as well as in the CerAMglass, a chemical laboratory of the department of Industrial Engineering. The BIAMET laboratory focuses on the study of human cancer diseases, specifically Neuroblastoma, an aggressive childhood tumor originating from progenitor cells of the sympathetic nervous system, and Osteosarcoma, a malignant bone cancer affecting young adults and adolescents. The scaffolding technique is considered a strategy for curing or repairing tissues affected by tumors and, for this reasons, tests of cellular biocompatibility are carried out to demonstrate the scaffold biological efficiency. In the CerAMglass laboratory, new approaches to the formulation of bio-glasses are being studied, such as the development of silicate ceramics from polymeric precursors, as well as additive manufacturing for creating scaffolds for BTE.

The aim of this thesis is to perform the biological validation of bio-glass scaffolds with different compositions and to study the photothermal effect of the bio-ceramic material for treating cancer diseases. The structure of the thesis is as follow.

In the first Chapter, a general overview of bone anatomy and pathology is presented, with a focus on bone malignant cancers. The chapter also includes a presentation of the materials and the techniques commonly used for scaffold fabrication in BTE, particularly describing the different bio-ceramic materials and bio-glass manufacturing techniques and properties.

In the second Chapter, the materials and the methods used for scaffold production and characterization are presented. Additionally, the protocols for cells seeding, culturing and analyzing onto the scaffolds are described. First, the two scaffold compositions are introduced: the considered bio-glass is 70S30C (70 mol% SiO_2, 30 mol% CaO) realized with and without the Fumed Silica (FS), a polymeric precursor used for the mixture stabilization. This is followed by a description of the heat treatments and printing technique. Then, the four considered cell lines (SK-N-AS, SaOs-2, hMSC, BJ) are described followed by detailed descriptions of the biological protocols used in this study, including the splitting protocol, cell counting and seeding, Live&Dead assay, immunoflourescent staining, and SEM protocol. The chapter also includes a description of Photothermal Therapy (PTT) and, to prove the efficiency of the IR treatment used to analyze the photothermal effect of the 70S30C bio-glass, the MTT protocol is followed.

In the third Chapter, the results obtained from all the performed experiments are reported. In particular, the results obtained are critically discussed to demonstrate that the bio-glass scaffolds are suitable for BTE, as they provide an adequate substrate for cellular culture. Furthermore, the photothermal effect is proved by Live&Dead images and the MTT, which confirms the death of cells due to the increase in temperature caused by IR irradiation.

The Conclusion reports a summary of this work, underlying its results and outlines for possible future works.

Chapter 1

Bone tissue: anatomy and engineering

1.1 Bone tissue anatomy

In this first section the anatomy of bone tissue will be presented and discussed, with focus on its structure and formation.

1.1.1 Connective tissue

The term "tissue" is used to describe a group of cells present in the body which share the common characteristics of embryonic origin and morphology and which are organized in order to achieve the functions of the tissue itself. Although there are many cells in the human body, they are divided into four tissue categories: *epithelial*, *connective*, *muscle*, and *nervous*. Each category consists of specific functions that contribute to the general health and the maintenance of the body [1].

Connective tissues play many roles in the body but, most importantly, they support and connect other tissues. Moreover, connective tissue, composing fibrous capsules and bones, has the role to protect the delicate organs and skeletal systems. Transport of liquids, nutrients, waste and chemical messengers is guaranteed by specialized fluid-related tissues such as blood and lymph which are examples of liquid connective tissue. Adipocytes are connective tissue cells that are responsible for synthesizing, accumulating and releasing lipids. They store excess energy in the form of fat and contribute to body thermal insulation. Connective tissue types are classified on their surface properties and the types of fibers that composed them. Connective tissue itself includes loose and dense connections: these two tissues contain various cell types and protein fibers suspended in a viscous ground substance [1].

In the loose connective tissue, the fibers are loosely organized and leave large spaces between them. The dense connective tissue contains instead more collagen fibers than

the loose tissue. Therefore, it has a higher resistance to stretching. There are two main categories of dense connective tissue: normal and irregular. In the dense regular on the fibers are parallel, thereby improving strength and stretch resistance to the direction of the fibers' direction. In the dense irregular tissues, the fibers direction is random and this arrangement gives the tissue greater resistance in all directions and less resistance in a particular direction [1].

1.1.2 Bone structure

Bones are the hardest connective tissue. It protects the internal organs, supports the body, promotes movement, produces blood cells, stores minerals, and releases fat. The rigid extracellular matrix of bones contains most collagen fibers embedded in mineralized soil material that contains hydroxyapatite, a type of calcium phosphate [1].
It is possible to make a classification of bones based on its shape. Long bones are tubular (e.g., the humerus in upper limb, femur in lower limb); short bones are cuboidal (e.g., bones of the wrist and ankle); flat bones consist of two compact bone plates separated by a spongy bone (e.g., skull); irregular bones are bones with various shapes (e.g., bones of the face); and sesamoid bones are round or oval bones that develop in tendons [2].
All bones are internally vascularized, and covered externally by a fibrous inter-tissue membrane called periosteum, except at the joints where the articular cartilage exists. This membrane has the unique capability of forming new bone and receives blood vessels whose branches supply the outer layers of compact bone [2].
Nerves accompany vessels that supply bone and periosteum. Most nerves entering the inner cavity with the artery are vasomotor fibers that regulate blood flow. Furthermore, the periosteum is provided with a wide range of sensory nerve fibers and is highly sensitive to any type of injury [2].
Macroscopically, bone exists in two forms: *compact* and *cancellous* as reported in Figure 1.1.

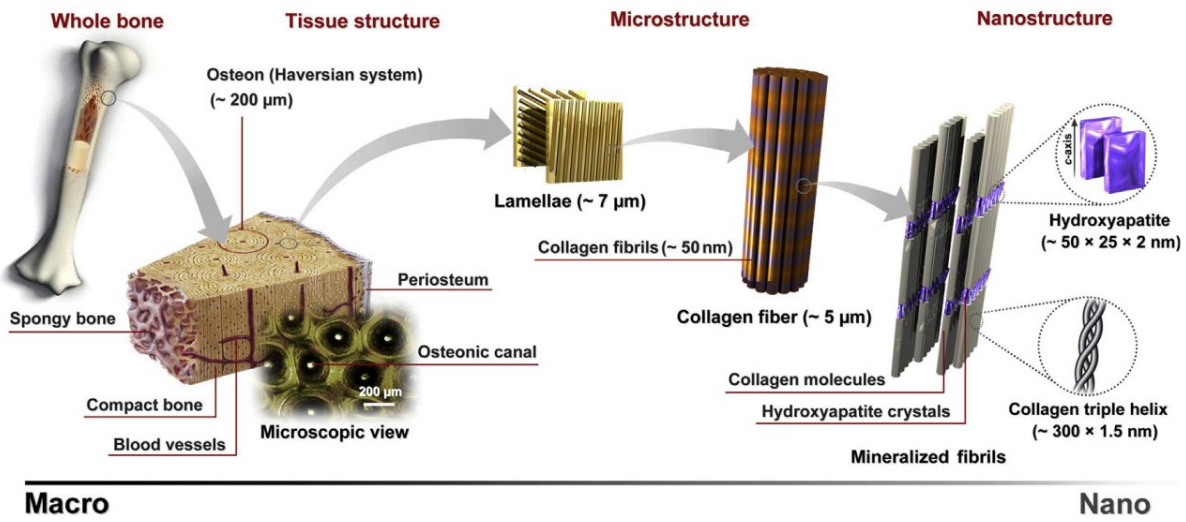

Figure 1.1. Hierarchical structure of the bone, adapted from [9].

The compact bone is hard and dense, similar to ivory. Currently, it is present on the surface cortex of the bone and becomes thicker along the length of the skeleton and on the surface plate of the flat bone. The collagen fibers in the mineral matrix are organized into lamellae, which are embedded in the osteocytes. Most of these lamellae are arranged in central cylinders around vascular channels (Haverine channels) to form a Haverine system or osteons, usually parallel to each other and to the bone's long axis. The Haversian channels communicate with the medullary cavity and with each other by operating the Volkmann channels on both sides, which contain anastomose vessels [3].

It is estimated that there are 21 million osteons in the typical adult skeleton. The diameter is between 100 and 400 µm and usually contains 5–20 lamellae. Each osteon is permeated by the canals of its resident osteocytes, which form pathways for the diffusion of metabolites between the osteogenesis and blood vessels [4].

Osteons are distinguished from their neighbors by a cement line that contains little or no collagen and is strongly basophilic because it has a high content of glycoproteins and proteoglycans. Cement lines are sometimes referred to as reversal lines because they mark the limit of bone erosion prior to the formation of a new osteon [4].

Cancellous bones are composed of sponge works of trabeculae of varying width, length and thickness (50−400 µm), arranged not chaotically but in very real patterns, to withstand local stresses and strains. Cancellous bones are found inside the short bones and at the articular ends of the long bones [3].

Long bone medullary cavities and cancellous bone interstices are filled with red or yellow medullary. At birth, all of the bone’s marrow is red and there is active

hemopoiesis everywhere. As age advances, the red marrow becomes atrophied and replaced by yellow fatty marrow without hemopoiesis. This change begins in the distal parts of the limbs and progresses gradually over time. In young adult life, the red marrow only remains in the ribs, sternum, vertebras, skull, skeleton bones, and the proximal ends of the femur and humerus, which are often the site of malignant metastases [3].

1.1.3 Bone formation

Bones develop through two major processes: intramembrane and endochondral ossification (membrane and cartilage ossification). In general, skull bones, faces, and throat bones are ossified in membranes, while long bones are ossified in cartilage [3].
In intramembrane ossification, osteoblasts simply deposit bone within fibrous tissue, but there is no presence of cartilage precursors [3].
In the endochondral ossification, a model of pre-existing bone hyaline cartilage is gradually destroyed and replaced by bone. Most bones, including long bones, form in this way. The cartilage is not directly transformed into bone, it is gradually destroyed and replaced by bone.
During the years of growth, there is a continuous re-modelling of bones, either by destruction (as of the osteoclast) or replacement (as of the osteoblast), whether the original development was intramural or endochondral. Similarly, endochondral ossification, subperiosteal ossification, and reconstruction occur in the callus of fracture sites [3].
The first place of bone formation is the primary center of ossification and in long bones it is located in the middle of the spine (diaphysis). The end of the bone (epiphyses) remains cartilage and usually acquires a secondary ossification center only after birth. When ossification occurs over the epiphyseal plate, the diaphysis and the epiphysis fuse and bone growth ceases. The portion of the bone that experiences the most active growth is the final area to undergo ossification before the end fuses with the diaphysis [3].

1.1.4 Bone microstructure

Bone contains a mineralized collagen extracellular matrix surrounded by a variety of specialized cells, including osteoblasts, osteocytes and osteoclasts [4].

Osteoblasts are located on the surface of the matrix, which synthesize, transport, assemble, and regulate the mineralization of the matrix. Over time, osteoblasts may become inactive and experience a decrease in cytoplasmic volume. Some inactive cells remain on the surface of trabeculae or they may be embedded in the matrix (osteocytes). Osteocytes are connected through a complex network of cytoplasmic processes of the dendritic cells through tunnels known as canalicules. Osteocytes help control calcium and phosphate levels in the microenvironment, detect mechanical forces, and translate them into biological activity, a process called mechanical transformation [5].

Osteoclasts are multinucleated specialized macrophages that are generated from circulating monocytes responsible for bone absorption. By the incorporation of the cell surface, the osteoclasts adhere to the bone matrix and create an outer cell trench [5].

Approximately 10% to 20% of bone is water. The remaining dry weight (30 to 40%) consists mainly of organic components of the extracellular matrix. About 30% of the organic matrix is collagen, and the remainder consists of non-collagen proteins, glycoproteins, and carbohydrates; the proportion of these components depends on age, location and metabolic condition of the individual bone. Most of the collagen in bone is an ordered branching network of type I fibers, but a small amount of type V collagen is also present, probably to help regulate fibrillogenesis. Collagen fibers contribute greatly to the mechanical strength of bone and its resistance, as reflected in the energy needed to break bone. Collagen is usually synthesized by osteoblasts to form bone. New tropocollagen molecules lose some of their non-helical terminal regions, forming fibroids in the extracellular matrix, which then combine to form fibers. In primary bones, collagen fibers form a complex interwoven mesh that includes other organic molecules. This “osteoid” material is then mineralized to form woven bones (non-lamellar). Over time, the primary bone is replaced almost entirely by a normal laminated array of almost parallel collagen fibers, which forms the basis of the laminated bone. The collagen fibers of the periosteum are integrated into the cortical bone (exterior fibers) which anchor this layer of fibrous cells on its surface [4].

The bone organic matrix consists of small amounts of various macromolecules connected to the collagen fibers and surrounding bone crystals. They are secreted by

osteoblasts and young osteoblasts, and include many growth factors, as for example osteonectin, osteocalcin, and prostatic enzyme inhibitors, often in latent forms [4].

1.1.5 Bone re-modelling

As with all brittle materials, micro-damage accumulations due to cyclic loading can occur in bone, and bone tends to limit the risk of fracture through a process of re-modelling as reported in Figure 1.2. The new created matrix could have different volume or orientation compared to the old one, since the bone would adapt its architecture and structure to situations in which it experiences constant loads [4].

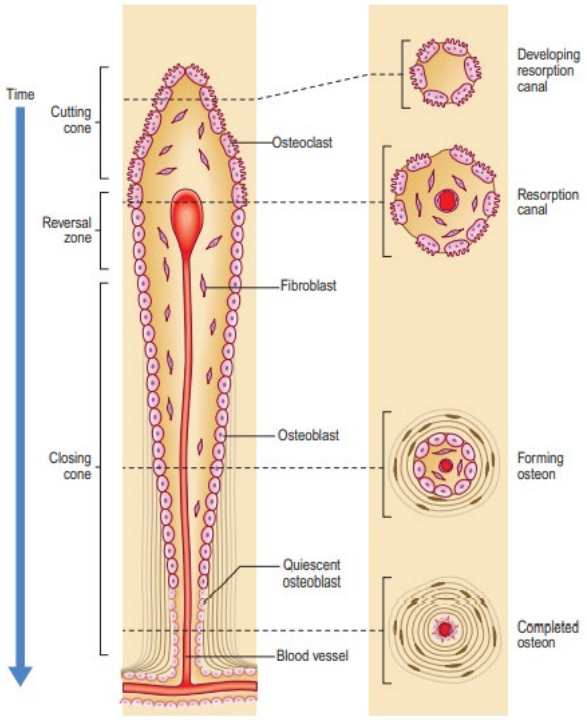

Figure 1.2. Bone remodelling timeline; adapted from [4].

Re-modelling also affects the local balance between bone resorption and deposition. The main objective of the bone is not to increase bone mass but to regenerate it and the process is ongoing throughout life, replacing about 10% of the bone every year. The bone re-modelling unit consists of a cutting cone and a closing cone. Activated osteoblasts form cutting cones, which excavate bone tunnels (resorption channels) and advance in front of growing central blood vessels at a speed of 50 μm/day. The cutting cone is usually 2 mm long and forms within 1–3 months. It takes the same amount of time to form a new (secondary) osteon after the completion of the closing cone.

Osteoblasts follow osteoclasts and fill the spaces created by new osteons, starting with the outer surfaces and walls of the tunnel [4].
Continual bone layers are deposited on the surface of the previous layer when osteoblast cohorts (such as osteocytes) are incorporated into the matrix that they secrete, until the most central lamella is close to the axis of the cylinder's blood vessels [4].
A highly mineralized basophil cement line marks the margins of the new osteon, showing the boundary between the absorption activity of the cutting cone and the bone matrix not modified by this activity. The remains of the circumferential lamellae of the old osteons form interstitial lamellae between the newer osteons [4].
The re-modelling rate decreases with age, which means that it is possible to estimate the age of skeletal material at death by looking at the numbers of osteons and osteon fragments. Conversely, increasing physical activity or constant loading of the skeleton could cause bone hypertrophy [4].

1.2 Bone tissue pathologies

In this paragraph, the main pathologies involving the skeletal system, and in particular bone tissue, will be described.

1.2.1 Fractures

Fractures are defined as a loose of bone integrity due to mechanical injuries and/or loss of bone strength, and they are some of the most common pathologic conditions affecting bone.
It is possible to categorize fracture types and affect treatment:

- Simple: the overhanging skin is intact;
- Compound: the bone is in contact with the skin surface;
- Comminuted: the bone is fragmented;
- Displaced: the distal ends of the bone at the fracture location are not aligned;
- Stress: a developing fracture that is caused by a period of increased physical activity in which the bone is subjected to cyclic loads;

- Greenstick: the fracture only partially extended through the bone and is common in infants when bones are soft;
- Pathologic: the bone's weakness is caused by an underlying disease process, such as cancer.

Bone has a considerable repair capability, a process that involves the regulation of the expression of multiple genes, which can be divided into overlapping phases with specific molecular, biological chemical, and biological mechanical characteristics [5].
The first signature of a fracture is the development of a hematoma due to the rupture of blood vessels surrounding the site of the injury. The clotted blood forms a fibrin network that closes the fracture site and, at the same time, creates a structure for the influx of inflammatory cells, fibroblasts and new capillaries. Meanwhile, platelets and migrating inflammatory cells release PDGF, TGF-β, FGF, and other factors that activate osteoprogenitor cells in the periosteum and surrounding soft tissues, stimulating the activity of osteoblasts and osteoclasts. For this reason, by the end of the first week, the main changes are the organization of the hematoma, the production of matrix in adjacent tissues and the re-modelling of the fractured ends of the bone.
A fusiform and predominantly noncalcified tissue, called *soft tissue callus* or *procallus*, is created to provide some anchorage between the fractured bone ends, but it is not characterized by the structural rigidity needed to support weight [5].
After 2 weeks, the procallus turns into *bony callus*. The osteoprogenitor cells start to create trabeculae of bone oriented perpendicularly to the cortical axis, and there is also the formation of cartilage along the fracture which helps the deposition of new bone trabeculae. As the bony callus become mature and is subjected to body-weight forces, there is resorption of the parts of the callus that are not stressed. In this way, the normal shape and size of the bone are restored as lamellar bone. The re-establishment of the medullary cavity signals the end of re-modelling.
A major obstacle to healing is the infection of fracture sites, especially common in open fractures. Malnutrition and skeletal deformities also hamper the healing of fractures [5].

1.2.2 Osteopenia and Osteoporosis

The term osteopenia is related to a decrease in bone mass, while osteoporosis a serious form of osteopenia that significantly increases the risk of fracture. These diseases can be

located in a particular bone or region, such as the disuse part of the limbs, or can involve the entire skeleton as a manifestation of metabolic bone diseases. The most common forms of osteoporosis are those associated with aging and menopause, and prevention and treatment strategies including exercise, appropriate calcium and vitamin D assumption are necessary [5].

Studies on bone formation and resorption are considered useful to understand osteoporosis pathogenesis. In young individuals, osteoblast have a major proliferative potential compared to older individuals. Thus, the capacity to create new bone, and so the ability to respond promptly to growth factors, decreases with age. Lack of physical activity can cause an increased rate of bone loss, since mechanical loads stimulate bone re-modelling. Defects in genes could cause variations in bone density. Calcium contributes to bone mass and insufficient intake of calcium, especially during the period of bone growth, could be a possible cause of the onset of osteoporosis. A lack of calcium could also reduce vitamin D levels and, for this reason, may be responsible of the development of senile osteoporosis. An important role in the postmenopausal osteoporosis is played by the estrogens deficiency that appears to increase the secretion of inflammatory cytokines. These cytokines stimulate the activity and the recruitment of osteoclasts, resulting in bones perforations and loss of bones interconnections [5].

Clinical manifestations of osteoporosis depend on the bone involved [5]. Usually, the bone structure is not adequate to support weight and, for this reason, fractures commonly occur, especially compression fractures of vertebrates that cause spinal deformities (the most common is the kyphosis) and reduced height [6].

The effects of osteoporosis cannot be reliably detected on a simple radiograph until 30 to 40% of the bone mass is lost. Since this pathology is difficult to diagnose in asymptomatic people, specialized imaging techniques should be used to investigate bone density, which is the parameter to evaluate [5].

1.2.3 Cancers

The most common types of malignant bone cancers are osteosarcomas, chondrosarcoma, and Ewing sarcomas. However, metastatic cancers and multiple myelomas are more prevalent than primary bone tumors [6].

Osteosarcoma

Osteosarcoma is the most common form of malignant tumor, accounting for approximately 20% of all bone cancers. It primarily affects males younger than 20 years of age and can occur in any bone, although it typically affects the metaphysis of long bones or the site near the knee, such as the proximal part of the tibia or the distal femur. It has different histological variations: the osteoblastic tumors show a prominent osteoid formation, while the chondroblastic tumors form cartilage matrix and can have relatively few bone differentiations [6]. Osteosarcoma usually presents a painful mass that gradually enlarges and sometimes sudden bone fractures are the first symptoms. The tumor often breaks through the cortex, raises the periosteum, and creates reactive periosteal bone, which is clearly visible with radiography.

Due to its good vascularization, the tumor site can appear as an area of increased density on radiographic images. Additionally, extensive necrosis may be seen at the site of the cancer. Osteosarcoma is treated in a multi-modal approach, including non-adjuvant chemotherapy, given after surgery on the premise that all patients have occult metastatics when diagnosed. [5].

Chondrosarcoma

It is a malignant tumor which has the highest incidence in men between the ages of 30 and 60. Neoplasms can arise as primary tumors or from the transformation of existing cartilage tumors, and they typically affect the axial skeleton, especially the pelvis, shoulder, and ribs.

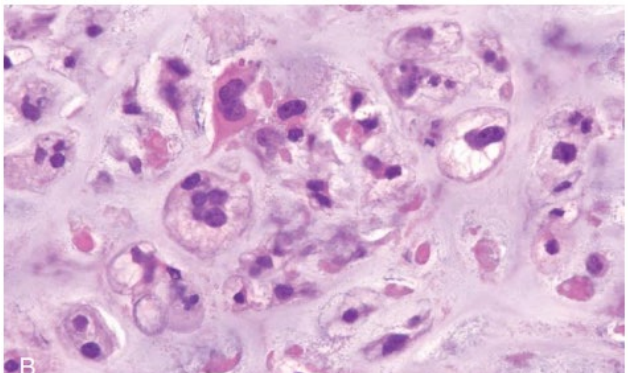

Figure 1.3. Chondrosarcoma in a third state; adapted from [5].

Common chondrosarcomas are large, hard, painful tumors composed of luminous grey-white translucent cartilage nodes with a gelatinous matrix. It is possible to find spot of calcification and also sites of necrosis, which could create cysts. The tumor is able to

penetrate through the cortex and affect surrounding tissues. There is a direct correlation between the grade of the tumor and the biological behaviour, and it is possible to identify 3 tumor grades, from 1 to 3 (as reported in Figure 1.3). Grade 1 is characterized by low cellularity and has a 5-year survival rate of 80-90%, while grade 3 has higher cellularity and giant tumor cells with a 5-year survival rate of 43%. Fortunately, most conventional chondrosarcomas are class 1 diseases and rarely metastasized, while 70% of grade 3 tumors are associated with metastasis, especially to the lungs. Conventional chondrosarcoma treatment is extensive surgical excision, often combined with chemotherapic treatments [5].

Ewing sarcoma

It is a malignant bone tumor with primitive round cells that are not clearly differentiated (Figure 1.4). It accounts for about 6-10% of primary malignant bone tumors and is the second most common bone sarcoma in children, affecting 80% of patients under 20 years of age.

Ewing sarcoma generally invades the cortex, periosteum and soft tissues and it is characterized by painful masses, often associated with infections, anemia, leukocytosis. The tumors are soft, white and often contain areas of bleeding and necrosis. They are composed of layers of small, round cells which could appear clear because there is a high glycogen content.

This type of tumor is an aggressive malignant condition treated with neoadjuvant chemotherapy, followed by surgical excisions with or without radiation [5].

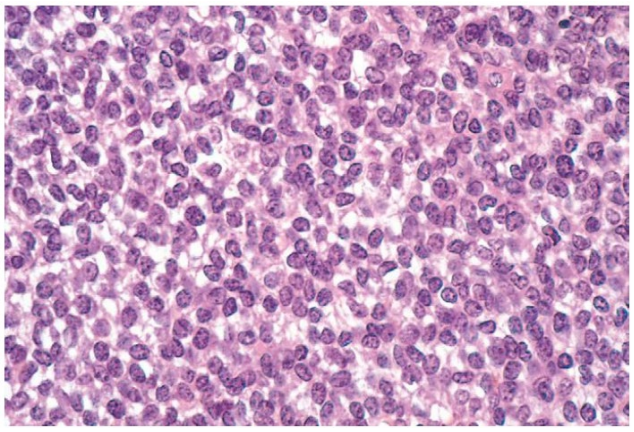

Figure 1.4. Ewing sarcoma composed of small round cells; adapted from [5].

1.3 Mechanical behavior of bone tissue

Bone tissue can be classified into two types: cortical bones (compact or dense) and trabecular bones (cancellous or spongy). The distinction between these two types of bone tissue can be made by considering the porosity: the porosity of the compact bone ranges from 5% to 15%, while the porosity of the trabecular bone is between 40% and 95%. It is possible to find cortical bone in the diaphysis of long bones and surrounding the trabecular compartment in the metaphysis and epiphyses. Trabecular bone is also located in the vertebrae [7].

1.3.1 Cortical bone

The material behaviour of the cortical bone is anisotropic, meaning it exhibits different properties depending on the direction of loading. The strength and compression of the cortical bone along the path oriented to the diaphyseal axis are greater than those along the radial and circumferential directions. These properties have been observed in the radial and circumferential directions, suggesting that cortical bones can be treated as transversely isotropic materials [8].

When the cortical bone is loaded in the longitudinal direction, it has a bilinear stress response, with different Yield points that separate the linear elastic region from the linear hardening region. It is also known that the fracture resistance is less than 3%. On the other hand, for the compression load along the longitudinal direction, there is a rapid hardening after yield, followed by softening, before failure at about 1.5 % stress. It is possible to underline that cortical bone loaded in the cross-sectional direction fail more fragilely, with a stiffness modulus ranging from 6 GPa to 10 GPa, compared to those loaded in the longitudinal direction, which have a stiffness modulus ranging from 17 GPa to 20 GPa. The impact of load speed on the modulus is only moderate, as a six-order increase in load increases modulus by only two factors and load by three factors. However, with the increase in load rate, the effects of strain and strengthening remain clinically relevant because the load rates can exceed the normal physiological range by more than 10 times [8].

When the cortical bone is loaded over the output point, material properties are degraded and this is a phenomenological definition of damage. Cortical bone damage is also

considered as a deterioration of the tissue microstructure and/or nanostructures and is collectively known as microdamage.

Microdamage may occur as a decomposition of protein–hydroxyapatite composites or as a slippage of lamellae along another lamella or along the cement line; the mechanism of bone fragility is associated with a decrease in modulus, and there is a relevant relationship between fracture resistance and micro-damage density. Microcrack accumulation increases exponentially with age in cortical bone and is significantly higher in the bones of women versus men [8].

The fracture of cortical bone may be caused by repeated loads (fatigue failure) or applied stresses that cause local loads beyond the tissue strength. The preferred alignment of osteons in the cortical bone provides an anisotropic stress. A fracture that spreads perpendicularly to the osteons is more likely to drift and rotate than a fracture that spreads parallel to the osteons (longitudinally oriented fracture), which can explain the anisotropic stress of the fracture.

The orientation dependence on these mechanisms may also explain the anisotropy of the increase fracture rigidity with the growth of fractures. Fatigue loading also causes progressive degradation of mechanical properties such as fracture resistance, module, and strength.

Cortical bone can be subjected to multiaxial loading conditions in the body, especially during traumatic events such as a fall. Multiaxial loading can cause more severe reductions in stiffness and fatigue life compared to a uniaxial loading [8].

Age related changes in the mechanical properties of cortical bone have been attributed to increased porosity, hypermineralization, microdamage accumulation, and decreased quantity of non-collagenous proteins. The strength of cortical bone under tension and compression declines by approximately 2% per decade from the third decade of life. The tensile ultimate strain also decreases by approximately 10% per decade, from a high of 5% strain at age 20 – 30 years to a low of less than 1% strain above age 80 years. In general, it can be said that cortical bone has greater resistance to compression fatigue than tension and high load frequencies [8].

Fracture toughness also decreases approximately 4% per decade. Common diseases such as osteoporosis and diabetes can cause marked changes in cortical bone's mechanical behavior. The effects of aging on the mechanical properties of cortical bone are not readily distinguishable from those of osteoporosis, while diabetes is associated with lower bone toughness as compared with normal cortical bone and this difference

may be related to heightened accumulation of AGEs (Advanced Glycation End products) in diabetic bone. Alteration in mineral content and in the spatial distribution of mineral, vitamin D deficiency, and chronic kidney disease, have also been linked to deficits in stiffness or toughness, or to changes in the manner of crack propagation [8].

1.3.2 Trabecular bone

Trabecular bone is a highly porous, heterogeneous, and anisotropic material found in the epiphyses of long bones and vertebrates. On the macrostructure scale, hard trabecular bones form a rigid and flexible structure, which creates the framework for bone marrow filling the intertrabecular space. At the microstructural scale, trabecular architecture is organized to maximize load transfer. It is the main loading bone in the vertebrate body and also transfers the load of joints to the long-term cortex bone. Like compact cortical bone, trabecular bone consists mainly of hydroxyapatite, collagen, and water. However, the trabecular bone content, tissue density (1.874g/mm3), and dust content (33.9%) are lower than cortical bone. As a result, the water content is higher (27% vs. 23% for cortical bones) and for this reason the trabecular bone is more active in reconstruction and is also less mineralized [7].

The orientation and organization of collagen and minerals are important factors in determining the mechanical properties of this bone tissue, as well as the size and the distribution of the lacunae and the porosity of the tissue, which is higher than in cortical bone. Actually, a high stress in longitudinal direction of lacunae could cause damages also in the trabecular bone itself.

Therefore, the mechanical behavior is related to the load direction, load intensity and even to the conditions of the cartilage which is adjacent the trabecular bone. It is not easy to identify the mechanical properties of the trabecular bone due to the small dimension of the trabeculae, the heterogeneous and anisotropic nature of the bone itself. Regardless, it was estimated, with buckling analysis or with nano-indentation, an elastic modulus around 14.13 GPa for dry trabecular bone and 11.38 GPa for the wet one as reported in Figure 1.5. It is necessary to point out that the reported elastic modulus may vary depending on the species and anatomical site of the bone [7].

Variations in density and architecture can lead to a heterogeneity in the elastic behavior and in the strength of trabecular bone, associated with the fracture of the bone itself. Approximately 70–90% of the variations in the modulus and strength of trabecular bone

can be explained by volume fraction or apparent density but if only an anatomic site is considered, the modulus and strength relations appear to be linear because the range of apparent density is less than an order of magnitude [8].

Testing technique	Bone type	Tissue modulus (Gpa)
Buckling	Human proximal tibia	11.38 (wet), 14.13 (dry)
Experiment-FEA	Human proximal tibia	23.6 ± 3.34
	Human greater trochanter	24.4 ± 2.0
	Human femoral neck	21.4 ± 2.8
	Human femoral neck	18.0 ± 2.8
	Bovine proximal tibia	18.7 ± 3.4
	Human vertebra	6.6 ± 1.0
	Human vertebra	5.7 ± 1.6
	Human proximal femur	10 ± 2.2
	Bovine proximal tibia	6.54 ± 1.11
Ultrasonic technique	Human femur	13.0 ± 1.47
	Human femur	17.5 ± 1.12
	Bovine femur	10.9 ± 1.57
	Human tibia	14.8 ± 1.4
	Human vertebra	9.98 ± 1.31
	Human tibia	14.8 ± 1.4
Nano-indentation	Human femoral neck	11.4 ± 5.6
	Human distal femur	18.1 ± 1.7
	Human vertebra	13.4 ± 2.0
	Human femural head	21.8 ± 2.9
	Human femur trochander	21.3 ± 2.1
	Human distal radius	13.75 ± 1.67
	Human vertebrae	8.02 ± 1.31
	Porcine femur	21.5 ± 2.1
	Human tibia/vertebrae	19.4 ± 2.3
	Sheep proximal femur	20.78 ± 2.4

Figure 1.5. Tissue elastic modulus of trabecular bone in different anatomic; adapted from [7].

Several studies have shown that axial elastic modulus is a better predictor of axial strength in bone structure than structural density. However, unlike elastic modulus, which is similar in compression and tension, the tensile strength of trabecular bone is lower than its compressive strength. Due to the heterogeneity of trabecular bone, it is difficult to establish general rules for strength and for this reason studies have shown that the anisotropy of trabecular tissue can be ignored because, in most cases, the elements of trabecular bone are loaded just uniaxially. Age, bone organ type, anatomic site and pathologies, such as osteoporosis, have a significant impact on strength of trabecular bone structure by affecting bone apparent density, architecture and tissue mechanical properties [7].

Regarding the anatomic site, the failure stresses for human bone can vary between 2 MPa for vertebral trabecular bone and 7 MPa for distal femoral bone. With a specific attention to the age, studies have demonstrated that the ultimate strength decreases by almost 7% and 11% respectively for proximal femoral and vertebral bone between the ages of 20 and 100, especially due to a decrease in volume fraction.

Several studies have also shown that the Yield strain is dependent upon anatomic site. For example, it is higher for the femoral neck in compression and higher for vertebrae in tension compared to other sites, but it has also been shown that, for all anatomic sites, the yield strain for compression is higher than for tension [7].

The occurrence of a damage has a direct effect on fracture risk in musculoskeletal diseases and bone re-modelling, and can happen by the implantation of prostheses or due to a bone joint disease [7]. In general, microdamage increases with age under both pre- and post-yield loading conditions. The incident of microdamage is related to architectural parameters and volume fraction, and it results in large modulus reduction. For example, microdamage is found to be more frequent in regions with low volume fraction and with a predominance of trabecular rods. The propagation of damage is also anisotropic because it is related to the orientation and to the local thickness of the trabeculae [8].

Creep is the tendency for bone to permanently deform under applied mechanical loads, and fatigue is the reduction of bone strength under cyclic loading. It was demonstrated by testing this tissue that trabecular bone shows the classical creep characteristics with three phases: high elastic strain response, steady state response, and necking. This result was obtained by applying “daily mechanical loadings” on trabecular bone to simulate the ordinary behavior of the trabecular bone when subjected to certain loads [7].

The cyclic compression load of trabecular bone can cause loss of rigidity and strength, and accumulate residual pressure, even under low applied load. The rate at which the module decreases and damage accumulates in fatigue increases as the amount of stress applied increases. The static and cyclic testing of human trabecular specimens under physiological loads (750 – 1,500 micro-strains) indicates that the time required to fully recover residual deformation is more than 20 times longer than the applied load. These results support the idea that non-traumatic fractures can be associated with long-term creep effects, whether accumulated during long-term static load or fatigue load.

The compressive fatigue life of trabecular bone is also a function of the loading direction: fatigue life is lower for loading oblique to the principal direction (off-axis) versus along the principal direction (on-axis) [8].

1.3.3 Whole bone

The study of the mechanical behavior of whole bones can be substantially more complicated than that of cortical or trabecular bone. However, investigations at the whole-bone level are the most directly relevant to understanding the occurrence of fractures, the biomechanics of healing them, and to figuring out the mechanical input and the outcomes of bone adaptation [18].

As bones are structural elements of the body, the skeletal system supports loads related to different daily activities, such as holding things, walking, pushing, and so forth. Loads can induce tensile, compressive, or shear stresses on the bone tissue. More complex stresses, such as those caused by bending or twisting of bone, can be decomposed into their three components of stress. To study these stresses, it is important to consider bone mechanical properties such as elasticity modulus, compressive, and tensile strength, which are highly dependent on the position of the bone, as well as the conditions and age of the individual (Figure 1.6). In addition, the mechanical properties of bone vary depending on the load orientation, considering orientation of the tissue (anisotropy) and the speed of load application (viscoelasticity). Therefore, bone tissue could be considered an anisotropic material and the bone elastic modulus is between 1 to 20 GPa [18].

Property	Cortical bone	Cancellous bone
Tensile strength (MPa)	50–150	10–100
Compressive strength (MPa)	130–230	2–12
Young's modulus (GPa)	7–30	0.02–0.5
Strain to failure (%)	1–3	5–7
Shear strength (MPa)	53–70	
Shear modulus (GPa)	3	

Figure 1.6. Different bone mechanical properties; adapted from [18].

It is essential to consider a physical property of osseous tissue, which is the permeability, that describes the porosity of the tissue. Permeability is estimated between $0.003 - 11 \times 10^{-6}$ $m^4/N{\cdot}s$ for trabecular bone in humans and $0.9–7.8 \times 10^{-11}$ $m^4/N{\cdot}s$ in cortical bone [18].

Since bone tissue deformation depends on time, it is considered a viscoelastic material because there is collagen 1 in the structure of bone tissue which plays an important role in severe injury fractures. The bone tissue exhibits stiffness behavior after a stress increases greater than the yield stress, and eventually breaks under a strain of less than 3%. However, under pressure loads in the longitudinal direction, hardness occurs rapidly after yield pressure, and failure occurs with a load of about 1.5%. Furthermore, the effects of load type on bone mechanical properties have shown that the pressure resistance of compression loading is higher than tensile and cutting loading in the longitudinal and transverse directions. Therefore, the compression characteristics of the bone are more significant in the longitudinal direction. It is also important to underline the different behavior of collagen related to the load rate, as collagen is one of the main components of bone ECM and is responsible for bone viscoelasticity. This exhibits a strongly viscoelastic behavior because, when stressed with a low strain rate, it opposes slight resistance since it is given sufficient time for filament entanglement. On the other hand, if it is stressed with a high strain rate, the collagen appears to be very stiff because the fibers do not have enough time to stretch [20].

It is crucial to ensure that scaffolds and transplants in the body have mechanical properties similar to the target bone; otherwise, bone damages may occur due to stress.

1.4 Bone Tissue Engineering (BTE)

Bone tissue engineering (BTE) plays an important role in bone tissue regeneration in order to restore original tissue integrity and functions of parts that have suffered micro or macro damages. BTE involves creating new methods of tissue repair and regeneration by focusing on the fabrication of scaffolds, which can reduce the problems related to the traditional treatments. The scaffold should emulate the physical structure, composition and biological functions of the bone extracellular matrix (ECM) [10].

1.4.1 Scaffold fabrication

Bone tissue engineering utilizes the populations of osteogenic cells, scaffolds made of osteoconductive biomaterials, and bioactive factors of osteoinduction to create a new strategy to mimic bone extracellular matrix.

The bone ECM is characterized by both an inorganic and organic phase. The inorganic phase provides both the strength and the stiffness of the bone, while the organic phase is responsible of energy. Additionally, the ECM regulates the formation of new bone tissue due to the interaction with osteoblast and osteoclast [10]. Different techniques have been used for scaffold fabrication, including thermally induced phase separation (TIPS), rapid prototyping (RP), and 3D-bioprinting [10].

The TIPS technique enables the fabrication of scaffolds for various tissues, like bone and teeth. In general, homogeneous polymer solutions are cooled, followed by high temperature heating and solvent removal, resulting in phase separation with a microporous structure. However, smaller pore sizes of 10–100 μm are not sufficient for bone tissue growth. Another disadvantage of this technique is the use of organic solvents, which can lead to problems such as long sublimation times and cell death to the solvent itself. These problems can be overcome by using additive manufacturing [10].

Rapid prototyping (RP) is an example of additive manufacturing in which specific patient information are matched with the scaffold properties using a computer-aided design (CAD) model. The result is a scaffold characterized by micro and macro porous distributed in the whole scaffold, which can promote cell distribution [10].

Similarly, 3D bioprinting also requires a CAD model to allow the 3D printing machine to recreate the structure. It is an emerging technology that provides an effective solution that helps to achieve patterns of complex tissue templates by depositing extracellular matrix, living cells, and other biomaterials. For this reason, the bioprinting process usually starts with the selection of cells and biomaterials related to the aim of the project goal. Inkjet, microvalve, laser-assisted, and extrusion bioprinting are the bioprinting techniques currently used [10].

1.4.2 Scaffold properties

Bioactive scaffolds should possess specific characteristics related to the tissue or organ that they aim to regenerate. However, certain attributes should be present in every scaffold to ensure its effectiveness.

Biocompatibility

It predicts an adequate integration of the scaffold into the host tissue without causing

toxic effects such as genotoxicity, cytotoxicity and/or immune response [11]. Unwanted effects, including cell toxicity, genotoxicity, immunogenicity, mutation, thrombogenicity and swelling, should be eliminated, minimized or controlled when placing a scaffold in the body. For example, inflammation should be avoided since it reduces the rate of regeneration and promotes tissue rejection [18].

Biodegradability

In vitro or in vivo, the ability of a scaffold to degrade over time is preferably controlled by a resorption rate in order to create a space for the growth of new tissue. In other words, as the number of cells increase, the empty space in the scaffold decreases and the degradation rate of the material is expected to match the cells' growth rate. This attribute is related to biocompatibility because degradation products must be non-toxic and metabolized or eliminated from the body, without causing any inflammations or other diseases. The degradation behavior of scaffolds should be strictly dependent on their application [18].

Porosity

Connected pores are necessary to promote cells and nutrients distribution in the whole scaffold and also to help the elimination of waste substances. Porous scaffolds are used to produce synthetic skin, bone and cartilage reconstruction, blood vessels, drug delivery, periosteal repair, etc. since the micropores (150 – 800 μm) can support vascular growth, nutritional transport, and promote bone tissue regeneration by facilitating artery formation, bone formation, and cell migration to implant sites [11].

The scaffold, for this reason, must have a large surface area due to its overall porosity and pore size. The ratio of surface area to volume of the porous structure depends on the size of the porous structure: large surface areas enable cell attachment and proliferation, while large pore volumes are necessary to contain and then provide sufficient cells for the healing or the regeneration process [18].

Different studies have shown that scaffolds with pore diameters of 500 to 800 μm are suitable for bone tissue regeneration because they provide sufficient space for cell growth.

Another important factor is the pore geometry as reported in Figure 1.7: it was shown that there is a greater cell proliferation on the short edges of rectangular pores compared to the long edges of scaffolds.

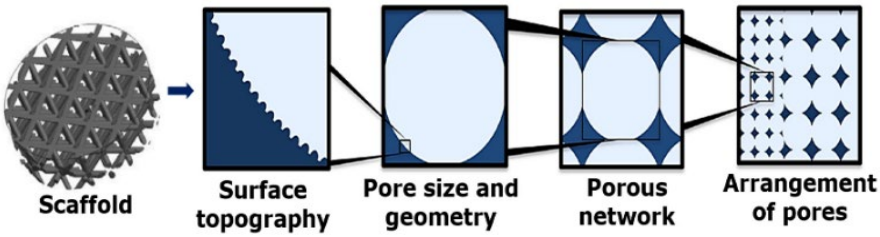

Figure 1.7. Scaffold porosity; adapted from [17].

Furthermore, concave surfaces facilitate tissue formation by allowing the appropriate cell adhesion space. On the other hand, convex surfaces of scaffolds restrict tissue growth [11].

Mechanical strength

It is an important factor that should be considered when creating a suitable scaffold for an engineered tissue. It is necessary that the implants have the same mechanical properties of the tissue they are replacing [10], such as elastic modulus, tensile strength, fracture toughness, fatigue, and elongation percentage [18]. The mechanical behavior of scaffolds is related to the bio-resorbability because changes in mechanical properties caused by decomposition processes should be compatible with bone regeneration processes. A scaffold for the BTE needs to have appropriate mechanical strength, the ability to withstand and transfer loads to the adjacent host tissue, and to mimic the anisotropic behavior of the natural bone [12]. The aim is to have a compressive strength in the range of 2–12 MPa and a modulus at least around 5 GPa which is the strength of cancellous bones [19].

Surface properties

Chemical and topological properties control and influence cell adhesion and proliferation. The first is related to the ability of cells to bind to the material, while the second is essential to osteoconductive behavior [11].

Osteoinductivity

In order to induce osteogenesis, osteoprogenitor cells are recruited to the site of regeneration and stimulated to differentiate into new bones through biomolecular signaling [11]. So, a bone scaffold must be osteoconductive and capable of inducing new bone formation. Furthermore, an ideal scaffold should form blood vessels in or

around the implant within few weeks from implantation to support nutrient and oxygen supply and to encourage waste transport [12].

1.4.3 Materials for BTE

In general, biomaterials are used to interface with biological systems in order to treat, increase or replace body tissues, organs or functions. The main difference between biological materials and other types of materials is their ability to remain in the biological environment without damaging it or being damaged themselves during the biological process [18].

Bone scaffolds are usually made of porous and degradable biomaterials that provide mechanical support in the repairing and retrieving of damaged or diseased bone. Naturally derived materials, ceramics, polymers and composites can be used as biomaterials.

1.4.3.1 Grafts

A commonly used biomaterial for bone regeneration is osseous tissue extracted from the same person (*autograft*). Autograft is considered a "golden standard" because it is osteogenic, osteoconductive and osteo-integrated. This material is normally taken from a location that is not subjected to mechanical loads and contain cells and growth factors that support the bone regeneration process. Since it is a material which is from the body of the patient, there is a less risk of rejection or disease transmission. Some of the disadvantages of autografts are the need for additional surgery, possible infections related to the tissue collecting, bone cancer, pain and, mostly, limited availability [18].

It is possible to have *allografts* when the bone tissue is from individuals of the same species or *xenografts* when tissue is from an individual of a different species. Allografts are ready-to-use and easy to handle, but require treatments, such as freezing drying, irradiation and acid washing to avoid receptor rejection and remove potential infections from implanted tissue. Xenografts usually produced by cows and corals may be osteoinductive and osteoconductive, low-cost and high-available, but they have the disadvantages of immunity and the risk of transmission of animal diseases [18].

1.4.3.2 Polymers

Polymers provide greater control over the physiological and chemical properties of scaffolds, including pore size, solubility, biocompatibility, enzyme reactions and allergic reactions. They also exhibit good mechanical properties, are biocompatible, biodegradable, and can be easily shaped. In bone tissue engineering the most common polymeric materials are: poly(lactic-acid) (PLA), poly(glycolic-acid) (PGA), poly(caprolactone) (PCL), poly (methyl methacrylate), poly(e-caprolactone), polyethylene, polypropylene [13].

Even if they have a good compressive strength and it is easy to control the degradation time, they may lose strength due to the rapid degradation in vivo and release acid components that can cause adverse response from the body. It is also possible to obtain scaffolds made of natural polymeric materials, such as proteins (collagen, gelatine, fibrinogen, elastin), polysaccharides (cellulose, dextran, glycosaminoglycans) and polynucleotides (DNA, RNA). Natural polymers have demonstrated great biocompatibility and controlled biodegradation, but there are concerns with their low mechanical properties as bone structures. Biopolymers may not provide sufficient architectural support and protection to osteogenic cells. In addition, impure substances in natural biopolymers can lead to immune reactions and pathogen transmission [13].

1.4.3.3 Composites

Recently, there has been a suggestion to combine different materials create composite with the advantages of all the used materials (metallic, ceramic, polymeric materials). This strategy can help to obtain a scaffold whose degradation could be controlled and properties improved. Polymeric/ceramic materials could be considered a promising solution for bone tissue engineering since they can promote both bone mineralization and cell differentiation [13].

Composites of natural ceramics, such as calcium phosphate (CP), hydroxyapatite (HA), and tricalcium phosphate (TCP), combined with Poly (L-lactic acid) (PLLA), collagen, gelatine, and chitosan could be used as scaffolds for BTE. To mimic bone properties, reinforcements of high-density polyethylene (HDPE) and Poly (l-lactide-co-glycolid acid) (PLGA) can be used with HA. Creating a coating of calcium phosphate on metals, glasses, inorganic ceramics and organic polymers (such as PLGA, PS, PP, and silicone) could enhance the biocompatibility and the bioreactivity of the scaffold [13].

1.4.3.4 Metals

Different materials could be used for bone scaffold, such as Iron (Fe), Magnesium (Mg), Titanium (Ti), and alloys like Fe-Mg, Mg-Ca. Bio-resorption capacity, high biodegradability, appropriate mechanical properties, non-inflammatory reactions, and support for the activation of bone cells are considered to be magnesium properties. Its elongation (from 3% to 21.8%), tensile strength (from 86.8 to 280 MPa) and elastic modulus (41 – 45 GPa) are similar to those of natural bone. However, the corrosion can cause a reduction of magnesium resistance. Porous titanium can be used to create scaffolds as a bone replacement material for its good biocompatibility but it could inhibit cell proliferation and reduce bone formation [13]. Titanium alloys are commonly used as joint replacements and fracture fixation implants because of their biocompatibility, corrosion-resistance and robustness [16]. Despite their good mechanical properties, such as high compressive strength, fatigue resistance, light weight and a good biocompatibility, metal implants present a minimum osteointegration with the surrounding bone due to the difference in stiffness with natural bone [10]. They could also prevent bone formation or stimulate bone loss and release toxic ions due to corrosion, which can cause an inflammatory response. Metals are more used for permanent implants than scaffolds since they are non-biodegradable [13].

1.5 State-of-the-art: bio-ceramic scaffold for BTE

Bio-ceramic is relative to a class of materials that can be used inside the human body and which have specific properties like biocompatibility, good physical and chemical stability, good mechanical features, anti-thrombus and anti-bacterial effect, and osteogenic ability. Many ceramic materials have high rigidity and biological activity that can serve as a temporary framework, providing an appropriate environment for cell adhesion and growth aiding in the restoration of bone tissue [15]. There are two different categories of bio-ceramic materials: bioactive and bioinert. Bioactive scaffold has the ability to directly bond with the host bone tissue, which is not the case for inert scaffolds. [14] Bioinert ceramics have high mechanical strength, good biocompatibility and chemical stability, while bioactive ceramics are biodegradable and osteoconductive [15].

1.5.1 Most used bioactive ceramic materials

1.5.1.1 HAp and TCP

Hydroxyapatite (HAp), Tricalcium phosphate (TCP) and their composites are the most commonly used bio-ceramics in BTE due to their ability to create porous, biodegradable, biocompatible osteoconductive scaffolds [10].

HAp (Ca_{10} $(PO4)_6$ $(OH)_2$) is the primary component of the bone matrix. It has good bioactivity, biocompatibility, non-toxicity, non-inflammatory properties, encourages bone growth, regeneration and osteointegration. However, it has a low mechanical strength and it is also brittle, with a slow rate degradation in vivo [16]. Hydroxyapatite (HA) can be combined with different materials like ZrO_2, carbon fibers and Al_2O_3 to improve the mechanical characteristics and the capability of HA to induce bone tissue regeneration. However, these materials are bioinert, an aspect that could reduce the bioactivity of HA significantly. In addition, there is the possibility to combine HA with natural polymers to obtain composite scaffolds with a good degradation rate. Polylactide-co-glycolide acid (PLGA) is one of the most widely used polymeric biomaterials, which possesses favorable biodegradability and generally good biocompatibility [21].

β-TCP has been found to have potential for both bone and cartilage regeneration [10]. Several studies have demonstrated the osteoinductive capability of this material, and also its ability to promote cell differentiation by creating cells-ECM interactions [21]. Moreover, it is always combined with alginate to create a gelatinous scaffold that can induce good mesenchymal stem cell (MSC) osteogenic differentiation [10]. Therefore, calcium phosphate is not widely used due to its not so good mechanical properties. For this reason, it is merely employed for filling bone defects or for covering orthopedic implants [21]. It is also possible to prepare a BCP scaffold made of 80 ±3% HA and 20 ± 3% β-TCP with an interconnected porosity of 70% that is able to support new bone formation [12].

1.5.1.2 Calcium sulfate

Calcium sulfate ($CaSO_4$) is an inorganic material with two hydrates: $CaSO_4 \cdot 0.5H_2O$ and $CaSO_4 \cdot 2H_2O$, which are obtained by different dehydration methods. The dense type α and porous type β are the most common forms for medical applications, including

medical gypsum, medical cement and ceramic particles. Calcium sulfate can combine with recombinant human bone morphogenetic protein (rhBMP)-2 or platelet-rich plasma to promote bone defect repair [14]. It was demonstrated its ability to accelerate bone regeneration process due to its piezoelectric behavior [17].

1.5.1.3 Bioinert ceramics: Alumina and Zirconia

α-Aluminum oxide (Al_2O_3) is a crystal that exhibits a strong bond force, high melting point (2050 °C), hardness, good chemical corrosion resistance and elastic modulus. In medical applications, alumina is mostly used for artificial joints or teeth.

It is possible to find three crystal forms of pure zirconia under normal atmospheric pressure: monoclinic, tetragonal and cubic which exist in different temperature ranges and transform into each other at certain temperatures. Of the three forms, tetragonal zirconia is the most used for medical application in artificial joints, dental crowns or all-ceramic teeth [14].

The advantages of using bioinert ceramic materials are related to their wear resistance, high strength and hardness, good crystal and chemical stability, hydrophilicity, and corrosion resistance. They are also considered biologically inert and able to mediate adhesion and stimulate osteogenic differentiation of human mesenchymal stem cells [14].

1.5.2 Bio-glasses

Bio-glass materials (BGs) are used for different biomedical applications, such as implants in non-load situations, fillers and scaffolds. The identify property of the Bioglass® is the presence of silica (SiO_2), in which every silica atom is connected with 4 oxygen atoms, creating a tetrahedral 3D network. The best composition is the one that leads to the so-called 45S5 bio-glass, characterized by 45% of SiO_2, 24.5% of Na_2O, 24.5% of CaO and 6% P_2O_5 (wt %), in which the presence of Na_2O and CaO create a bioactive surface with the biological environment. It is used for BTE due to its ability to allow stem cells differentiation into an osteoblastic phenotype, to its both osteo-conductive and osteo-productive effects. They also present interconnected porous which is similar to the trabecular bone and enable cell movement within the material [25]. But many studies have demonstrated that its poor mechanical properties are strictly related

to the porosity: high level of porosity could enounce the bone formation on BGs, it is also results in their low density [22].

An important feature of these materials is related to the possibility to create strong connections with the surrounding tissues and to the opportunity to modify their composition; this aspect allows to obtain specific properties, which makes these materials suitable for different tissues applications [23]. Clinical applications of these materials include orthopedic and maxillofacial surgery, in the treatment of chronic osteomyelitis [25].

These materials are considered bioactive since they can degrade in the body environment, promoting bone formation due released calcium and silica ions [25], stimulating angiogenesis and inducing the creation of an HA layer, similar in composition and structure to that of natural bones, on the implant surface [22]. Strictly related to the material composition is the formation rate of HCA and also the bioactive potential, which decreases as the silica content increases over 60 w/t %. The formation of HCA includes different steps [23].

The first step is related to an ionic exchange between Ca^{2+} and Na^{+} ions in the material and H^{+} and H_3O^{+} ions coming from the surrounding environment. There is also the formation of Si-OH and a silica layer on the surface of the material with the release of alkaline and $(PO_4)^{3-}$ ions, with causes an increase of pH in surrounding fluids. The increase in pH or OH- concentration, causes the Si-O-Si bond of the glass network to be attacked, resulting in the dissolution of silica into $Si(OH)_4$ and Si-OH on the glass surface. The silica ions released is demonstrated to have an impact on bone formation around the glass surface. There is the creation of a silica layer poor in Na^{+} and Ca^{2+} ions from the previous released Si-OH groups, whose thickness varies between 1 and 2 μm and characterized by a micro-porosity [23].

Ca and $(PO_4)^{3-}$ ions migrate from both the surface of the glass and body fluid solution, while on the surface of the glass there's the formation of a layer composed of amorphous calcium phosphate (ACP) Hydroxyl and carbonate groups are incorporated from the solution as the dissolution continues. Crystallization of the amorphous layer into hydroxy-carbonate-apatite then occurs. It is similar to natural bone in terms of composition and structure leading to the direct anchoring of the implant into the tissue. The connectivity of the layer depends on the modifying cation (Ca, Na, Al, Ti, Ta) which can be incorporated in the solution formula and could slow down or accelerate the dissolution rate [23].

1.5.3 Bio-glass scaffolds manufacturing

The principal methods used to fabricate bio-glass scaffolds are sol-gel, solid freeform fabrication, freeze casting.

1.5.3.1 Sol-gel

Sol-gel products are nano-porous with a bioactive level and degradation rate higher than other bio-glasses. The *sol* is a stable colloidal suspension of nanoparticles (amorphous or crystalline) in a liquid, while the *gel* is a continuous porous network which surrounds and supports the liquid phase. In most cases, gel formation allows the formation of covalent bonds between the particles in the sol, and the structure of the network depends on the nature of the particles. In order to stabilize the sol, repulsive forces between the particles are required, which must be overcome successively to allow the gelling process. This is possible through, for example, the steric encumbrance of an organic layer or for the presence of electrostatic repulsion [23].

This method is typically used due to the possibility of obtaining different products by modifying the process parameters in different ways, and it is characterized by 5 steps:

1. Mixing of reagents at 25°C to induce the formation of covalent bonds. There is also a phase of stirring the solutions at mild conditions to obtain a homogenous mixture;

2. Gelation: in this phase, there is an increase in the viscosity of the solution due to formation of a 3D network between the molecules;

3. Aging: thermal treatments are conducted at 60°C. At the end of these, the gel has less porosity and better mechanical strength;

4. Drying: in this step, thermal treatments are carried out at 120°C < T < 140°C in order to eliminate the liquid phase of the solution from the pores. The reduced porosity and the improved mechanical resistant are both relevant to avoid cracking during this phase;

5. The final step is the thermal stabilization, conducted on the dried gel at 700°C.

Typical of this process is the mesoporous structure, with the pore size of 10 - 30nm, an aspect that promotes HA formation and the interaction with body fluids.

Advantages of using bio-glasses produced by the sol–gel method are several. It is possible to functionalize the glass with biomolecules during the formation of the

scaffold without compromising their physico-chemical properties. Furthermore, considering the composition, it is possible to simplify the glass formulation, by avoiding the addition of high amounts of Na_2O to lower the melting temperature and facilitate glass processing. In addiction it is easier to dope sol–gel glasses with trace elements, compared other glasses, which allows for the preservation of the glass bioactivity while promoting special therapeutic functions related to ion releasing (e.g., antibacterial properties, angiogenesis) [23].

1.5.3.2 Solid freeform fabrication (SFF)

It is a rapid prototyping technique that can be used to create object layer-by-layer following a predesigned computer-aided design (CAD) model. In this way, it is possible to obtain a controlled and optimized architecture for the scaffold to accelerate the bone-regeneration process or to guide bone formation inside and around the implant. Several SFF techniques have been used for scaffold fabrication, including three-dimensional printing (3D printing), ink-jet printing, stereolithography (SL), selective laser sintering (SLS).

1.5.3.3 Thermal bonding

This methos includes freezing the solution containing colloidal particles in a nano-porous mold, followed by a sublimation of the solvent under cold temperature. After a drying phase, the scaffolds are sintered to remove impurities from the macropores, which improves mechanical strength. Due to the directional freezing of the suspension, it is possible to obtain a scaffold with oriented microstructure, an aspect that allows to have a higher strength in that direction compared to the other directions [24].

This technique is used to prepare 45S5 scaffolds, but it has been shown that the pore dimensions are too small to support tissue ingrowth. For this reason, the addition of an organic solvent, like 1,4-dioxane, to the aqueous solvent results in an increase in pore diameters, from 10 - 40μm to 100 - 150 μm. In this way, these oriented scaffolds could support cells proliferation and differentiation, as well as their infiltration [24].

1.5.4 Bio-glass mechanical properties

As mentioned earlier for the other materials, artificial material should be able to mimic the mechanical properties and structure of the natural tissue. However, it is important to say that the main problem related to these group of materials is the poor workability and the not good mechanical strength [24]. There is a risk of cracks forming during the implantation process or in the post-operative phase, which makes these bio-glasses unsuitable to be used in under-loading conditions [23].

It has already reported that porosity in these materials results in low mechanical properties: as the level of porosity increases from 30% to 95%, the compressive strengths span almost three orders of magnitude, ranging from 0.2 to 150 MPa as reported in Figure 1.8.

Material Property	Trabecular Bone	Cortical Bone	45S5 Bioglass
Compressive strength (MPa)	0.1–16	130–200	500
Tensile strength (MPa)	n.a.	50–151	42
Compressive elastic modulus (GPa)	0.12–1.1	11.5–17	n.a.
Young's modulus (GPa)	0.05–0.5	7–30	35
Fracture toughness (MPa·$m^{1/2}$)	n.a.	2–12	0.7–1.1

Figure 1.8. Comparison between mechanical properties of cortical and trabecular bone to the mechanical properties of 45S5 Bio-glass [23].

However, it has been shown that porous scaffolds can be manufactured with a compressive strength comparable to the values associated with human cortical and trabecular bones. This aspect may be in contrast to the fact that they are not suitable to be used for repairing defects in under-loading body districts [24].

The architecture also affects the strength of the scaffolds. Scaffolds with oriented pores have higher compressive strength in the orientation direction that in other directions. Studies have demonstrated that the compressive strength along pore orientation is 2-3 times higher than the value of the same strength perpendicularly to the pore orientation direction. For this reason, controlling the glass composition and the architecture could lead to obtain a scaffold with both proper strength and porosity.

The fracture toughness of this class of materials is very low (0.5 – 1 MPa·$m^{1/2}$), and they result to be sensitive to the presence of small cracks, which could cause their

failure when loaded over their compressive strength. As a results, these materials are considered brittle [24].
The incorporation of biodegradable polymers, creating BG composites, could improve properties such as degradation rate, which should be controlled, elastic modulus, strength [25].

1.6 Aim of the thesis

As previously discussed, in bone tissue engineering (BTE) bio-ceramics can be used to create the scaffold, since they have mechanical properties which are similar to those of natural bone and they can recreate the microstructure of bone tissue while being shaped with a good porosity using 3D bioprinting. This work utilizes bio-glass 70S30C with two different compositions to create scaffolds using stereolithography 3D bio-printing. This composition was chosen due to the capability of this material to release Ca^{2+} and $(SiO)^{4-}$ ions which would promote the formation of hydroxyapatite (HA), a component of natural bone, due to the interaction with the biological environment. The obtained HA has a similar composition to that of natural bone, a fundamental feature to promote mineralization of the scaffold after implantation. The aim of this thesis is to demonstrate both the biocompatibility of the bio-glass scaffold with different cell lines and its photothermal effect when exposed to an IR source light. Specifically, validating the photothermal property involves testing the material's ability to increase its temperature when irradiated with IR waves. It is then important to verify whether the increase in scaffold temperature could lead to the death of cancer cells cultured inside it.

Chapter 2

Materials and Methods

2.1 Selection of the scaffold biomaterial

One possible alternative to the 45S5 bio-glass is the 70S30C bio-glass, which consists of 70 mol% SiO_2 and 30 mol% CaO. This composition is chosen for its ability to promote cells adhesion and proliferation due to its porosity. Using a 3D printing technique, it is possible to fabricate scaffolds with this composition that have macropores with a diameter of 200 – 600 μm, which are mutually interconnected. The used technique for the solution preparation is similar to the sol-gel technique, that promote the fabrication of a 3D interrelated porous solid network [26].

2.1.1 Scaffold solution preparation

These bio-glass scaffolds are produced from a polymeric preceramic solution using a Masked Stereolithography Apparatus (MSLA) bio-printing process. In this technique, thin layers of photosensitive resin are first inserted into the bottom of the vat made of fluorinated ethylene propylene (FEP). UV light passing through an LCD screen below the vat is used to harden the resin. The light from an array of LEDs passes only through the white pixels of the display, which in turn hardens the photosensitive material and defines a projection area for each printed layer.

The precursor solution for the 70S30C bio-glass consists of two phases: an oil and a water one. The oil phase is formed by melting a silicon resin powder, the H44 (poly-methyl-phenyl-silsesquioxane, Wacker-Chemie GmbH, Munich, Germany) in 15 gr of FunToDo resin (an acrylic and photosensitive resin consisting of acrylate monomers and glycol diacrylate monomers mixed with a phosphine oxide-based photo initiator, SB, from Fun To Do, Alkmaar, The Netherlands). The solution is left at room temperature for one day to homogenize.

For the water phase, 85 gr of FunToDo resin are mixed with 5 gr of Span 80 (Sorbitan Monooleate, Tokyo Chemical Industry co., Ltd., Tokyo, Japan), a surfactant that facilitates the blending of the aqueous and oil phase. Then, 5 gr of hydrophobic silica (FS. Aerosil R106 Fumed Silica Cyclotetrasiloxane, Octamethyl-, $C_8H_{24}O_4Si_4$, Evonik Industries AG, Hanau, Germany) are added. The solution is manually mixed, and then subjected to point ultrasonic treatment (Sonopuls, Bandelin, Berlin, Germany) for several cycles of 15 minutes each at increasing power levels, starting from 50% and up to 70%. Calcium nitrate tetrahydrate ($Ca(NO_3)_2 \cdot 4H_2O$, Scharlau, Irstanbul, Tukey) is added and melted using point ultrasonic for 5 cycles of 15 minutes each at a power of 90% to guarantee the complete dissolution of the salts.

The oil and water phases are then manually mixed, with the quantities of the components shown in Table 2.1. The silica precursors are H44 and hydrophobic silica which, after the treatment in N_2 at 700°C, allow for a silica oxide percentage of 70%. The calcium oxide precursor is calcium nitrate tetrahydrate, from which a 30% calcium oxide percentage is derived.

The aim of this process is to obtain the 70S30C bio-glass using a polymeric pre-ceramic, hydrophobic silica, instead of sol-gel precursors. To demonstrate this, another scaffold composition was prepared using the same technique but without adding hydrophobic silica. Instead, a higher percentage of H44 was included to obtain a silica percentage of 70% after heat treatment. The composition is shown in Table 2.2.

Table 2.1. Composition of the 70S30C solution with the adding of FS.

Component	Quantity (gr)
Acrilic resin	85
Silres h44	30.55
Span 80	5
Hydrofobic silica	5
Calcium nitrate tetrahydrate	28.05

Table 2.2. Composition of the 70S30C solution without the adding of FS.

Component	Quantity (gr)
Acrilic resin	65
Silres h44	34.96
Span 80	4
Hydrofobic silica	0
Calcium nitrate tetrahydrate	22.44

2.1.2 Heat treatment (N_2)

H44 and FS (if present) give silica and gas as products. H44 also produces a significant amount of separated amorphous carbon, called pyrolytic carbon, according to the following reaction [39]:

$$Si_3O_{4.6}C_{8.45} \Leftrightarrow 2.3\ SiO_2 + 0.7SiC + 7.75C$$

Calcium nitrate, instead, gives calcium oxide as well as a gas phase. The final product is a bio-glass scaffold consisting of silicon oxide and calcium oxide combined with a distinct phase of pyrolytic carbon. The process is shown in the Figure 2.1.

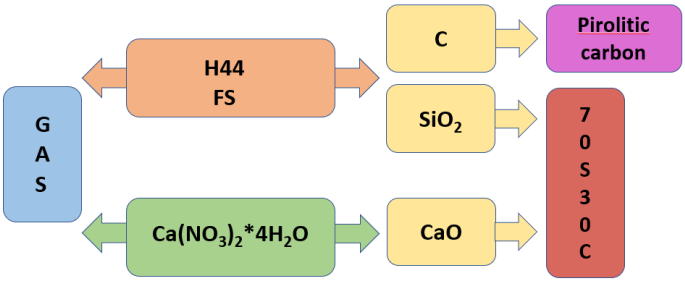

Figure 2.1. Heat treatment scheme. Adapted from [27].

Pyrolytic carbon is a biocompatible and non-thrombogenic material, and it has also specific photothermal properties, related to the possibility to heat the scaffold if it is treated with an IR lamp. This property is called *photothermal effect* and it could be exploited to treat cancer diseases with photothermal and photodynamic therapy (PTT or PDT).

2.1.3 Heat treatment (air)

During the heat treatment with air, it is possible to identify different events which characterize the process. The samples are heated up from room temperature (25°C) to around 200°C, mainly affecting the calcium nitrate tetrahydrate, $Ca(NO_3)_2 \cdot 4H_2O$ and the silicone, both present in the scaffolds' compositions (with and without Fumed Silica (FS)). During this process the Ca salt in $Ca(NO_3)_2 \cdot 4H_2O$ will melt at a temperature of 40°C and as the heating process continues, between 130°C and 160°C, it will also start to lose the water phase (dehydration) in an endothermic reaction. As the temperature further increases, a second endothermic reaction involving H44 (poly-methyl-phenyl-silsesquioxane), the silicon phase of the solution, takes place. Specifically, at 200°C the H44 silicon will be crosslinked. Both the endothermic reactions are characterized by a water release as a reaction product.

When the temperature increases over the 350°C, there will be a heat release related to the decomposition of the acrylic resin which is hardened at this temperature. The final effects are, for this reason, correlated with both the $Ca(NO_3)_2 \cdot 4H_2O$ and the silicone H44.

In order to make the H44 polymeric-ceramic transformation to occur, it is necessary to reach a temperature between 300°C to 550°C; in this range the $Ca(NO_3)_2$ would be decomposed into CaO, as a sign of the interaction of the salt with the matrix [44].

2.1.4 Printing process

The printing process of 70S30C scaffolds requires the definition of a geometric model: the chosen model is a gyroid with 90% of porosity. The model consists in 6 gyroid scaffolds, each with a side of 10mm, in which curved membranes form helicoidal spaces, as shown in Figure 2.2 [27].

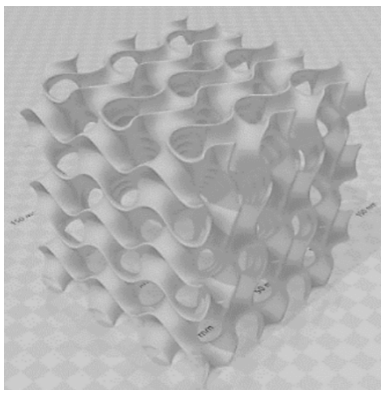

Figure 2.2. Gyroid model with 90% of porosity. Adapted from [27].

The formulation (2.1) considered for the scaffold modelling is:

$$\frac{2\pi x}{cs} * cos\left(\frac{2\pi y}{cs}\right) + sin\left(\frac{2\pi y}{cs}\right) * cos\left(\frac{2\pi z}{cs}\right) + sin\left(\frac{2\pi z}{cs}\right) * cos\left(\frac{2\pi x}{cs}\right) = 0 \quad (2.1)$$

where *cs* is equal to the cell size [28].

The used bio-printer (Figure 2.3) for masked stereolithography (Original Prusa SL-1S, Prusa Research a.s., Prague, Czech Republic) works with a wavelength of 405nm.

Figure 2.3. Original Prusa Research SL-1S used to print the scaffolds.

The exposure time for the first layer is set at 35 sec, while it is 17 sec for the subsequent layers. After printing, the samples are cleaned with air pressure and isopropanol and treated with UV to further harder them. The samples obtained are shown in Figure 2.4.

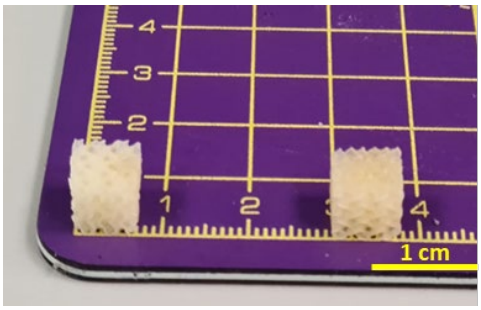

Figure 2.4. 70S30C scaffold with (on the right) and without FS (on the left) before the heat treatment.

In the end, the samples are subjected to a heat treatment in two steps: 0.3°C/min up to 500°C for 5 h, then 1°C/min up to 700°C for 1 h [27]. After the heat treatment the resulted samples have dimensions of ~4,5 mm x 4,5 mm x 4,5 mm as shown in Figure 2.5, values obtained manually.

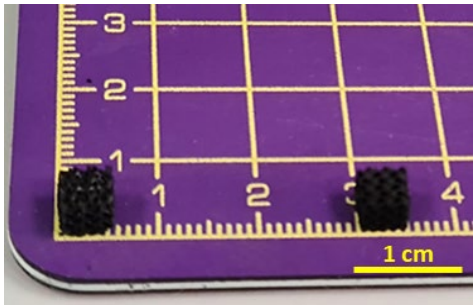

Figure 2.5. 70S30C scaffold with (on the right) and without FS (on the left) after the heat treatment.

The samples lose more than 50 percent of their volume during nitrogen heat treatment because the resin H44 turns to SiO_2 and C, the FunToDO resin disappears, the $Ca(NO_3)_2$*$4H_2O$ turns into CaO and what remains is a glass of silica and calcium oxide with a pyrolytic carbon phase.

2.1.5 Scaffold characterization

In this section all the test performed to describe the mechanical and chemical properties of the scaffold produced are described.

2.1.5.1 Cellular solids

Bio-glasses can be considered cellular materials usually characterized by networks of membranes or trabeculae. These materials consist of a repetition of monomeric units, called *cell,* and their properties are related to different aspects:

- Properties of the solid material;
- Cellular lines and shapes;
- Relative density: this is the ratio between the density of the foam (ρ) and the density of the solid material (ρ_s), defined as $\boldsymbol{\rho_{rel} = \rho/\rho s}$ or $\boldsymbol{\rho_{rel} = 1 - P}$, where P is the porosity percentage of the material. It is also defined as the volume fraction of solid. Different cellular materials have low relative densities (~10 – 20%), which means that they can be deformed up to large strains (~70 – 80%) before densification occurs. Densification is the collapse of the cells [27, 39];
- Porosity: to be defined cellular, a material must have a porosity >70% [27].

These materials exhibit a similar behavior in compression and tension, at least when the strain is not too high. As the strain increases, cells become more oriented with the loading direction, leading to an increase in the stiffness of the material until failure [39]. For cellular materials, it is possible to define also geometrical density, apparent density and true density. Geometrical density is calculated by considering the entire volume of the solid without excluding porosities and is defined as:

$$\rho_{geom} = \frac{m}{V} \tag{2.2}$$

where m and V are equal to the mass and the volume of the solid material, respectively.

Bulk density also considers the open porosity and is defined as:

$$\rho_{app} = \frac{m}{V - VOP} \tag{2.3}$$

True density is defined by considering the open (VOP) and closed (VCP) porosities present within the cellular material and is defined as:

$$\rho_{true} = \frac{m}{V - VOP - VCP} \tag{2.4}$$

Depending on the cell structure, these materials are *bending-dominated* or *stretch-dominated* [27].

Bending-dominated

In a bending-dominated structure, the solid is mostly deformed in bending [40]. According to the Gibson Ashby model (Figure 2.6), the connectivity level is low and the thickness of the membranes is lower than the cell dimension. This allows for the definition of relative density based on a proportional relationship between the membranes thickness and the width of the cell:

$$\rho_{rel}=C_1\left(\frac{t}{L}\right)^2 \tag{2.5}$$

where t is the membranes thickness and L is the width of the cell.

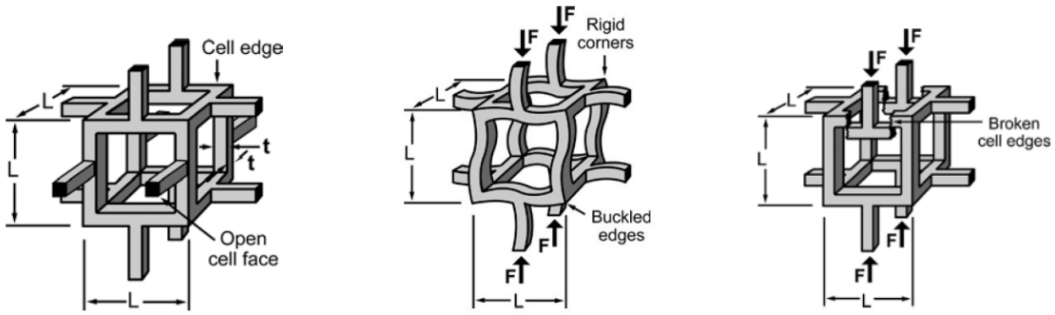

Figure 2.6. Gibson Ashby model of a cell. Adapted from [27].

The relative density allows for the definition of two relationships: one between the Young' modulus of the solid material and the foam, and another between the compression stress and the bending stress:

$$\frac{E}{Es} \sim (\rho_{rel})^2 \tag{2.6}$$

$$\frac{\sigma cr}{\sigma fs} \sim 0.2(\rho_{rel})^2 \tag{2.7}$$

The mechanical behavior is linear elastic until failure after which the body continues to crack at a constant tension. Eventually the tension rises again when all the porosity is removed and the material is packed on itself [27].

Stretch-dominated

Stretch-dominated solids are typically loaded in tension, showing stiffnesses and strengths higher than bending-dominated materials [40]. The traversal borders of these structures are always subjected to traction and compression and never to bending and so

these materials guarantee a higher efficiency. Figure 2.7 shows an example of a micro-truss structure that can be considered stretch-dominated.

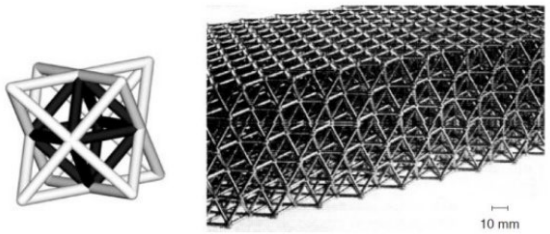

Figure 2.7. An example of micro-truss structure. Adapted from [27].

In this case the relationship between the Young' modulus of the solid that composes the foam and the relative density is as follows:

$$\frac{E}{Es} \sim 1\text{-}P \tag{2.8}$$

The relationship between compression and bending stress is [27]:

$$\frac{\sigma cr}{\sigma fs} \sim (\rho_{rel}) \tag{2.9}$$

2.1.5.2 pH tests

To evaluate the release rate of Ca^{2+} ions in different environments, three different pH tests were conducted using cell culture medium, Phosphate Buffered Saline (PBS) and ultrapure-MilliQ® water. Samples with FS, treated in air and N_2, and samples without FS, treated only in N_2, were tested. The pH was evaluated using a pH-meter for all the samples. The steps performed are as follows:

1. The samples were placed in a 12-well plate;
2. 3 ml of ultrapure-MilliQ®, PBS and medium were poured on different samples;
3. pH evaluation was done after 1, 5, 24, 48 and 72 hours for all the samples.

The samples were stored in an incubator at 37°C to replicate the biological conditions.

2.1.5.3 Porosity evaluation

The porosity was evaluated using a helium pycnometer (Ultrapyc 3000 Anton Paar, Graz, Austria) to measure the density values of different samples. It is necessary to

consider the average density and the geometric density. The geometric density includes the porosity, and for this reason, the real density needs to be measured, which does not include open and close porosity [27]. As a result, an average density value of 2.2 g/cm^3 is measured for both the scaffold containing and not containing FS. The geometric density of the scaffold containing FS is 0.2665 g/cm^3, from which a porosity of 80% is calculated. The geometric density of the scaffold not containing FS is 0.3382 g/cm^3 which results in a porosity of 74.50% [27].

2.2 Biological validation

To verify cell adhesion and proliferation on the 70S30C scaffold, a biological validation was conducted with different cell lines. Also, several protocols were performed in order to provide adequate outcomes.

2.2.1 Cell lines

Cancer (SK-N-AS and SaOs-2) as well as healthy (hMSCs and BJ) cells were seeded on the scaffold to perform the biological validation and check cells proliferation.

SK-N-AS: neuroblastoma cell line

Neuroblastomas are composed of small, primitive-appearing cells with dark nuclei, poor cytoplasm, and not defined cell borders. This cell line derives from bone marrow of child since this cancer frequently occurs at an early age [5].

SaOs-2: osteosarcoma cell line

Osteosarcomas cells could vary in size and shape, and are frequently characterized by large hyperchromatic nuclei [5]. This cell line usually comes from primary osteosarcomas and shares some fibroblastic features [29].

hMSCs: human mesenchymal stem cell

Mesenchymal stem cells (MSCs) are multipotent stem cells capable of differentiating, under appropriate culture conditions, into various cell types: for example, osteocytes, chondrocytes, adipocytes, myocytes, and tenocytes [30].

BJ: fibroblast cell line

Neonatal foreskin fibroblasts are specialized, innervated, cutaneous mucosal tissue that covers and protects the glans. Human foreskin cells have been demonstrated to be a source of innumerable cell types such as endothelial cells, keratinocytes, melanocytes, stem cells and fibroblasts [31].

2.2.2 Cellular protocols

Cells used to perform experiments were maintained in flasks with a surface of 75 cm^2 and placed in an incubator at 37°C, humidified at 5% of CO_2. Every two or three days the cell-type specific culture medium was changed to provide fresh nutrients and remove dead cells.

For SK-N-AS and SaOs-2 lines medium contains:

- A base medium called DMEM (Dulbecco's Modified Eagle Media provided by Thermofisher Scientific);
- Some additional elements added to the DMEM base with different v/v %: 10% v/v of Fetal Bovin Serum (FBS), 1% v/v of PenStrept (an antibiotic to prevent possible contaminations) and 1% v/v of MEM (a modified Basal Medium Eagle media containing higher concentrations of essential nutrients).

The solution for the medium for the hMSCs was composed by:

- 90% MesenCultTM MSC Basal Medium (Human) that is a standardized basal medium designed for the in vitro culture of human mesenchymal stem cells;
- 10% MesenCultTM MSC Stimulatory Supplement (Human).

For the BJ line medium is composed by:

- A base medium called EMEM (Minimal Essential Medium provided by Thermofisher Scientific);
- Some additional elements added to the EMEM base with different v/v %: 10% v/v of Fetal Bovin Serum (FBS), 1% v/v of PenStrept (an antibiotic to prevent possible contaminations).

When the cells reach approximately 80% confluence, they are split using a specific protocol which is described below.

2.2.2.1 Splitting protocol

First, the culture media and Trypsin/EDTA solution (Biochrom GmbH) were placed in a 37°C water bath (Bagnomaria Serie Pura, Julabo, Sacco srl) to warm them up. Then, the flask containing cells was removed from the incubator and placed under the biological hood. The splitting protocol consists in different steps:

1. The culture medium was removed from the flask by aspiration with a serological pipette and stored in a 15 mL Falcon tube;
2. A volume of 5-7 mL of PBS (Phosphate-Buffered Saline Solution: it is an isotonic solution containing different salts but without calcium and magnesium ions) stored at room temperature under the hood was used to remove any trace of culture media (that contains trypsin inhibitors) inside the flask. PBS is then discharged;
3. 3 mL of Trypsin 0.25% (a serine protease enzyme used to cleave proteins bonding cells to the dish) was added to the flask, which was placed in the incubator for 4 or 5 min, depending on the cell type: SK-N-AS require 4 min, while hMSC and BJ 5 min. Instead, SaOs-2 cells require 10 minutes in the incubator to allow the Trypsin to act;
4. The previously stored medium was introduced into the flask to inhibit the action of Trypsin. By gently pipetting, cells were aspirated from the bottom surface and placed in a 15 ml Falcon tube;
5. The Falcon tube was centrifuged at 1500 rpm for 5 min for SK-N-AS and BJ, at 300 rpm for 8 min for hMSCs and SaOs-2 cells, setting the soft deceleration to limit cellular damage. This induces the sedimentation of cells, which form a dense pellet at the bottom of the tube, while residues remain in the supernatant fluid. The liquid is discharged;
6. Cells were counted (more detail about this will be provide in the following paragraph) and an appropriate aliquot of cell suspension (usually a volume containing $1x10^6$ cells for SK-N-AS and SaOs-2 or a lower quantity of cells,

around $5x10^5$ for hMSCs and BJ) was added to a new 75 cm^2 flask, with 8-9 mL of fresh culture media to maintain the cell culture.

2.2.2.2 Cell counting

Cell counting procedure was performed to know the total number of cells suspended in a certain volume of liquid. This operation is fundamental since the cells must be seed on the scaffolds with a specific cell density.

It is possible to count the cells using a Bürker chamber, shown in Figure 2.8.

Figure 2.8. Bürker chamber.

It consists of a rectangular microscope slide with a rectangular indentation that creates a chamber, made of two 3 x 3 mm big squares, with a depth of 0.1 mm. Each of these is divided in 9 squares (1 mm side) each delineated by three lines and divided in 16 smaller squares (0.2 mm side) (Figure 2.9).

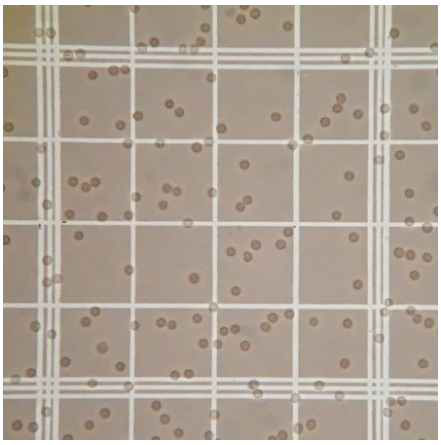

Figure 2.9. One of the 9 squares divided by three parallel lines; the small points visible inside the squares are cells.

The steps for cell count are as follows:

1. The cell pellet was suspended in fresh culture media and pipetted to avoid cells sedimentation and clustering;

2. 10 µL of cell suspension was collected with a micropipette and positioned on one side of the Bürker chamber to form a bubble. Then, 10µL of Trypan Blue (Invitrogen) was added to the cell suspension. Trypan blue is chosen because is a cell stain that colours in blue only dead cells to count only the living cells;
3. 10µL of cell suspension and Trypan blue were introduced between the chamber and the glass slide;
4. The chamber was observed at the microscope with a 10 X magnification. At least 3 principal squares are considered and the cells are counted.

To calculate the total number of cells the following equation 2.10 is considered:

$$N_{cells} = N_{average} \cdot d_1 \cdot d_2 \cdot K \cdot Vsosp \quad (2.10)$$

Where $N_{average}$ is the number of cells counted using the Bürker chamber [adim], d_1 is the dilution factor of cell suspension [adim], d_2 is the dilution factor for the use of Trypan Blue [adim], K is a constant related to the geometry of the Bürker chamber [μL^{-1}] and V_{sosp} is the total volume of cell suspension [µL] after the detachment process.

2.2.2.3 Scaffold cells seeding

Before seeding, the scaffolds were sterilized with 30 min of UV treatment, then washed two times with PBS, placing them on a stirrer, to allow the PBS to fill all pores of the scaffolds. Then scaffolds were placed in a 48-well plate, preconditioned with fresh culture medium, and incubated at 37°C for 1h. This preconditioning treatment with the culture medium was necessary to prepare the substrate for an adequate cell adhesion and growth. Then, a specific volume of cell suspension composed of medium and cells and calculated according to the number of cells available, were added onto the scaffolds, after removing the preconditioning medium. Cells were seeded at the optimized concentrations of $1x10^6$ for SK-N-AS and SaOs-2, and $5x10^5$ cells/µL for hMSCs and BJ. After a 15 min incubation at 37°C, each well was filled with 500 µL of fresh culture medium to promote cells surface attachment and growth. The scaffolds were further incubated for 24 hr and then the media was replaced every 24 hours for up to 21 days. The steps for the cells seeding were summarized in Figure 2.10.

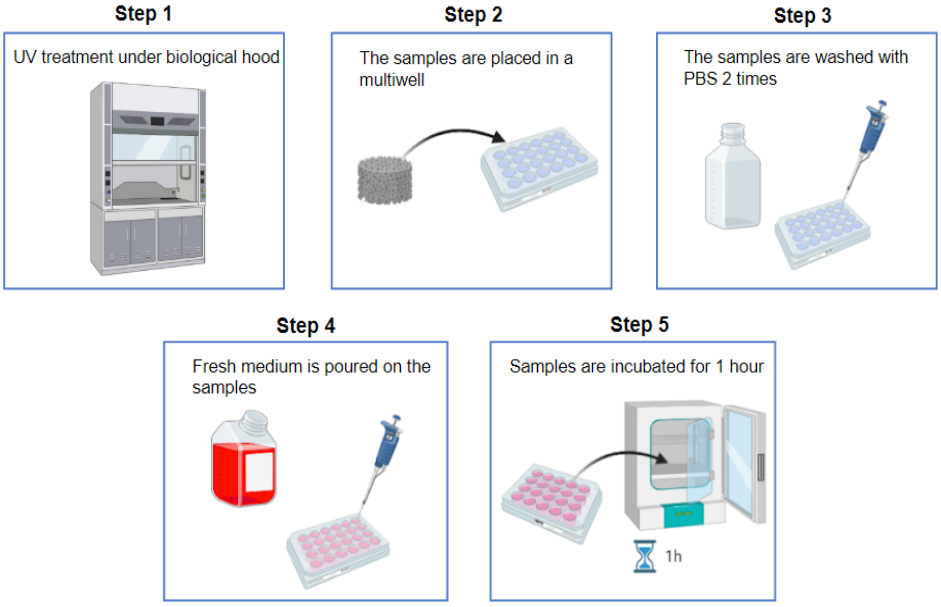

Figure 2.10. Scheme of the scaffold preconditioning protocol.

2.2.3 Live and Dead protocol

To evaluate cell viability inside the scaffold, a cell viability assay was performed on cells seeded over the scaffolds after different days from cells seeding. The Live&Dead assay consists in staining cells using fluorophores that have specific affinity to one substrate, so they mark one specific target selectively. The staining solution was prepared diluting three cell markers (reported in Figure 2.11) in PBS:

- Hoechst 33342: used in a volume ratio 1:500; it is a blue fluorescent dye which marks all cell nuclei. Its excitation wavelength is equal to 361 nm while the emission one is equal to 461 nm;
- Calcein-AM: used in volume ratio of 1:1000; it is a green fluorescent dye which marks the living cell cytoplasm. Its excitation wavelength is equal to 495 nm while the emission one is equal to 515 nm.
- Propidium: used in volume ratio of 1:250; it is a red fluorescent dye which marks dead cell nuclei. It is excited at 488 nm and emits at a maximum wavelength of 617 nm.

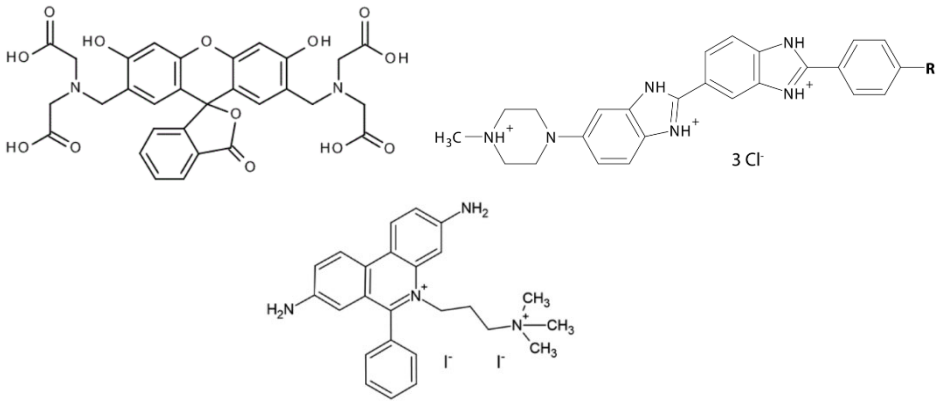

Figure 2.11. Chemical structures of Calcein-AM, Hoechst and Propidium.

At first, the medium was removed from the well and the samples were washed with PBS to remove every trace of Fetal Bovine Serum (FBS), which could interfere with Calcein and Hoechst's staining. Then the staining solution was prepared by mixing in PBS Calcein, Hoechst and Propidium, and poured on the samples. The well was placed in incubator at 37°C for 25-30 min.

The scaffolds were analyzed using a fluorescence microscope which has a fluorescence lamp able to excite the fluorescent dyes and to capture the emitted light through different filters (one for each stain, since they have different emission wavelengths). The steps followed are summarized in Figure 2.12.

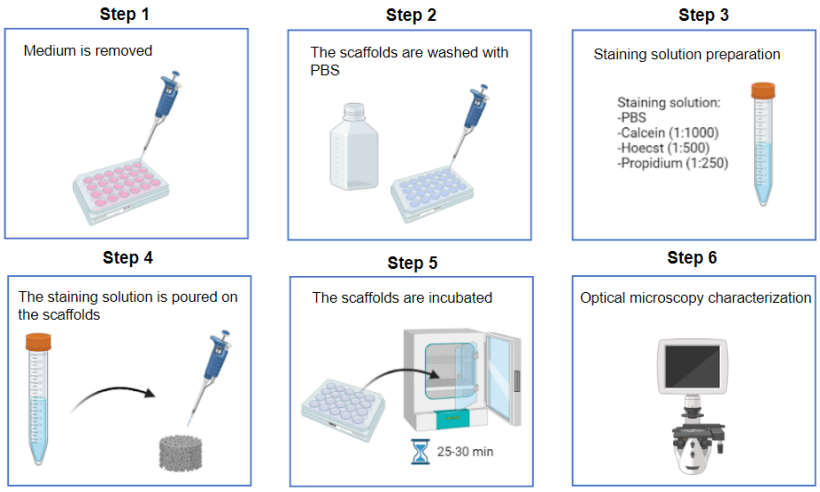

Figure 2.12. Live&Dead protocol steps.

After the staining, a cells count was performed using the ImageJ software. In this way it was possible to evaluate how many of the cells populating the scaffold at the time of staining, are alive and how many are dead. This is a qualitative analysis as the counted

images represent only small portions of the entire scaffold. For the counting, images were analyzed for the tumor cell lines at 10x magnification, which guarantees a good resolution and allows to have an appropriate vision of the cells' form and number. The counting was performed after 7 and 14 days from seeding to prove if the cells were able to proliferate over the scaffolds during days.

2.3 Immunofluorescence (IF staining)

Immunofluorescence (IF) is an immunochemical technique that allows detection and localization of a large variety of antigens in different types of tissues or cells. This method provides the combination of specific antibodies tagged with fluorophores. IF allows an excellent sensitivity and amplification of signal since it includes various microscopy techniques [32].

There are two main methods available for IF, and the choice between them depends on the scope of the experiment and the specific antibodies used: direct or indirect.

In the direct method, fluorophore label is conjugated directly to the primary antibody that will be reacting with the target epitope (Figure 2.13).

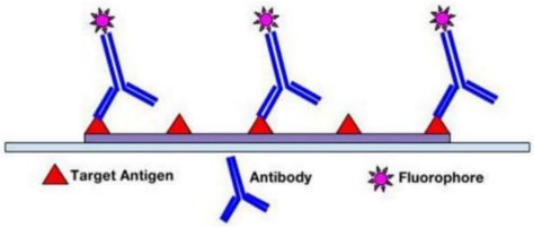

Figure 2.13. Direct immunofluorescence; adapted from [32].

On the other hand, the indirect method involves a two-step incubation process: 1) a primary antibody binds to the target epitope, 2) a fluorophore-tagged secondary antibody recognizes and binds to the primary antibody (Figure 2.14).

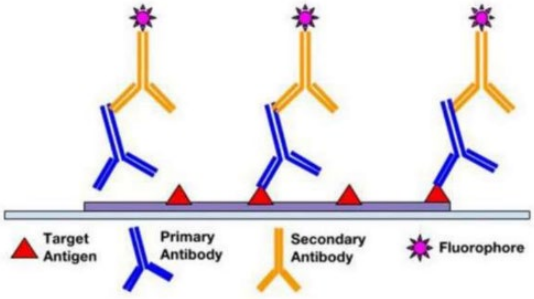

Figure 2.14. Indirect immunofluorescence; adapted from [32].

Even if the direct method is quicker, the indirect one is most commonly employed for the possibility to obtain a high sensitivity, signal amplification, and its ability to detect several targets in the same sample [33].

In choosing the proper antibodies, several criteria must be considered. To prevent the secondary antibody from cross-reacting with endogenous immunoglobulins in the tissue sample, the primary antibody should be derived from a different species than the one used in the sample and so the secondary antibody must be against the host species of the primary antibody [34].

Secondary antibodies are usually conjugated with fluorescent labels which emit upon photoexcitation. To achieve adequate signal amplification, researchers can use polyclonal or biotinylated secondary antibodies. Polyclonal secondary antibodies recognize multiple epitopes for each primary antibody, thereby increasing binding and signal levels [35]. In addition, multiple fluorochrome-protein (avidin or streptavidin) complexes can be bound to a single biotinylated secondary antibody to increase signal levels. Using a combination of all these methods could allow also a greater signal amplification [32].

Fixation is an essential preliminary step in IF staining in order to prevent autolysis and preserve cells morphology while maintaining the antigenicity. The fixation method is able to immobilize target antigens without disturbing cellular architecture. In this way, the antibodies can better access to the targeted cellular components. There is no universal fixative for every antigen, so the optimal fixation method may need to be determined empirically based on the given antigen and sample type. Commonly used fixatives include formaldehyde, glutaraldehyde, methanol and acetone [36]. Before applying antibodies to tissue samples in IF staining, it is important to perform a blocking protocol to prevent antibodies from binding to non-target epitopes. Blocking reagents should be chosen with no affinity for the target epitopes, high binding rates to non-target reactive sites, and stabilization of cellular morphology [32].

The best combination of blocking reagents, blocking duration, and antibody types should be optimized based on the specific experiment. In general, most blocking buffers fall into of the following categories:

- Protein solutions: concentrated protein buffers that bind all proteins present in the sample. As antibodies are forced to compete with the blocking protein for specific epitopes, non-specific binding can be reduced. Common examples include bovine serum albumin (BSA), non-fat dry milk, and gelatin.

- Normal serums: blocking reagents containing antibodies from the same species as that of the secondary antibody. This property is useful to block non-target reactive sites to which secondary antibodies would otherwise bind.
- Protein-free commercial buffers: these buffers are also widely available, with different compositions specific for various antibodies as well as increased shelf life [37].

2.3.1 Fixation and staining with Phalloidin and DAPI

The adopted procedure for immunofluorescence is the following:

1. After a minimum of 7 days from the cell seeding (§2.2.2) the scaffolds were washed with PBS for 1 time;
2. Under a chemical hood, a solution of PBS and 4% of Paraformaldehyde (PFA) was prepared, starting from a solution of 37% PFA, stored at room temperature. The solution was poured over the scaffolds;
3. After 25 minutes, the PFA solution was removed and the samples were washed with PBS for 3 times;
4. The multi-well dish containing the fixed samples was stored at 4°C until the immunofluorescence staining;
5. A solution containing 0.1% of Tryton X-100 was poured over the samples. Tryton X-100 is a non-ionic surfactant able to permeabilize the cell membrane to allow the entry of the antibody inside the cells. The solution is obtaining starting from a solution of 10% Tryton, stored at room temperature;
6. After 10 minutes, the samples were rinsed with PBS 1 time;
7. A solution containing Rhodamine Phalloidin at a concentration of 1:400 in PBS was prepared. Rhodamine Phalloidin is a fluorescent dye commonly used to visualize and quantify F-actin in tissue sections and cell cultures. When bound to F-actin, Rhodamine Phalloidin emits an orange-red fluorescence, allowing for easy detection of F-actin in cells and cell membrane components [38].

8. After 40 minutes a solution containing DAPI at a concentration of 1:1000 in PBS was prepared and poured over scaffold; DAPI (diamidino-2-phenylindole) is a blue fluorescent dye that fluoresces selectivity for DNA with high cell permeability that allows efficient staining of nuclei;
9. After 15 minutes the IF solution was discarged and the samples were rinsed with PBS for 1 time.
10. The samples were finally investigated using a confocal microscope which offers a better resolution and a higher signal-to-noise ratio compared to traditional fluorescence microscopes.

2.4 SEM protocol

The scanning electron microscopy (SEM) is a technique that exploits the interaction between electrons and the atoms that make up the specimen under examination. It allows for imaging at very high magnifications, surpassing the resolution limit of optical microscopy and even achieving resolutions at the atomic level. SEM can visualize the biological structure with high resolution, but an optimal view of the structure requires a sample preparation process. Since the samples contain seeded cells, it is priority to protect them and prevent their detachment from the scaffold during preparation. For this reason, SEM samples preparation requires:

1. Stabilization and preservation of the biological structures;
2. Dehydration of the samples;
3. Gold coating.

Biological samples are typically treated with protein and lipid cross-linking reagents, like glutaraldehyde (2.5% GA) and osmium tetroxide (OsO_4) respectively, dehydrated with an organic solvent, such as ethanol (EtOH) or acetone, and critical-point dried through carbon dioxide [41].

Step 1

It is necessary to preserve adherent cells that have been seeded on the scaffold. For this reason, they need to be fixed, a process that includes the following steps:

- Most of the medium was removed from the 48-cell well plate containing the samples, conserving a small quantity to prevent the samples from drying out;
- The samples were washed with 0.6 µL of PBS poured on each scaffold;
- A solution made of PBS and 2.5% GA was prepared under the hood and poured over the samples, making sure that the samples were completely covered;
- The fixing solution is left to act for 40 to 50 minutes at room temperature, without removing the cover of the well plate;
- The samples were washed 3 times, each time for 5 min with 0.6 µL of PB (0.1 M phosphate buffer pH 7.2). It was prepared by dissolving 35.5 g of sodium phosphate dibasic in 500 mL of H_2O.
- The samples were dehydrated using a graded ethanol series by subsequent exchanges of the following dilutions in distilled water, as follows:

  25% ethanol, 1× 5 min
  50% ethanol, 1× 5 min
  75% ethanol, 1× 5 min (samples were stored overnight at 4°C at this step)
  95% ethanol, 1× 5 min
  100% ethanol, 3 × 10 min [41].

Step 2

Conventional SEM requires the removal of water from the samples under consideration, even though biological specimens are composed mostly of water. Water removal was performed by critical-point drying (CPD). The steps to be carried out are as follows:

- Place the critical-point dryer specimen container in a solvent-resistant container, such as a PE specimen cup, and fill it with 100% dry ethanol to the top of the holder;
- Using fine-tipped forceps, place the samples in the slot of the CPD holder, being careful to avoid damaging them;
- Place the CPD container with the samples inside it;
- Insert the specimen holder into the chamber of the CPD instrument, filled with 100% ethanol as recommended by the manufacturer;

- The chamber should be precooled to approximately 10°C or lower per manufacturer's specification. This is controlled by adjusting the set points on the instrument to the desired temperature;
- When the chamber has reached 10°C, completely evacuate the ethanol and release the transition agent, which is mixed with CO_2 and less dense than ethanol with liquid CO_2 [41].

Step 3

After fixing and drying the samples, a thin layer of a conductive metal is coated onto the scaffolds to minimize damages and improve topographical contrast and imaging quality for SEM using secondary electron detection. The choice of metal depends on the application, with gold, gold/palladium and platinum alloys, or platinum (Au, Au/Pd, Au/Pt, and Pt, respectively) commonly used for low-resolution imaging, while iridium (Ir), tungsten (W), or carbon (C), are better choices for high-resolution imaging. Applying a minimal layer is crucial to avoid obscuring structural details. The coating steps are as follows:

- Place a double-sided adhesive tab on the aluminum SEM stub and remove the protective layer;
- Place the fixed and dried samples carefully on the stub using fine-forceps and being to avoid damaging the cells;
- After the placement of the scaffolds, the contact between the scaffold substrate and the aluminum stub can be improved by applying a thin layer of conductive paint around the samples. In order to have a complete dry, it is necessary a period of 4 hr or overnight in a desiccator;
- Place the dried aluminum stub with the samples in the sputter coater for the metal coating step;
- After making sure the correct target is in place, setting tilt and rotation conditions (e.g., usually ± 90 degrees and 360 degrees rotation according to desired result) are fixed;
- Open the valves to a specific emission to obtain the desired thickness;

- At this point, it is possible to turn off the power supply and releasing the vacuum;
- Remove the sample and store it in a desiccator until ready for examination.

To obtain adequate SEM imaging, it is necessary to balance the selection of appropriate SEM voltage, considering a good signal-to-noise ratio, depth of penetration and resolution. The working distance should be adjusted to ensure the cell is in focus while the surrounding "background" cells are slightly blurred. The selection of a good voltage can affect the ability to see small structural details, such as proteins [41].

2.5 IR treatment for photothermal therapy (PTT)

Photothermal therapy (PTT) has recently been applied in cancer treatment for the possibility to use a non-invasive technique, to provide localized treatment and yield good therapeutic effects. The most common laser used in PTT is near-infrared (NIR) light, which has less tissue absorption and scattering, resulting in a deeper penetration. It is characterized by a wavelength range of 750 – 1350 nm, known as the *biological window*. This range can be divided into the first near-infrared (750 – 1000 nm, NIR-I) window and the second near-infrared (1000 – 1350 nm, NIR-II) window. While most PTTs focus on the NIR-I region, its tissue penetration depth is limited. In contrast, the NIR-II region can provide deeper tissue penetration [42].

In general, the therapeutic effect of PTT is strictly dependent on the photothermal materials used. Their photothermal conversion efficiency, photothermal stability, and biocompatibility are essential elements. Photothermal materials, including inorganic, organic, and organic–inorganic composite materials, have been investigated in terms of the mechanism, preparation, and cancer therapy applications. Inorganic materials have advantages such as convenient preparation, strong NIR absorption, modifiability, and photostability. However, their poor biodegradability can lead to potential cytotoxicity, which reduces their clinical application.

Organic materials exhibit superior biocompatibility and biodegradability compared to inorganic materials, but their complicated synthesis procedures and poor photostability limit their potential application [42].

As a result, composites of organic and inorganic materials have been developed to leverage their individual strength. These composites can be formed by chemical conjugation or through physical affinity. Thanks to this combination, problems such as low photothermal conversion efficiency or poor biocompatibility of certain photothermal materials can be overcome. In addition, better therapeutic effect, drug delivery, and high photothermal conversion efficiency can be achieved.

In general, NIR photothermal materials can penetrate deeper into living tissue with fewer biological interferences and better therapeutic effects simultaneously. Moreover, biological cells and tissues have little absorption in the NIR wavelength region, making them less susceptible to damage from low-intensity NIR laser radiation. Due to these virtues, NIR photothermal materials have shown applications in cancer therapeutics, such as in PTT [42].

When exposed to an IR laser or light, photothermal materials transform the laser energy into heat to induce the death of cancer cells and it is possible to identify three processes:

1. Absorption
2. Scattering
3. Reflection

Among these processes, only the absorbed light can be used for heat generation. So, if a photothermal material absorbs more available light, the heat generated by the photothermal conversion process will increase proportionally. For this reason, the performance of PTT not only depends on the photothermal conversion efficiency but also on the light absorption capacity of the photothermal material [42].

Photothermal materials can be injected intravenously into the body and targeted to cancerous regions using either active or passive strategies. Active targeting involves modifying the ligands on the surface of the photothermal materials to specifically bind to receptors on cancer cells. Additionally, encapsulating the photothermal reagents within cell membranes may also enhance cancer targeting.

Passive targeting involves the enhanced permeability and retention effect (EPR), which causes photothermal reagents to accumulate at tumor sites [42].

The targeting effect of photothermal materials can be visualized using various imaging techniques. The IR light absorbed by the photothermal material can also generate heat and emit fluorescence. This fluorescence can be used for imaging to monitor the

distribution of photothermal reagents in the organism and at the cancer site. Furthermore, the heat generated by IR light causes a local temperature increase in the tissues, resulting in the generation of acoustic waves through thermal expansion. These waves can be converted into photoacoustic (PA) images based on the collected acoustic data. Therefore, photothermal materials based on NIR light can achieve specific targeting of tumor sites while also visualizing the distribution and morphology of tumors. This capability could provide better PTT efficiency [42].

This work investigates the photothermal effect of the 70S30C bio-glass. In this preliminary test, a common IR lamp with a power of 150 W is used as the source of IR light. The average power density of irradiation is adjustable by changing the distance between the source and the samples. All samples were exposed to IR irradiation at approximately 15 cm of distance to the IR lamp. It was measured using a photothermal camera that, at this distance, the scaffold reaches the temperature of 50°C that is sufficient to cause cell death. The samples were treated with the lamp for different durations (from 30 seconds up to 10 minutes) under a biological hood to maintain the cells in sterility condition as reported in Figure 2.15.

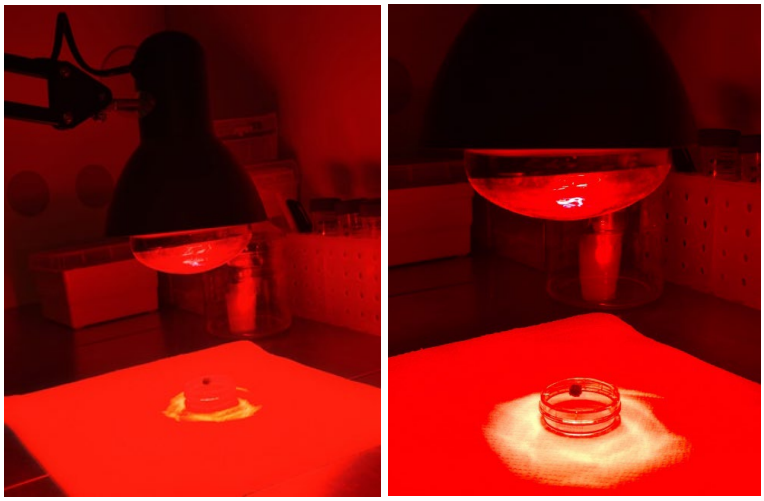

Figure 2.15. Set up for the IR irradiation of the samples under the biological hood.

The scaffolds were placed inside the multi-well after IR irradiation with fresh medium to investigate the mortality of cells after 24 hours. To verify the efficiency of the IR treatment the vitality of cells was evaluated both with Live&Dead assay (Following the same protocol described in Section 2.2.3) and with MTT test.

2.6 MTT protocol

Cell proliferation and viability can be measured by the MTT (3-4,5-Dimethylthiazol2,5-diphenyltetrazolium bromide) assay. The MTT assay is used to measure cell metabolic activity, which is an indicator of cell proliferation and viability and cytotoxicity. This colorimetric assay is based on the reduction of a yellow tetrazolium salt (MTT) to purple formazan crystals by metabolically active cells. Indeed, viable cells contain NAD(P)H-dependent reductase enzymes able to reduce MTT to formazan. The insoluble formazan crystals are then dissolved with a solubilization solution of DMSO, and the resulted colored solution is quantified by measuring the absorbance at 500-600 nanometers using a multi-well plate spectrophotometer. The darker the solution, the higher the number of metabolically active viable cells is.

This quantitative assay allows for easy and rapid handling of a high number of samples and has applications in a variety of areas, such as:

- quantification of cell growth and viability;
- measurement of cell proliferation in response to growth factors, cytokines and nutrients;
- measurement of cytotoxicity, such as quantification of the effects of cancer necrosis factor alpha or beta or macrophage-induced cell death or evaluation of cytotoxic or growth-inhibitory agents, such as inhibitory autoantibodies;
- study of cell activation [43].

In this work, MTT treatment was performed to demonstrate the efficiency of the IR treatment on the cells within the scaffold. The steps performed were as follows:

1. Depending on the experiment, the samples were treated with the IR lamp after 1, 2, or 3 weeks of cell seeding. After placing them in a 48 or 96 multi-well, 400 or 150µL of fresh medium was poured over the scaffold, and the samples were incubated for 24 hours;
2. MTT solution was added to each well, with the total volume of the solution added being 10% of the entire medium volume inside each well. The samples were then incubated for 4 hours;

3. After the incubation time, the solution of medium and MTT was slowly removed, in order to not destroy and remove the formazan crystals;
4. Next, DMSO was added to the samples, and it was necessary to pipette it onto the scaffolds to break the crystals and obtain a colored solution.
5. The absorbance in each well was measured using an Elisa Reader (Anthos 2020 ver1.8, Anthos Lab Tec Instruments®, Austria) at 492 nm, with 620 nm as reference, after removing the scaffolds from the multi-well.

The results of the MTT assay were analyzed using Graphpad, software to obtain the vitality of cells for all the IR treatment time tested.

Chapter 3

Results and Discussions

In this chapter, the results obtained from all the performed experiments are reported and critically discussed to demonstrate that the scaffolds are suitable for cellular cultures, and that the IR treatment induces cancer cells apoptosis due to the photothermal potential of the 70S30C bio-glass.

3.1 pH-test results

The pH measurement is necessary to verify whether or not there is release of Ca^{2+} and $(SiO_4)^{4-}$ ions by the scaffolds in culture media, and weather the scaffold is capable of allowing HA formation from the released ions in the biological environment. The ions released by the scaffold can affect cell culture in various ways. For instance, they can influence proliferation, differentiation, and gene expression. The cell-specific effects also depend on the type and concentration of ions released.

Both samples that underwent heat treatment in N_2 and in air are considered so that any differences in pH could be assessed for the different treatments. The following tables contain pH values, measured by a pH-meter at room temperature, after taking the multi-well containing the samples from the incubator after different incubation time.

Table 3.1. Summary of the pH values measured for the samples after 1 hour of incubation.

SAMPLE	pH in cell culture media	pH in PBS	pH in MQ water
with FS in N_2	6.60±0.12	7.6±0.03	8.0±0.01
with FS in air	7.6±0.04	7.4±0.07	7.8±0.06
without FS	7.5±0.06	7.1±0.04	7.5±0.12

Table 3.2. Summary of the pH values measured for the samples after 5 hours of incubation.

SAMPLE	pH in cell culture media	pH in PBS	pH in MQ water
with FS in N_2	6.9±0.08	7.0±0.04	7.3±0.1
with FS in air	7.0±0.06	6.9±0.1	7.3±0.1
without FS	7.0±0.05	6.3±0.03	6.9±0.06

Table 3.3. Summary of the pH values measured for the samples after 24 hours of incubation.

SAMPLE	pH in cell culture media	pH in PBS	pH in MQ water
with FS in N_2	6.9±0.06	7.0±0.1	7.8±0.14
with FS in air	6.9±0.1	6.9±0.03	7.6±0.07
without FS	6.9±0.08	6.6±0.1	7.2±0.05

Table 3.4. Summary of the pH values measured for the samples after 48 hours of incubation.

SAMPLE	pH in cell culture media	pH in pbs	pH in MQ water
with FS in N_2	6.8±0.02	7.1±0.05	7.4±0.08
with FS in air	6.9±0.05	7.1±0.05	7.3±0.02
without FS	7.0±0.1	6.8±0.01	6.9±0.16

Table 3.5. Summary of the pH values measured for the samples after 72 hours of incubation.

SAMPLE	pH in cell culture media	pH in pbs	pH in MQ water
with FS in N_2	6.8±0.01	7.0±0.03	7.4±0.07
with FS in air	7.1±0.3	7.0±0.03	7.2±0.08
without FS	7.0±0.02	6.7±0.04	7.0±0.08

The pH of the considered media is 7.3 for cell culture medium, 7.4 for PBS and between 5 to 7.5 for MQ water, respectively. Focusing particularly on the pH measured in the culture medium it is possible to notice that during the first 5 hours of incubation, there is a reduction in the pH value for the No-FS sample treated in N2 and the sample with FS treated in air, which indicates an acidification of the medium probably due to the release mainly of $(SiO_4)^{4-}$ ions. In the case of the sample with FS, the pH increases from 6.6 to

6.9, possibly mainly caused by a release of Ca^{2+}. In the next 3 days, the pH values remain similar. From this analysis, confirm that there is a heat treatment-induced release of different ions in the media and the scaffold compositions, as evidenced by the variation in the media pH values, as shown in Figure 3.1.

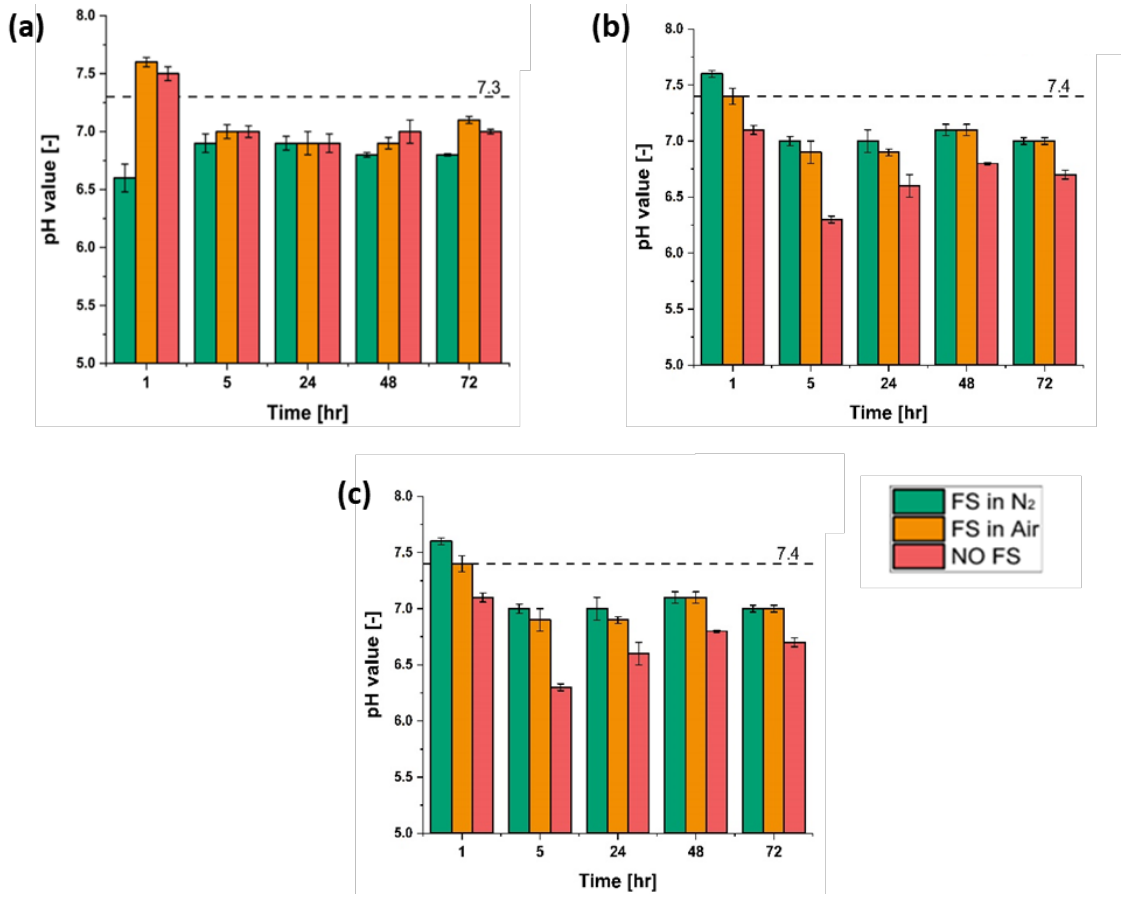

Figure 3.1. Plot of the pH values after 1, 5, 24, 49 and 72 hr for all the scaffold sample tested; (a) in cell culture media, (b) in PBS and (c) in MQ water.

Overall, the pH values in all the media considered are around 7.0 ± 0.5. This aspect is relevant since the pH in the biological environment must be around 7.5 to maintain a correct cell culture environment. Therefore, it is possible to confirm that the ions released by the scaffold in the culture media slightly increase the pH levels, but this alteration is nontoxic for the cell culture. Additionally, for the biological experiment performed, the culture media was replaced every 12 hours, thus maintaining the correct value of the pH.

3.2 Porosity evaluation results

The Table below shows the density value measured with a helium pycnometer. The first density considered is the geometric density, calculated from the nominal volume and mass of the samples. However, this density considers a volume that includes porosity. Therefore, it was necessary to calculate the bulk density, which is the density that excludes open porosity, and the true density, which excludes both open and closed porosity, through the relationships explained in Section §2.1.5.3. First, a higher porosity value means that there is more space available for cell growth and proliferation, which can be beneficial for tissue engineering applications. Second, the porosity can affect the mechanical properties of the scaffold. Therefore, it is essential to balance the porosity and mechanical properties to ensure good performance in a specific tissue engineering application. Furthermore, the different porosity values can also affect the rate of degradation of the material, which can be important in designing scaffolds for tissue regeneration.

In this study, it was possible to identify a different porosity value for the 70S30C scaffolds compositions, which would lead to a preference for a composition between the two.

Table 3.6. Value for density in g/cm^3 and % of porosity, adapted from [28].

SAMPLE	ρ_{geom}	ρ_{BULCK}	ρ_{true}	Porosity (%)
Gyroid with FS	0.7978 ± 0.0944	2.0759 ± 0.0588	1.986 ± 0.6008	80%
Gyroid without FS	0.5789 ± 0.0696	2.0236 ± 0.0873	2.1791 ± 0.5269	74.5%

The value of porosity obtained are all lower than that theoretical value set at 85%. This is because the permeability of the gas used by the pycnometer must be considered. Overall, the porosity level resulting from the analysis is ideal for bone tissue engineering. Studies have demonstrated that a porosity level at least 70% could be feasible for scaffold for tissue engineering applications [45].

3.3 Live&Dead results for biological validation

To evaluate cell response to the scaffold architecture and composition, cellularized constructs were analyzed 14 days after seeding using Calcein-AM, a green fluorescent

marker staining the cytoplasm of live cells, Hoechst, a blue marker which stains all cells nuclei, and Propidium, a red fluorescent marker that stains in red dead cells nuclei. The figures below (from Figure 3.2 to Figure 3.9) report representative images for the biocompatibility validation of SK-N-AS, SaOs-2, hMSCs and BJ cell lines cultured on 70S30C scaffold. Overall, the scaffolds consistently show good seeding efficiency, high cell density and distribution, and good cell proliferation during the time interval tested. 14 days after seeding, all cells in the scaffolds are adhering to the surface and inside the porosity. In particular, hMSCs and BJ cells correctly assume their typical elongated morphology. Moreover, cells are homogeneously distributed throughout the entire 3D structure of the scaffold. The scaffold without FS in its composition show high levels of autofluorescence, detrimental to the accuracy and reliability of the analysis. Autofluorescence is a phenomenon where the scaffold material itself emits fluorescent light when excited by the imaging system. This can interfere with the fluorescent signals from the cell markers, making it difficult to distinguish between the scaffold material and the cells. As a result, the analysis of cell adhesion, proliferation, and differentiation on the scaffold may be inaccurate or biased. For this reason, only scaffolds containing FS (Fumed Silica) were investigated to prove the cellular adhesion and proliferation.

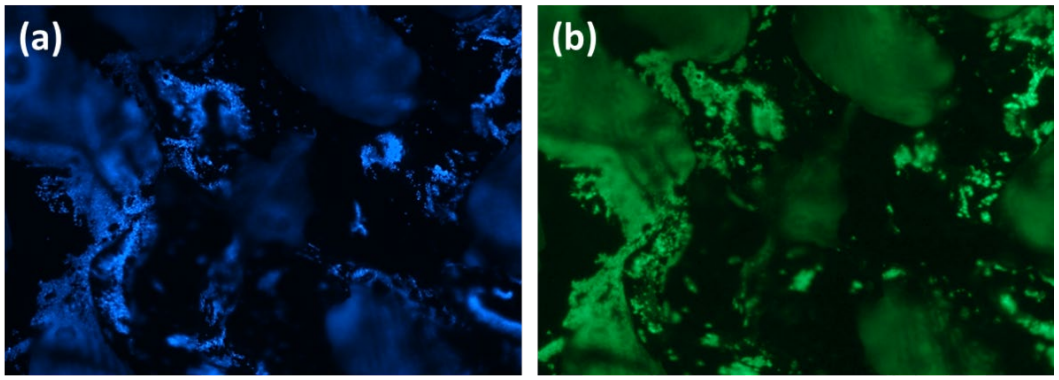

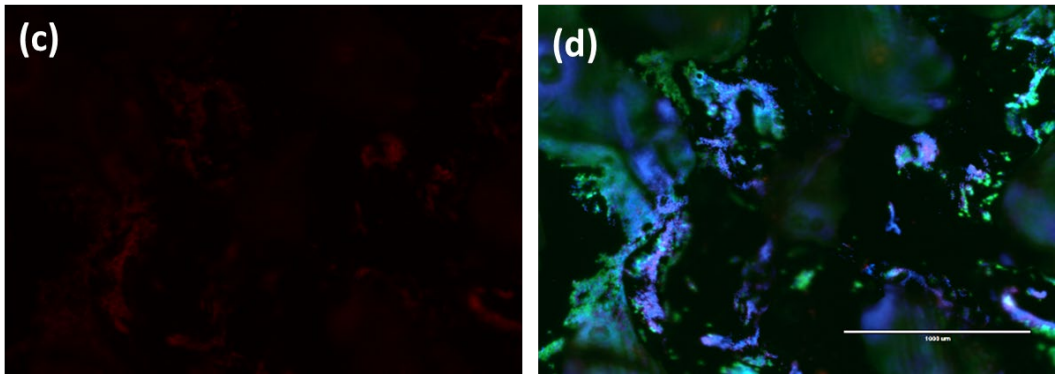

Figure 3.2. Results of Live&Dead assay for SK-N-AS cells 14 days after seeding. (a) Cells nuclei marked in blue with Hoechst; (b) Live cells nuclei marked in green with Calcein; (c) Dead cells nuclei marked in red with Propidium; (d) Merge. 4x Magnification, scale bar 1000 µm.

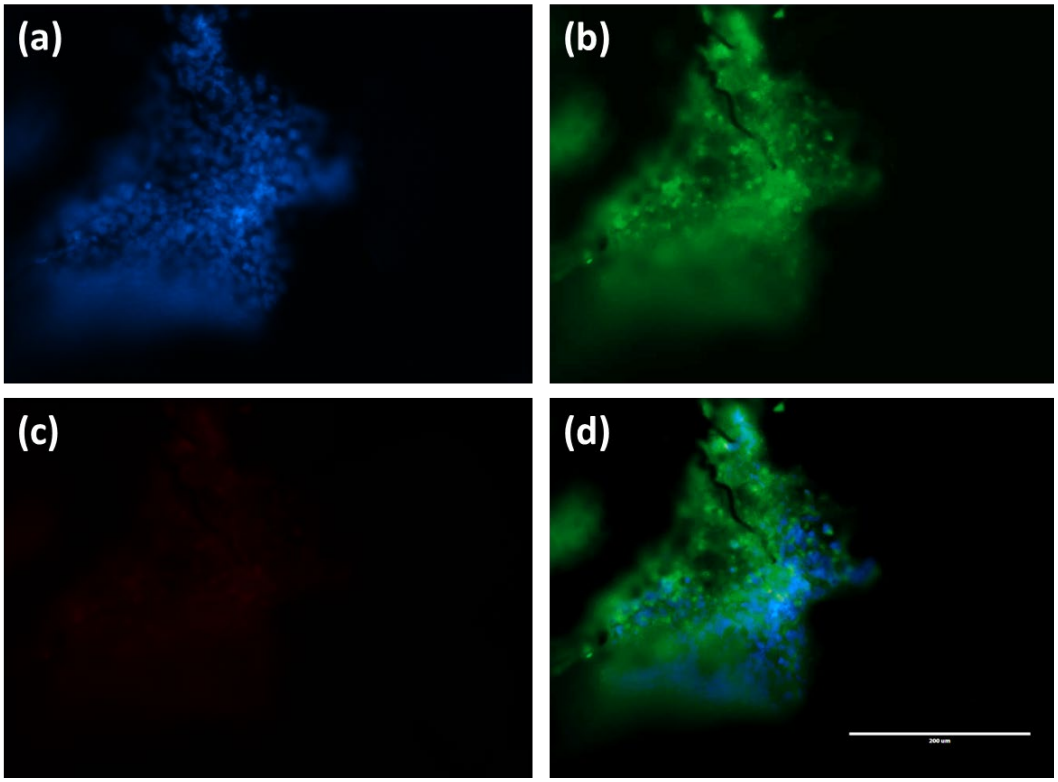

Figure 3.3. Results of Live&Dead assay for SK-N-AS cells 14 days after seeding. (a) Cells nuclei marked in blue with Hoechst; (b) Live cells nuclei marked in green with Calcein; (c) Dead cells nuclei marked in red with Propidium; (d) Merge. 10x Magnification, scale bar 200 µm.

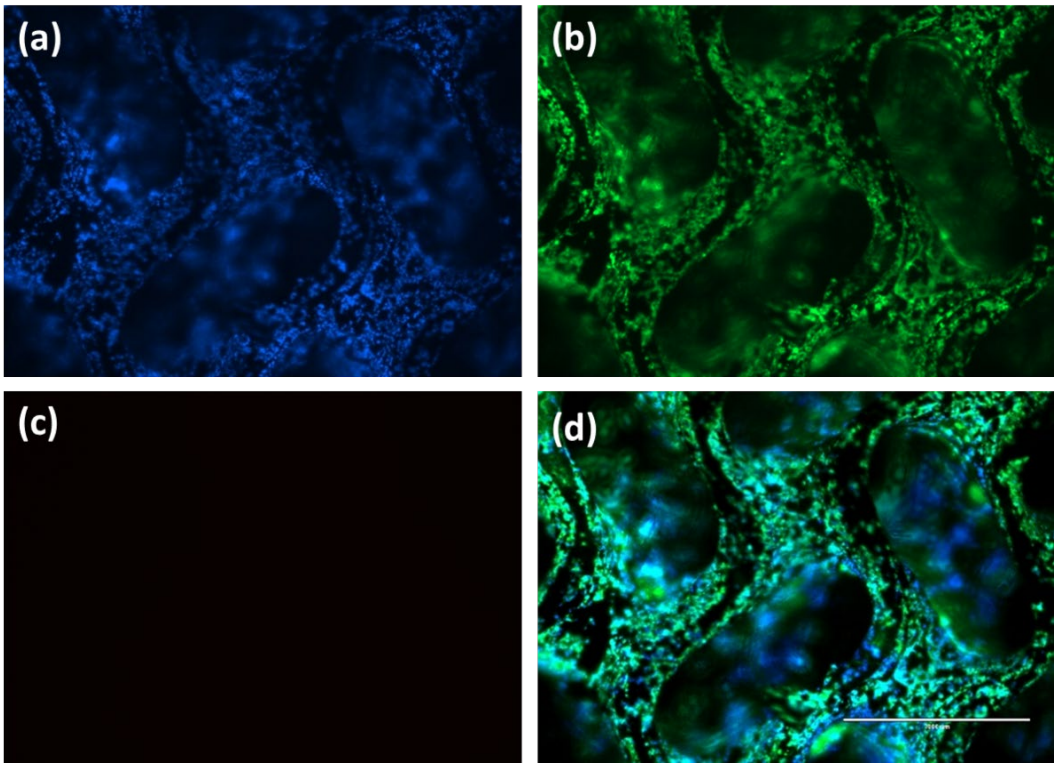

Figure 3.4. Results of Live&Dead assay for SaOs-2 cells 14 days after seeding. (a) Cells nuclei marked in blue with Hoechst; (b) Live cells nuclei marked in green with Calcein; (c) Dead cells nuclei marked in red with Propidium; (d) Merge. 4x Magnification, scale bar 1000 µm.

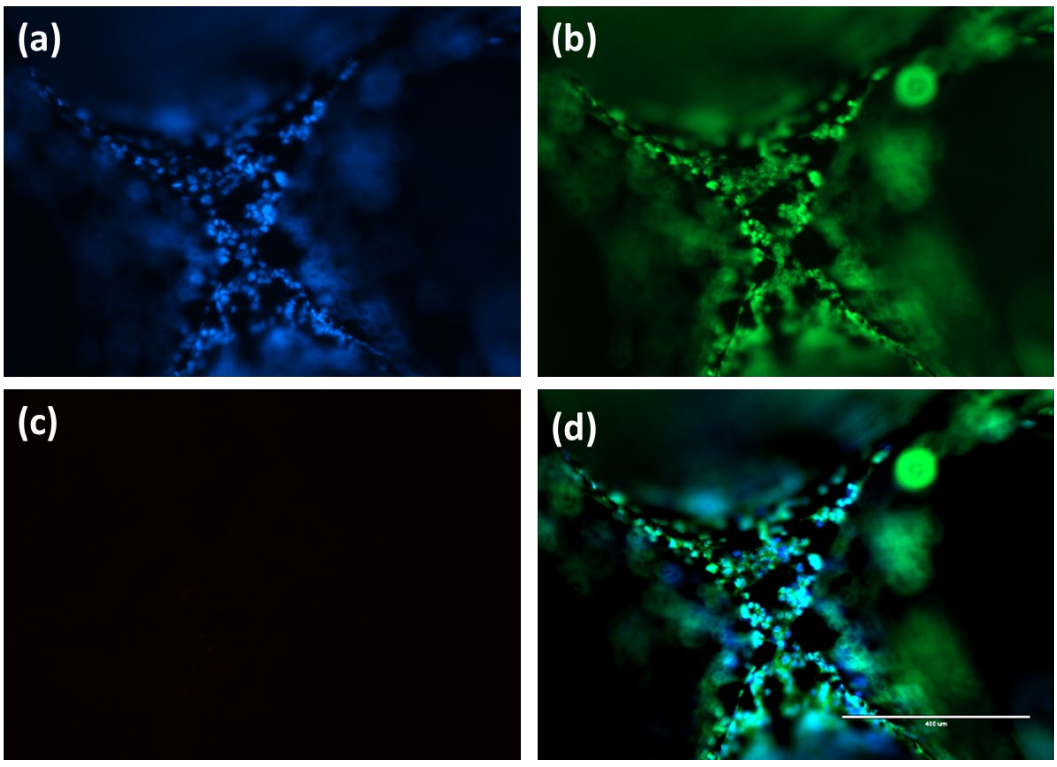

Figure 3.5. Results of Live&Dead assay for SaOs-2 cells 14 days after seeding. (a) Cells nuclei marked in blue with Hoechst; (b) Live cells nuclei marked in green with Calcein; (c) Dead cells nuclei marked in red with Propidium; (d) Merge. 10x Magnification, scale bar 200 µm.

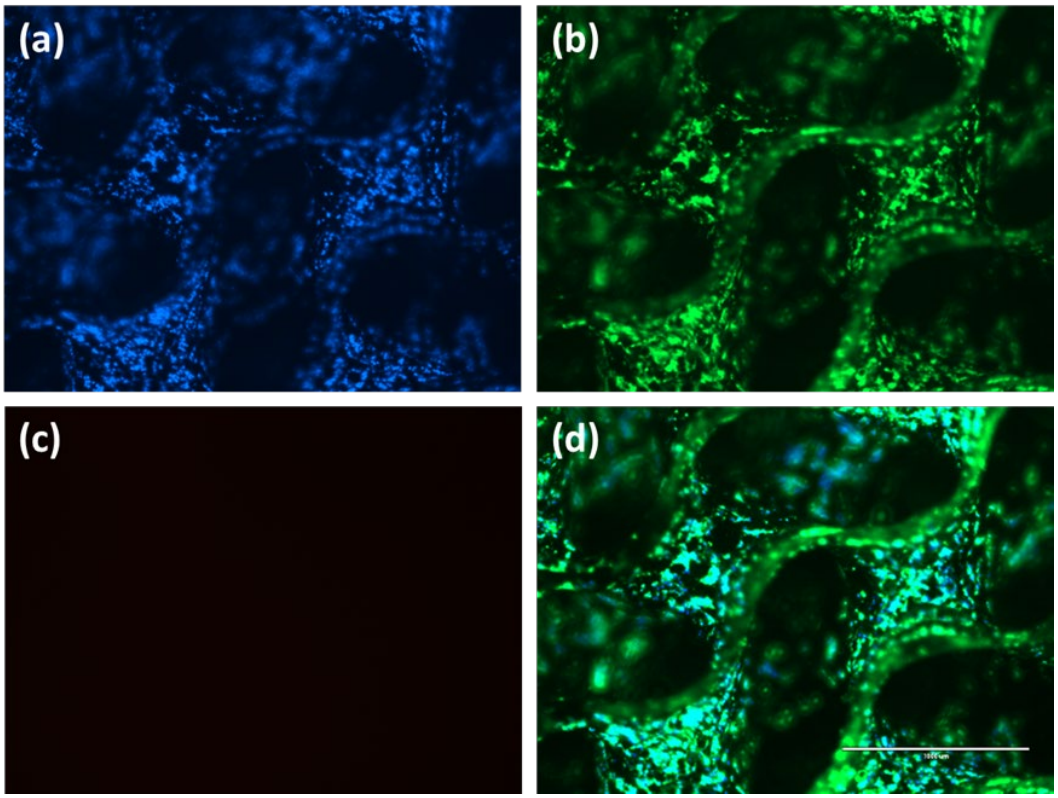

Figure 3.6. Results of Live&Dead assay for hMSCs 14 days after seeding. (a) Cells nuclei marked in blue with Hoechst; (b) Live cells nuclei marked in green with Calcein; (c) Dead cells nuclei marked in red with Propidium; (d) Merge. 4x Magnification, scale bar 1000 µm.

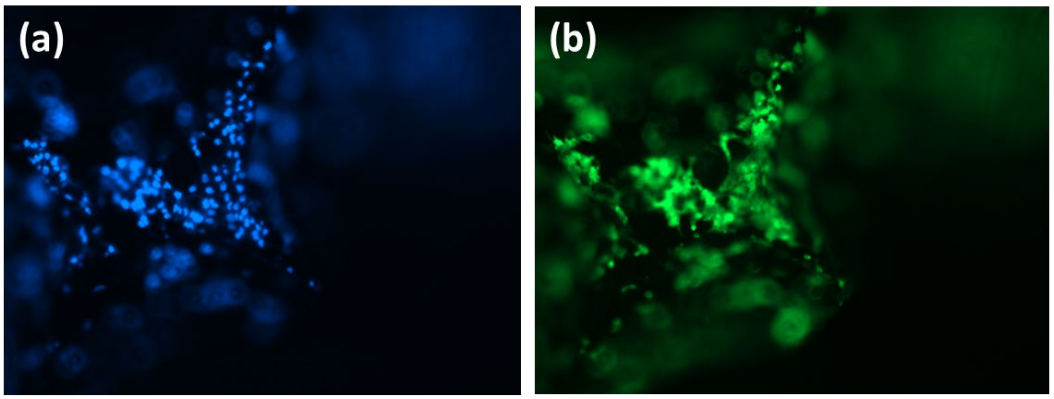

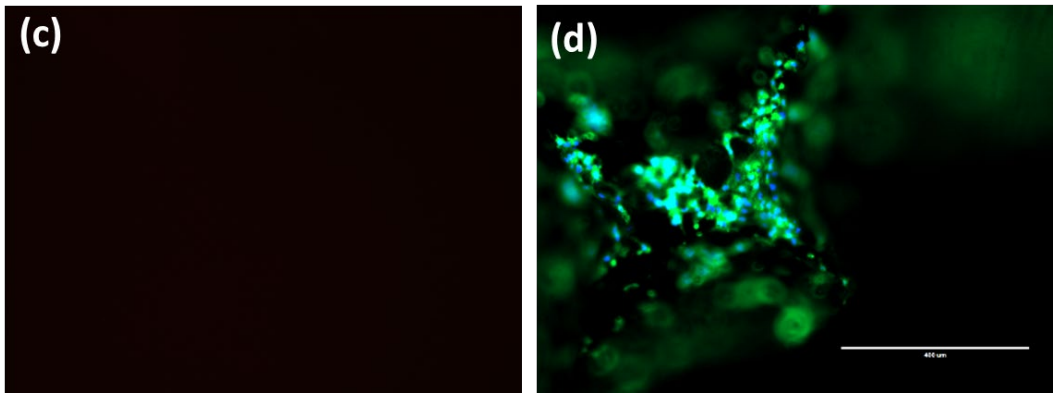

Figure 3.7. Results of Live&Dead assay for hMSCs 14 days after seeding. (a) Cells nuclei marked in blue with Hoechst; (b) Live cells nuclei marked in green with Calcein; (c) Dead cells nuclei marked in red with Propidium; (d) Merge. 10x Magnification, scale bar 200 µm.

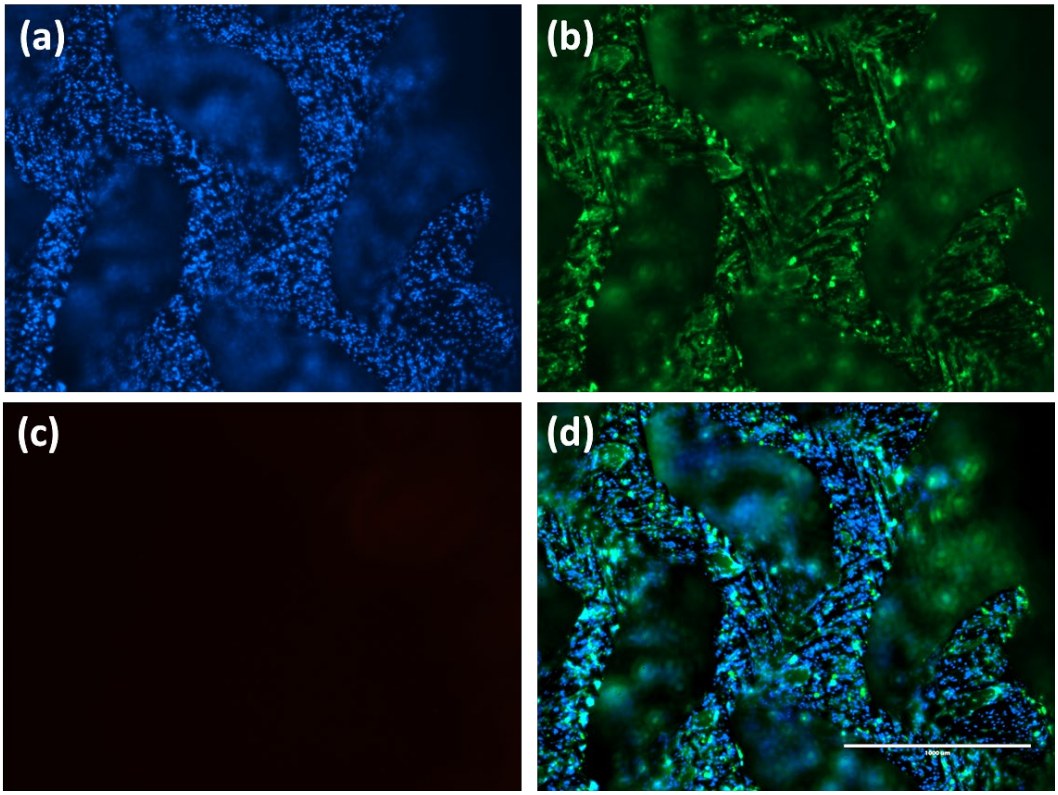

Figure 3.8. Results of Live&Dead assay for BJ cells 14 days after seeding. (a) Cells nuclei marked in blue with Hoechst; (b) Live cells nuclei marked in green with Calcein; (c) Dead cells nuclei marked in red with Propidium; (d) Merge. 4x Magnification, scale bar 1000 µm.

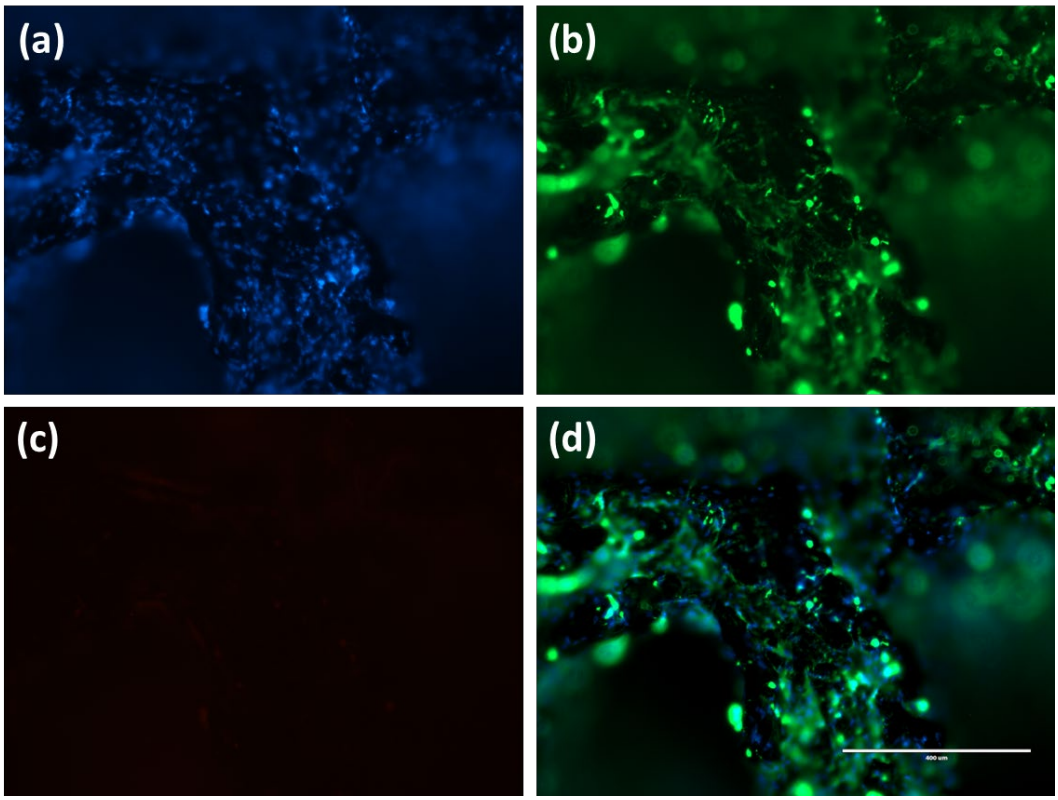

Figure 3.9. Results of Live&Dead assay for BJ cells 14 days after seeding. (a) Cells nuclei marked in blue with Hoechst; (b) Live cells nuclei marked in green with Calcein; (c) Dead cells nuclei marked in red with Propidium; (d) Merge. 10x Magnification, scale bar 200 µm.

It is possible to observe that after 14 days after seeding, the majority of the cells cultured on the scaffolds are alive since Propidium marks only a few dead cells nuclei while the Calcein signal is predominant. This result confirms the biocompatibility of the scaffold and the possibility to obtain, with this composition, an optimal culture condition over a long period of time.

It is necessary to underline that the imaging of 3D scaffolds is difficult to obtain with standard laboratory microscope, since it is only possible to focus on small areas of the scaffolds. For this reason, magnifications of 4x and 10x have been preferred due to the possibility to observing both the scaffold and the cells with better resolution. In particular, the scaffolds in which the FS is absent are characterized by a high Calcein absorbance, making the scaffold difficult to observe with the optical microscope. Therefore, the scaffolds made with the FS were preferred over those without it.

Cell viability counting was performed on the scaffolds containing FS, and this analysis was conducted only for the two cancer cell lines seeded on them. Images with a magnification of 10x were analyzed using ImageJ after 7 and 14 days from seeding, to obtain a quantification of the cells' viability. The results are reported in Table 3.7.

Table 3.7. Summary of the results for the viability of both the cancer cell lines tested.

Cell line	Viability (%)
SK-N-AS (DAY 7)	~95±0.02
SK-N-AS (DAY 14)	~97±0.02
SaOs-2 (DAY 7)	~97±0.02
SaOs-2 (DAY 14)	~99±0.02

From this qualitative analysis related to both the SK-N-AS and SaOs-2 cell lines, the viability resulted is very high. Therefore, both the cancer cells are selected to be tested using the IR lamp to verify the possibility to induce tumor cell apoptosis.

3.4 Immunofluorescence staining results

To confirm the biocompatibility and the cytocompatibility of the 70S30C bio-glass scaffold, a further staining was carried out with DAPI and Rhodamine Phalloidin. DAPI and Rhodamine Phalloidin are fluorescent dyes used in the staining process to visualize different cellular structures. DAPI is a nuclear stain that binds to the DNA in the cell nuclei and fluoresces blue. It is commonly used to visualize the nuclei of the cells and to assess cell proliferation and viability. Rhodamine Phalloidin is a stain that binds to the actin filaments of the cell membranes and fluoresces orange. It is used to visualize the cytoskeleton of the cells and to assess cell morphology and adhesion. Together, DAPI and Rhodamine Phalloidin staining can provide valuable information on the distribution, morphology, and viability of the cells on the scaffold. This information is crucial to assess the biocompatibility and cytocompatibility of the scaffold and to optimize the scaffold design for specific tissue engineering applications.

The scaffolds were observed with a confocal microscope at different magnifications, and it was possible to confirm that there was a high concentration of cells on the scaffolds after 7 to 21 days from seeding, both on the surface and inside the porosities.

All the cell lines were investigated through IF staining and, for SK-N-AS, both scaffold formulation with and without FS were considered (Figure 3.10 and Figure 3.11). However, again observing the autofluorescence in samples without FS, the biocompatibility study was focused on samples made by the mixture with FS for the other cell lines.

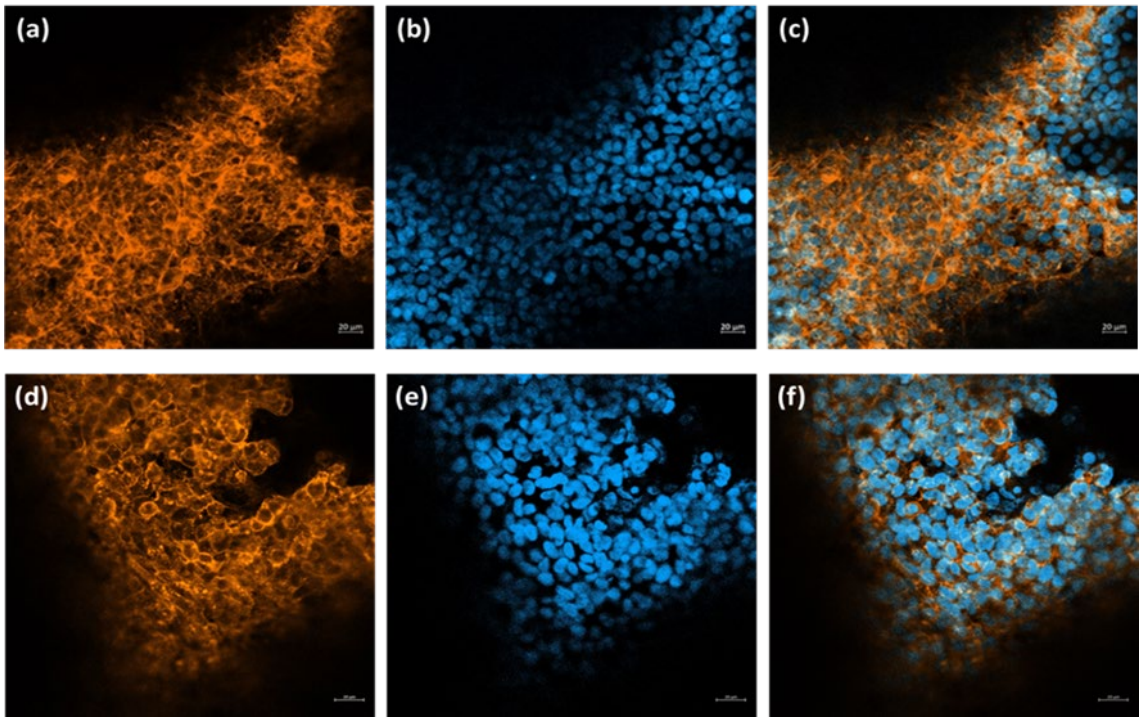

Figure 3.10. Results of the IF staining for SK-N-AS 14 days after seeding using scaffold composition with FS. (a and d) Actin filaments marked with Rhodamine Phalloidin; (b and e) Cells nuclei marked in blue with DAPI; (c and f) Merge. Magnification 20x, scale bar 20 µm.

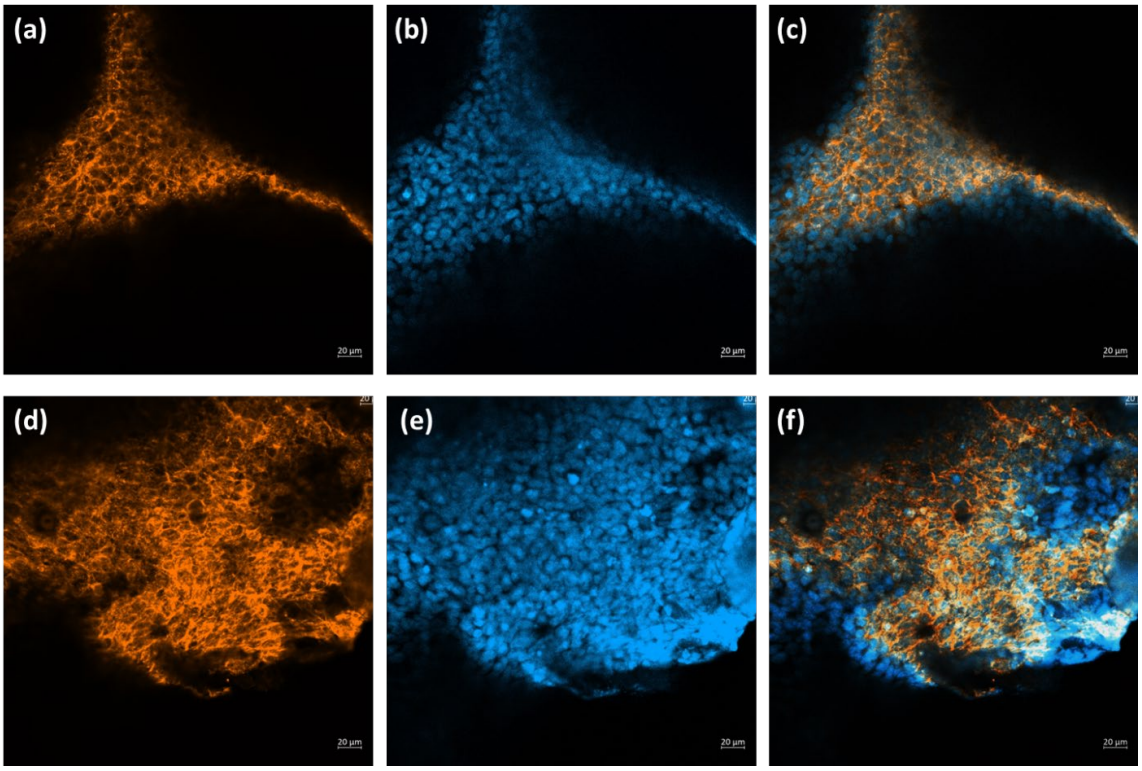

Figure 3.11. Results of the IF staining for SK-N-AS 14 days after seeding using scaffold composition without FS. (a and d) Actin filaments marked with Rhodamine Phalloidin; (b and e) Cells nuclei marked in blue with DAPI; (c and f) Merge. Magnification 20x, scale bar 20 µm.

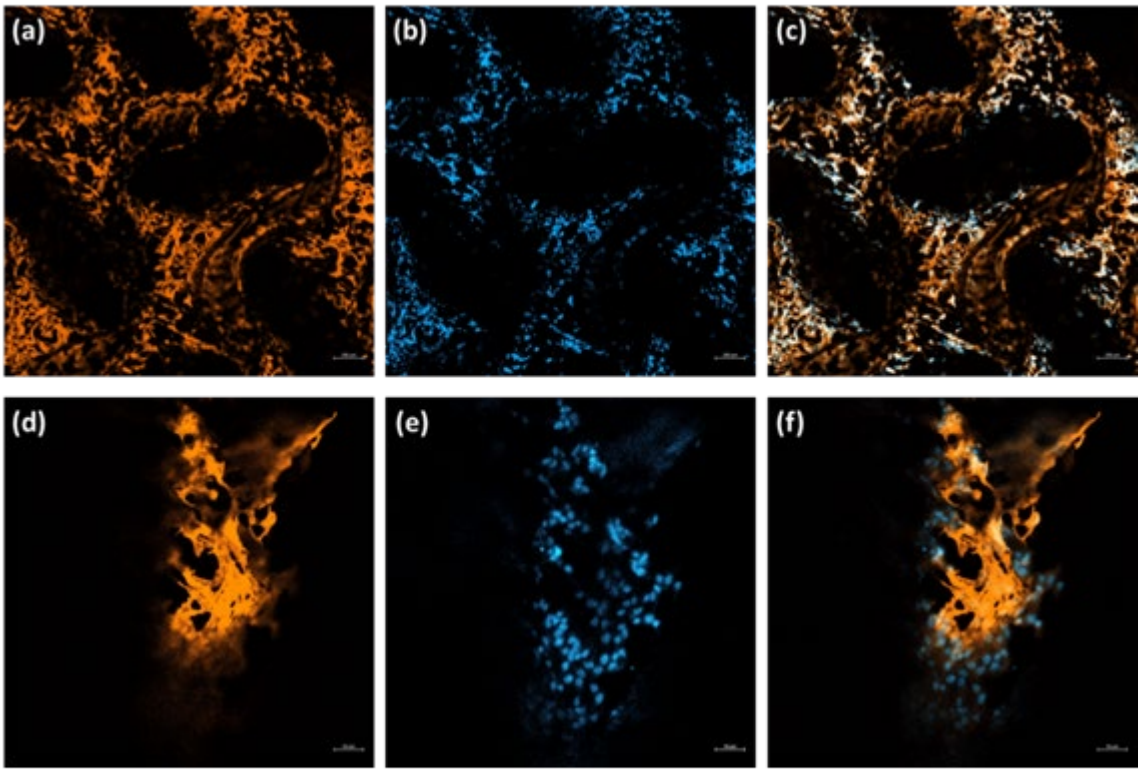

Figure 3.12. Results of the IF staining for SaOs-2 14 days after seeding using scaffold composition with FS. (a-c) Magnification 10x, scale bar 200 µm. Actin filaments marked with Rhodamine Phalloidin, cells nuclei marked in blue with DAPI and merge; (d-f) Magnification 20x, scale bar 20 µm. Actin filaments marked with Rhodamine Phalloidin, cells nuclei marked in blue with DAPI and merge.

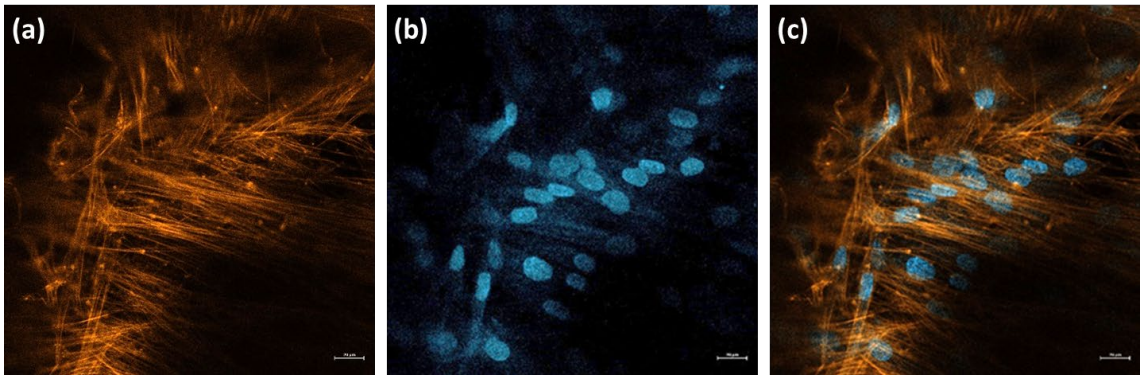

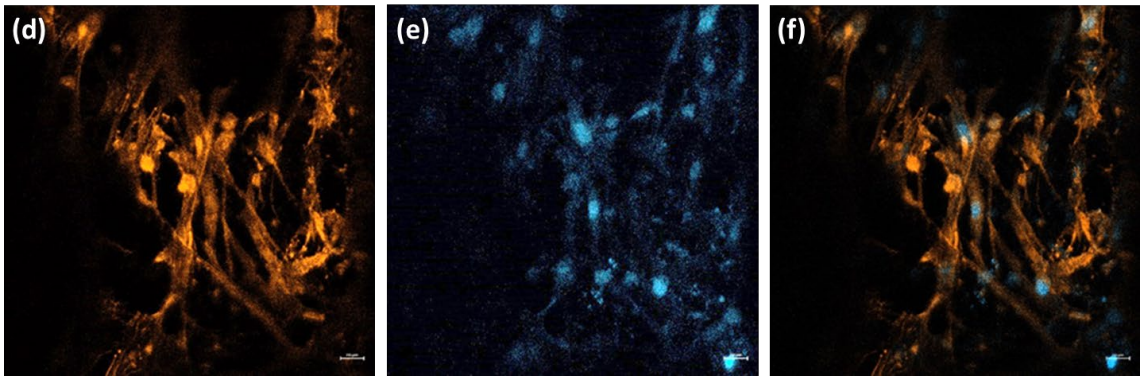

Figure 3.13. Results of the IF staining for hMSCs 14 days after seeding using scaffold composition without FS. (a and d) Actin filaments marked with Rhodamine Phalloidin; (b and e) Cells nuclei marked in blue with DAPI; (c and f) Merge. Magnification 20x, scale bar 20 µm.

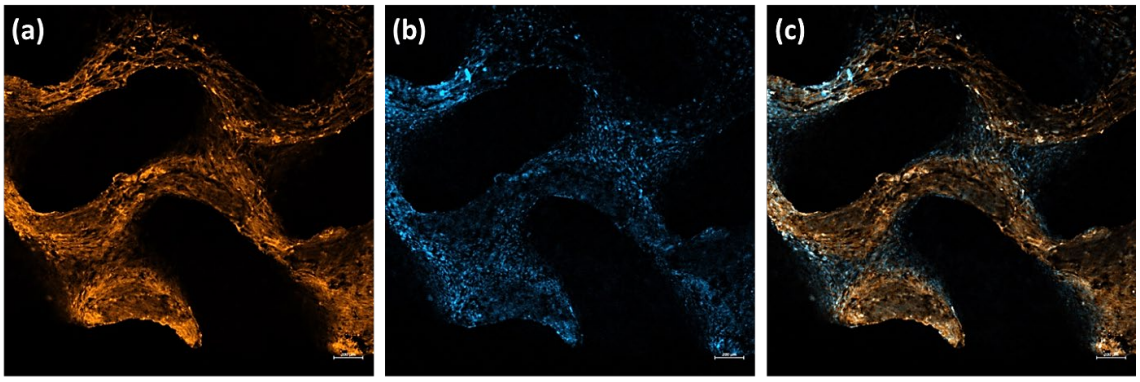

Figure 3.14. Results of the IF staining for BJ cells 14 days after seeding using scaffold composition without FS. (a) Actin filaments marked with Rhodamine Phalloidin; (b) Cells nuclei marked in blue with DAPI; (c) Merge. Magnification 2x, scale bar 400 µm.

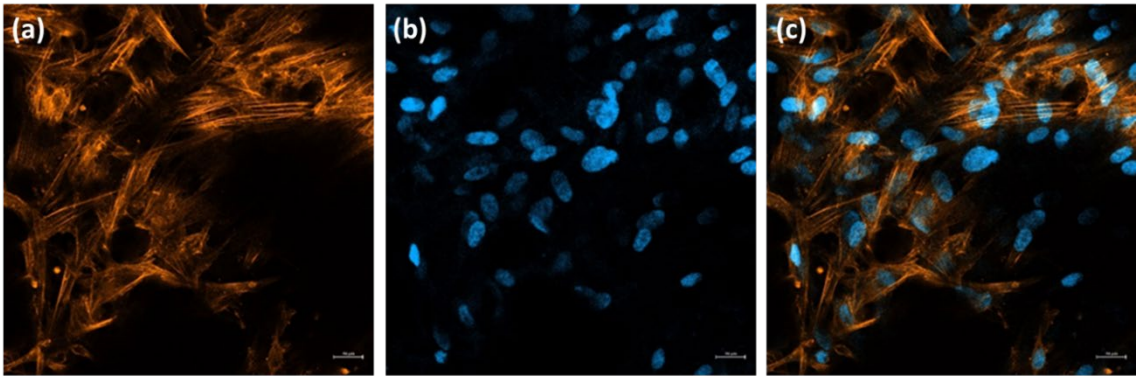

Figure 3.15. Results of the IF staining for BJ cells 14 days after seeding using scaffold composition without FS. (a) Actin filaments marked with Rhodamine Phalloidin; (b) Cells nuclei marked in blue with DAPI; (c) Merge. Magnification 20x, scale bar 20 µm.

All of the tested cell lines demonstrate a high concentration on both the surface and within the porosities of the scaffolds. In particular, under 20x or 25x magnification, hMSCs and BJ cells were observed to have an elongated shape, according with their correct phenotype. The chosen scaffolds formulation provides a good substrate for these cells, even for undifferentiated hMSCs. Therefore, it may be possible to investigate whether these cells can differentiate into an osteoblastic phenotype, given that the substrate has mechanical properties and features similar to natural bone. The differentiation of hMSCs into an osteoblastic phenotype could have significant implications for bone tissue engineering. This process could potentially allow for the creation of new bone tissue to repair or replace damaged or diseased bone. hMSC differentiation into this cell type could lead to the development of new approaches for bone regeneration. This could be particularly beneficial for individuals with bone fractures or defects, as well as those with osteoporosis or other bone disorders. Additionally, the use of hMSCs for bone tissue engineering could potentially reduce the need for traditional bone grafts.

3.5 SEM results

Human SK-N-AS and SaOs-2 cells were grown for 14 days on bio-glass scaffolds treated with N_2 to evaluate the scaffolds biocompatibility and the morphology of the adhered cells. Only the tumor cell lines were examined, and it was observed that cells were located on the surface of the scaffold (Fig. 3.17a), with some cells entering into the pores through small windows (Fig. 3.16). However, SEM observations revealed a normal morphological phenotype of these cell types on the surface matrix of the bio–glass scaffolds (Fig. 3.19a) with some evidences of attachments of cells via membrane processes (Fig. 3.16c).

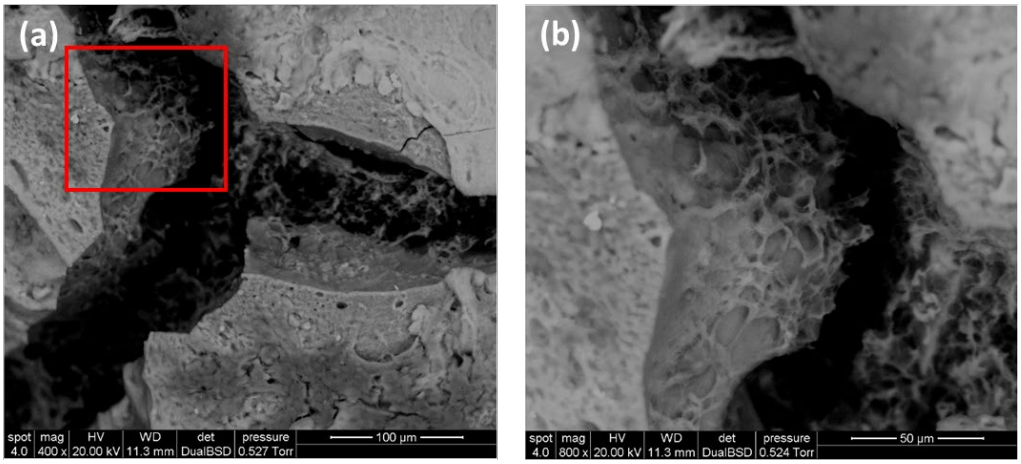

Figure 3.16. SEM images of scaffolds seeded with SK-N-AS cells after 14 days from seeding. (a) 400x, (b)Zoomed view of the area in the red box at 800x magnification.

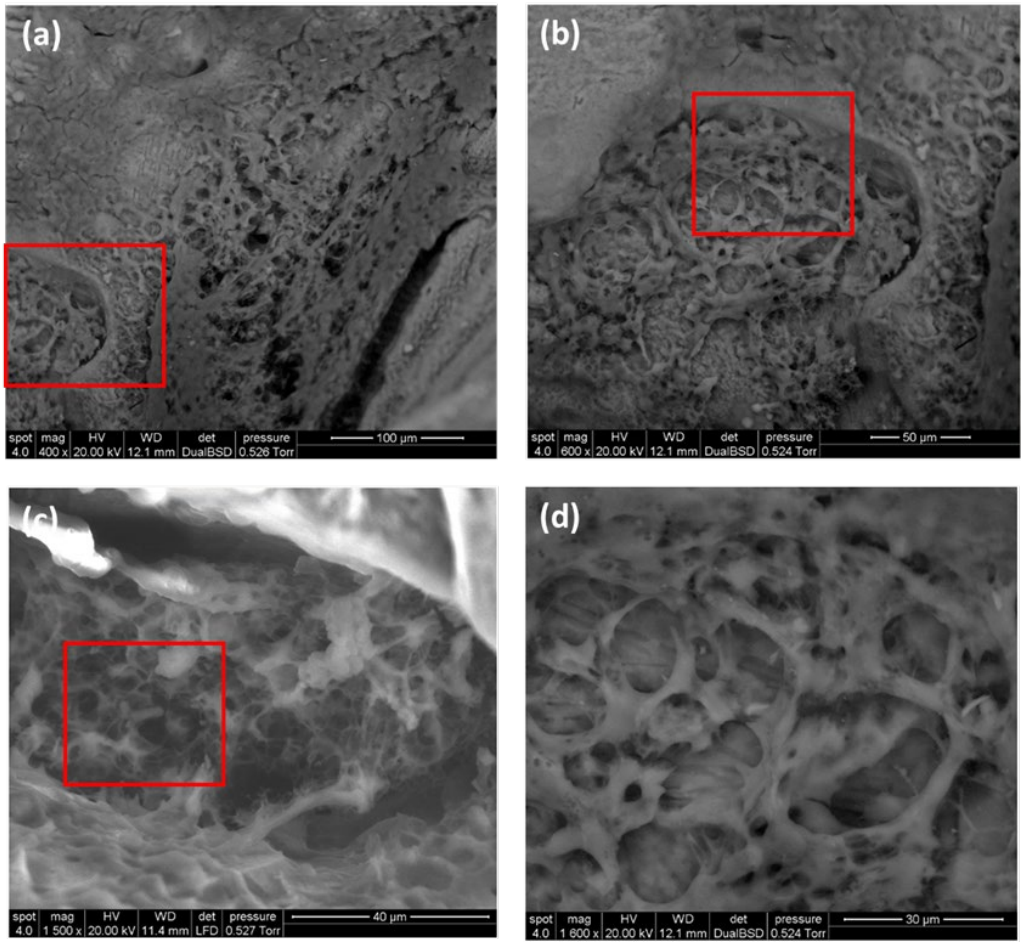

Figure 3.17. SEM images of scaffolds with SK-N-AS cells after 14 days from seeding. (a) 400x, (b) Zoomed view of the red box at 800x, (c) 1500x, (d) 1600x.

Element analysis of the scaffolds was conducted after cells seeding, and the results are shown below. Four EDS spectra were analyzed in the obtained figures (Fig. 3.17a, b) to

verify if the composition of the scaffold surface is consistent throughout. By analyzing the spectra, we can determine whether the composition is consistent throughout the surface or if there are any variations in composition in different areas of the scaffold surface. This information is important for evaluating the performance of the scaffold and its potential suitability for use in tissue engineering applications. For example, if there are variations in the composition of the scaffold surface, this could potentially impact the biocompatibility of the scaffold and its ability to support cell growth and differentiation.

(a)

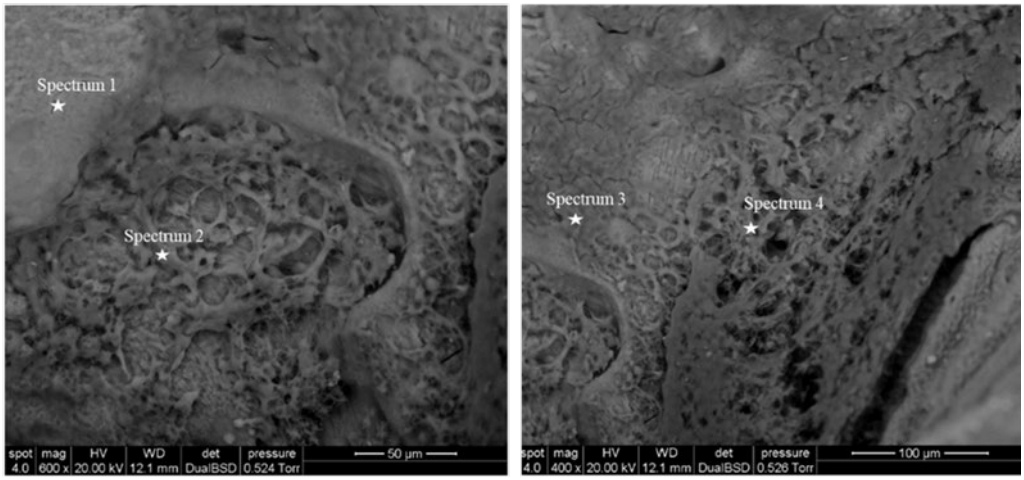

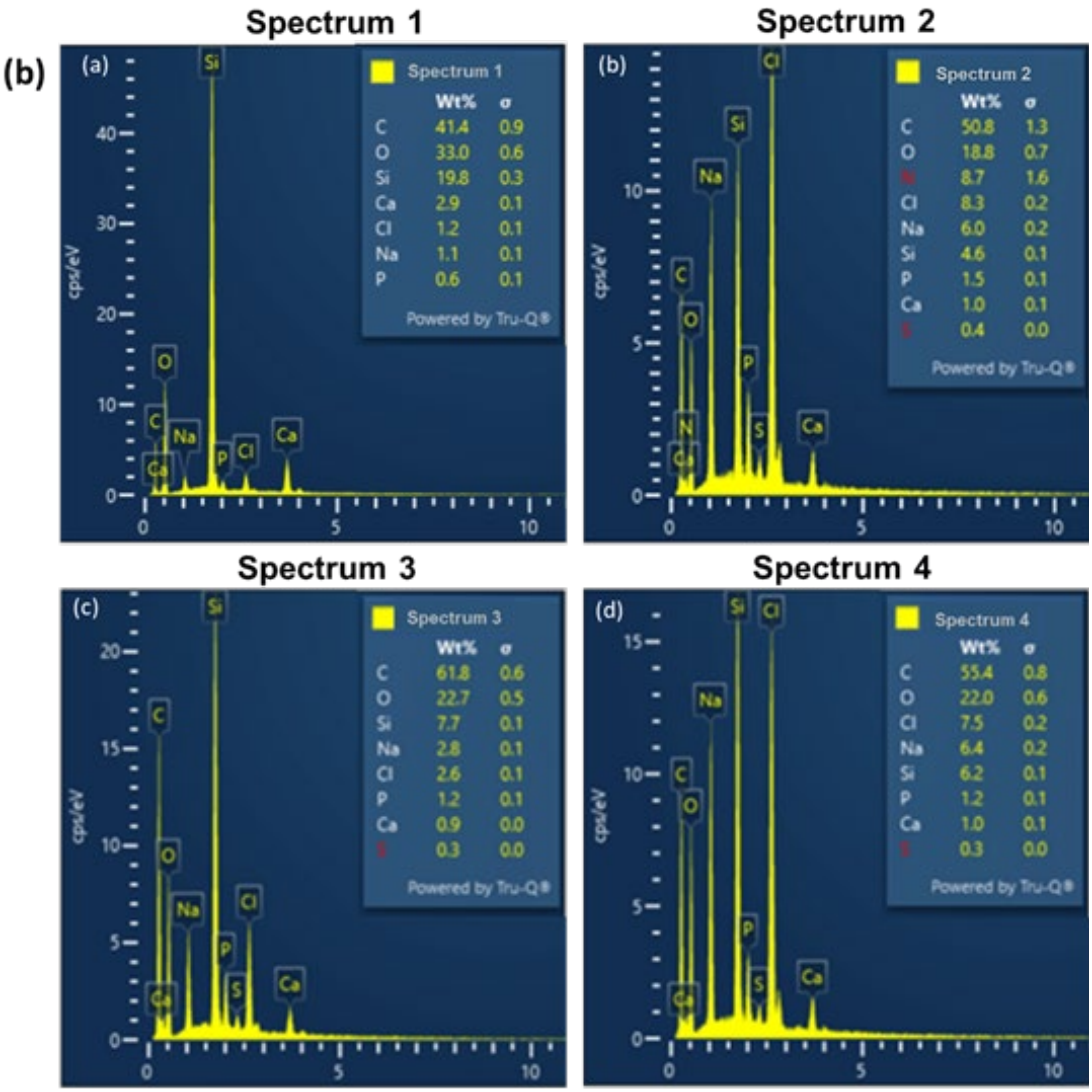

Figure **3.18.** (a) Area analysed with SEM; (b) EDS spectra of the 4 different areas of the scaffold seeded with SK-N-AS.

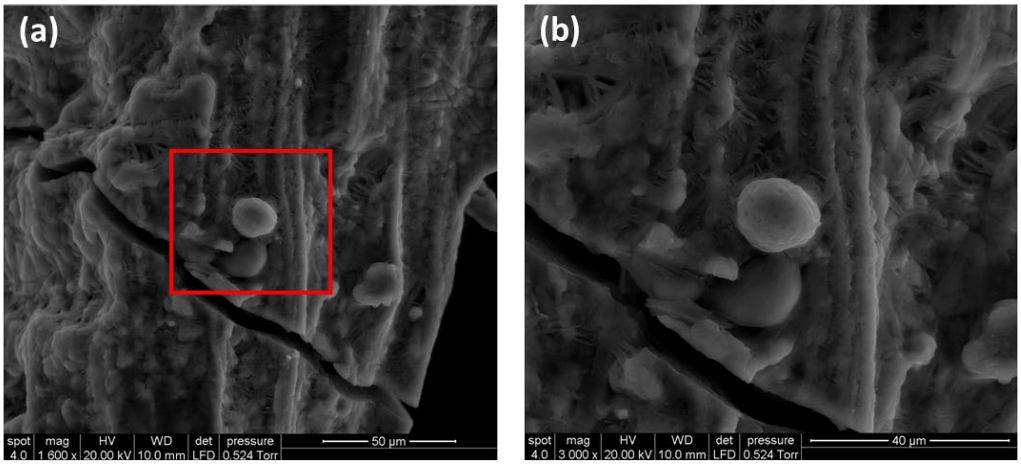

Figure 3.19. SEM images of scaffolds with SaOs-2 cells after 14 days from seeding. (a) 400x, (b) Zoomed view of the red box at 800x.

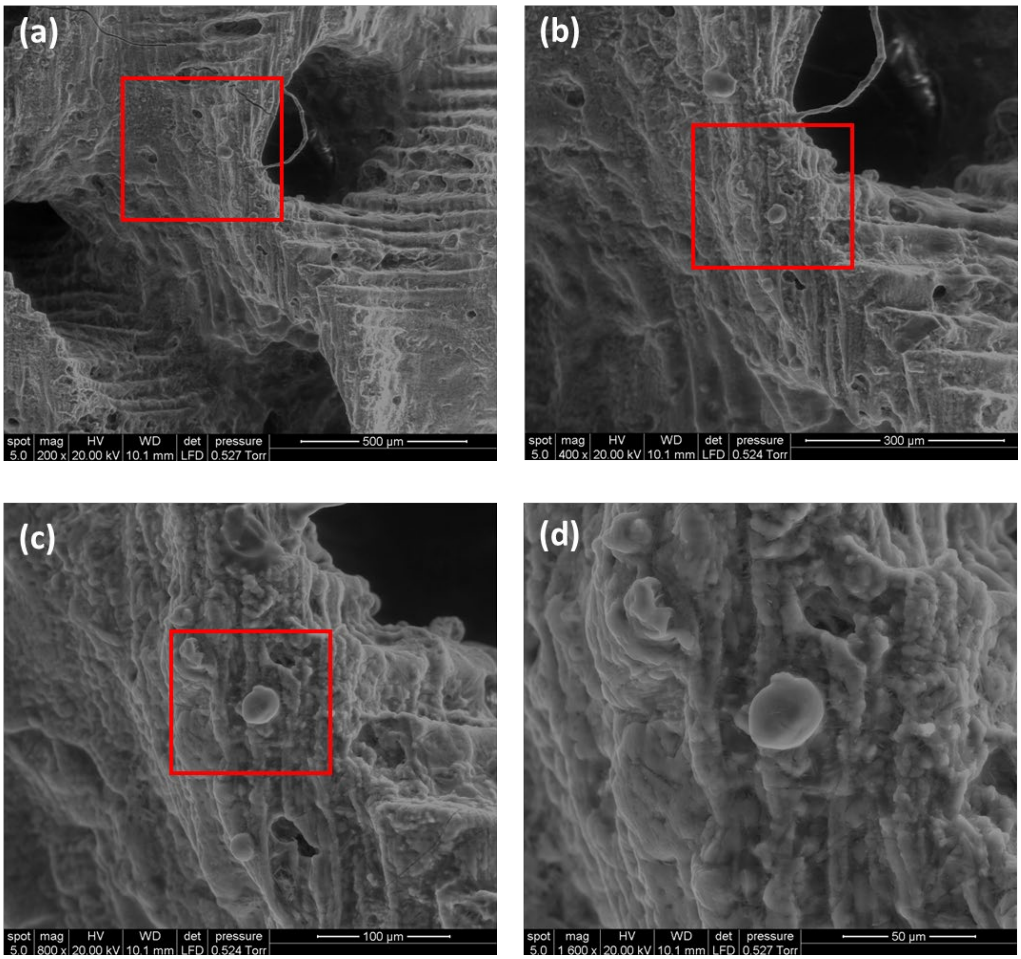

Figure 3.20. SEM images of scaffolds with SK-N-AS cells after 14 days from seeding. (a) 200x, (b) Zoomed view of the red box at 00x, (c) 1500x, (d) 1600x

The element analysis of the scaffolds after the cells seeding was conducted, and the results are shown below. In the figure obtained (Figure 3.21), four EDS spectra were analyzed to verify if the composition of the scaffold surface is consistent throughout.

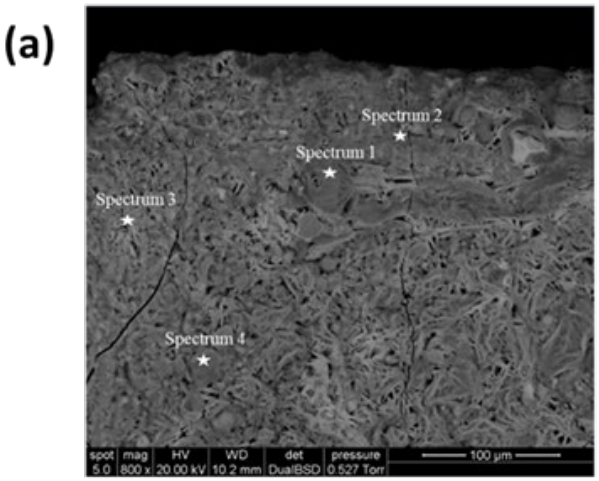

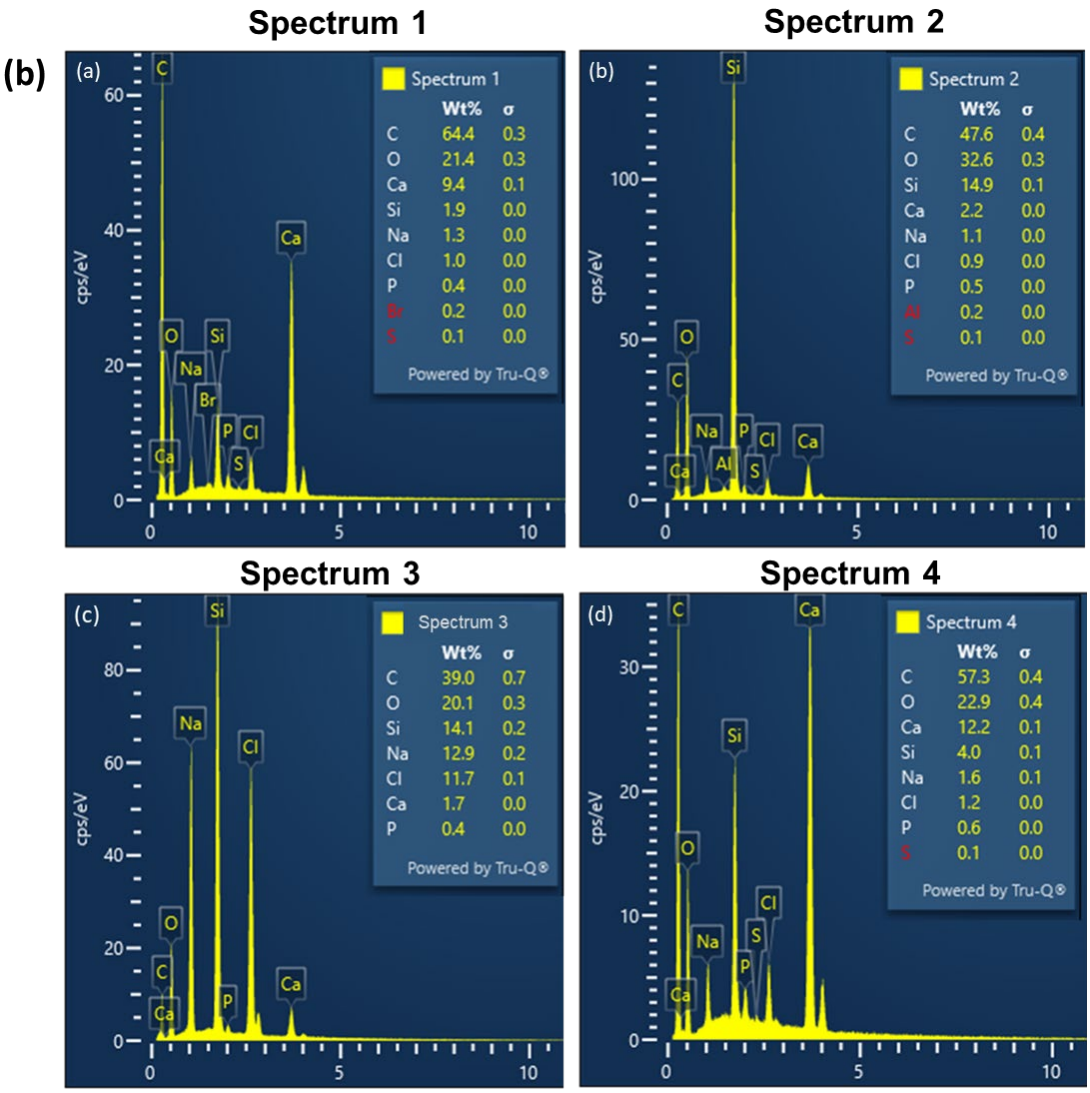

Figure 3.21. SEM images of scaffolds with SaOs-2 cells after 14 days from seeding. (a) 200x, (b) Zoomed view of the red box at 00x, (c) 1500x, (d) 1600x.

The previously presented SEM images demonstrate that cells adhered to and spread onto the ceramic surface of the scaffolds, indicating a good acceptance of the scaffold material by the living cells. To determine if the cells were able to migrate across the whole scaffold, different sections were examined. Cells were found at various levels of the scaffold from the initial seeding point at the top. At higher magnification, the cells appeared well-spread on their substrate. The SEM images and proliferation experiments strongly suggest biocompatibility of the scaffold material and the ability of living cells to migrate across the scaffolds.

The EDS spectra are different, as expexted, and this is related to the presence of cells on the surface of the scaffold. EDS spectra 1 and 3 in Figure 3.18 and 2 and 3 in Figure

3.21 were detected in the matrix of a 70S30C bioglass scaffold from preceramic polymer with FS. As predicted, the concentration of silica and oxygen prevails due to the presence of numerous Si-O-Si bonds. In contrast, spectra 2 and 4 in Figure 3.18 and the spectra 1 and 4 in Figure 3.21 show the EDS spectra detected in an area with a high concentration of cells on a 70S30C bioglass scaffold from preceramic polymer with FS. The height of the chlorine and carbon peaks is higher than that of the silicon or calcium peak. Additionally, the oxygen peak is also higher compared to Figure 3.18 (a, c) and 3.21 (b,c). The high concentration of these ions can be explained by the fact that cell membranes contain differents ions such as potassium, chlorine and magnesium. Therefore, in sections of the scaffold where cells were present, the concentration of these ions is higher than in other sections. Additionally, the presence of carbon in the EDS spectra is an indication of the presence of organic material, which in this case is likely to be cells. Carbon is a key component of biological molecules such as proteins, lipids, and nucleic acids, which are all present in cells. Therefore, the detection of carbon in the spectra provides evidence of the presence of organic material, which is likely to be cells.

3.6 IR treatment results

Scaffolds with cancer cells was irradiated with an IR lamp to determine whether the cells would be induced to die due to an increase in temperature beyond physiological levels. The temperature of the scaffold without cells was preliminary measured during the IR treatment using a thermal-imager. It was observed that the temperature reached over the 50°C after 15 seconds of treatment, as shown in Figure 3.22.

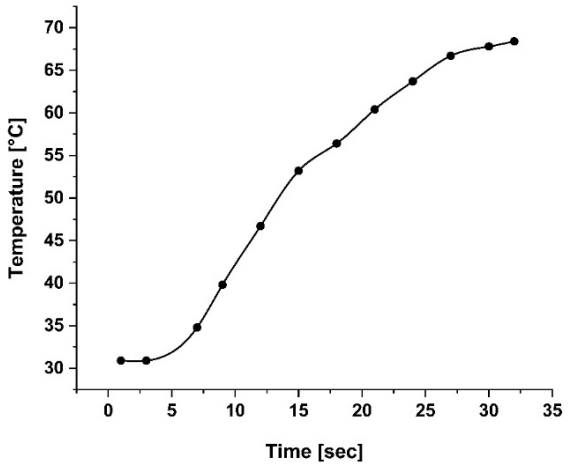

Figure 3.22. Temperature variation of the bio-glass scaffold during the IR treatment measured with a thermal-imager.

Cancer cells are known to be more sensitive to high temperatures than normal cells, and thermal therapy has been investigated as a potential treatment for cancer. By heating the tumor tissue to a temperature above 42°C, cancer cells can be selectively destroyed while leaving healthy cells relatively unharmed. In this case, the temperature of the scaffold containing cancer cells reached over 50°C, which is well above the threshold for thermal therapy.

3.6.1 Live&Dead results after IR treatment

To assess the effectiveness of the IR treatment on the cancer cells, a Live&Dead assay was carried out on the scaffolds after irradiation. Different treatment times were considered to determine if longer treatment times resulted in decreased cell viability. Both samples with SK-N-AS and SaOs-2 cells seeded onto the scaffold were examined.

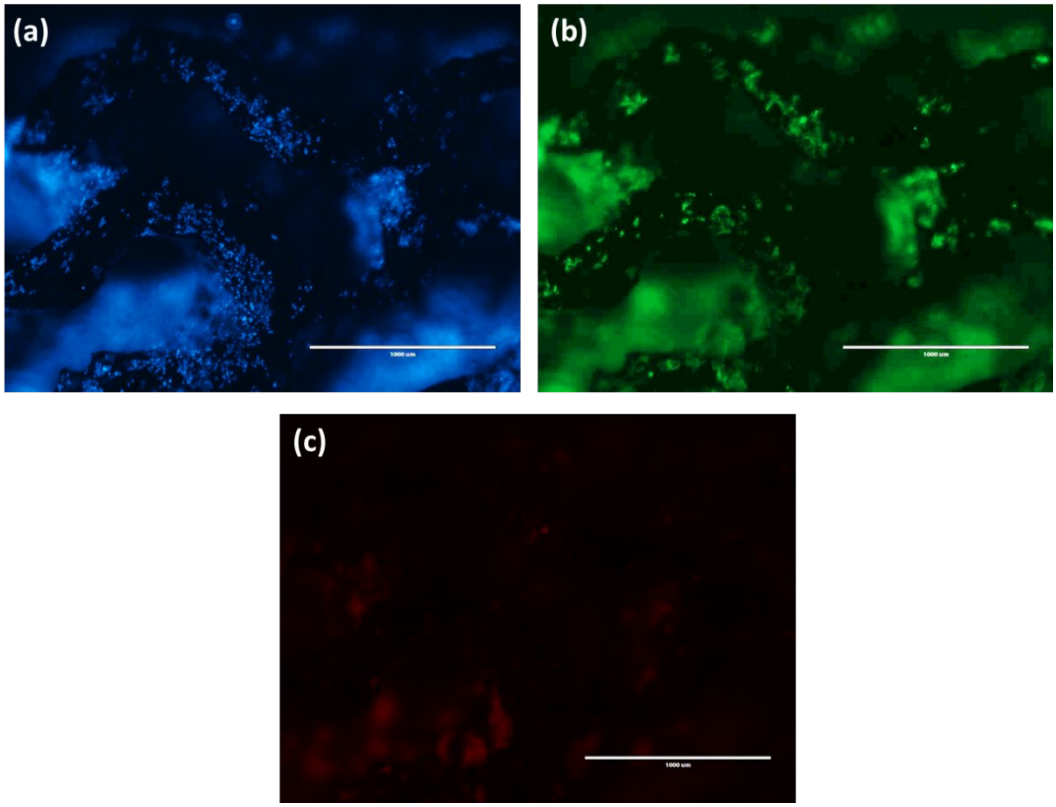

Figure 3.23 Results of Live&Dead assay for SK-N-AS seeded on the scaffold after IR lamp treatment for 30 sec. (a) Cells nuclei marked in blue with Hoechst, (b) Live cells cytoplasm marked in green with Calcein, (c) Dead cells nuclei marked in red with Propidium. 4x magnification, scale bar 1000 µm.

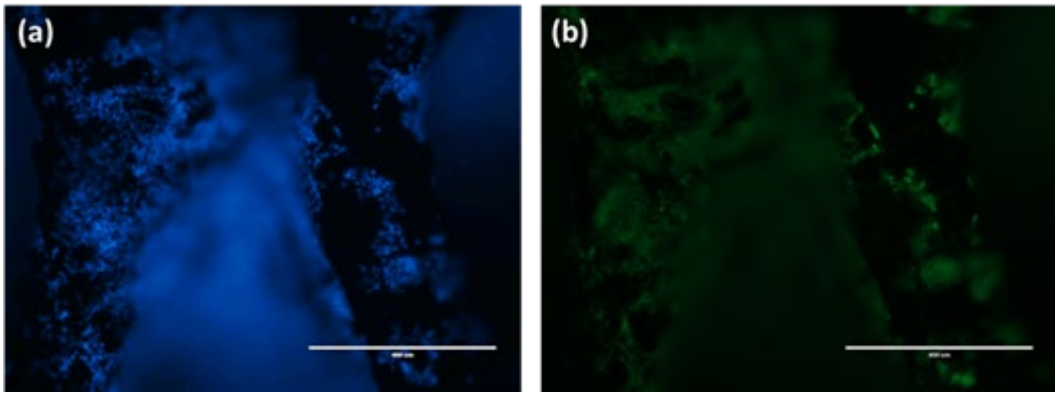

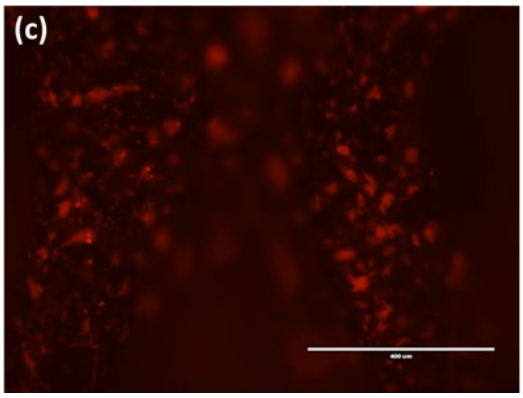

Figure 3.24 Results of Live&Dead assay for SK-N-AS seeded on the scaffold after IR lamp treatment for 5 minutes. (a) Cells nuclei marked in blue with Hoechst, (b) Live cells cytoplasm marked in green with Calcein, (c) Dead cells nuclei marked in red with Propidium. 10x magnification, scale bar 200 µm.

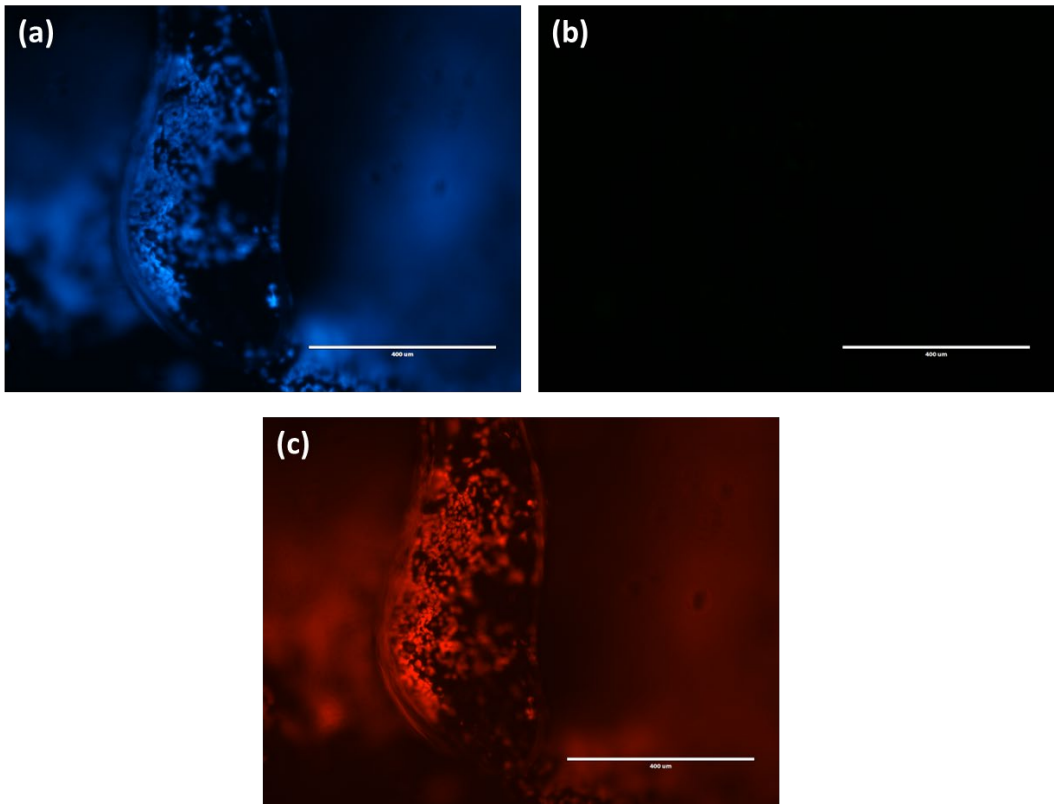

Figure 3.25 Results of Live&Dead assay for SK-N-AS seeded on the scaffold after IR lamp treatment for 10 minutes. (a) Cells nuclei marked in blue with Hoechst, (b) Live cells cytoplasm marked in green with Calcein, (c) Dead cells nuclei marked in red with Propidium. 10x magnification, scale bar 200 µm.

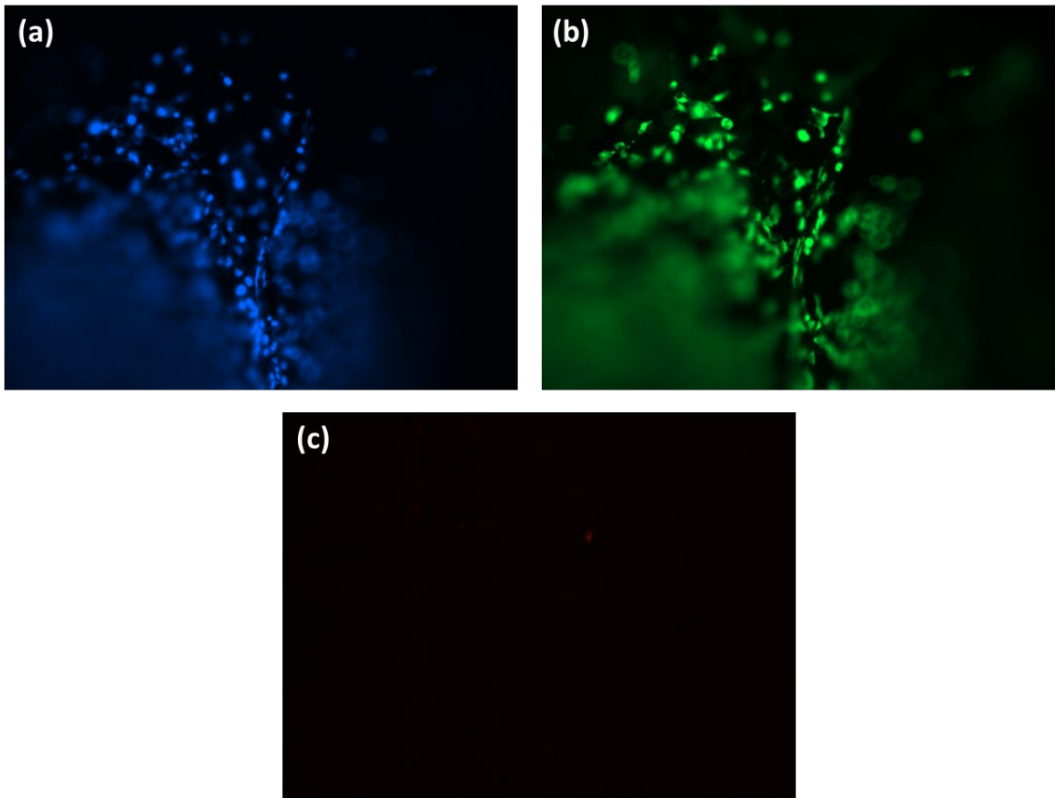

Figure 3.26. Results of Live&Dead assay for SaOs-2 cells seeded on the scaffold after IR lamp treatment for 30 sec. (a) Cells nuclei marked in blue with Hoechst, (b) Live cells cytoplasm marked in green with Calcein, (c) Dead cells nuclei marked in red with Propidium. 10x magnification, scale bar 200 µm.

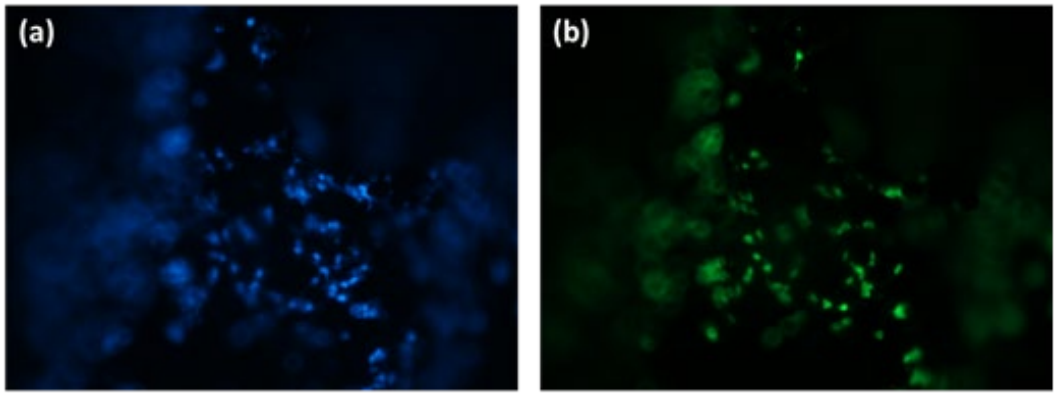

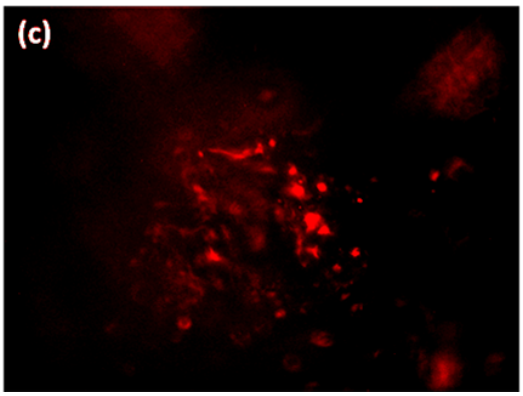

Figure 3.27. Results of Live&Dead assay for SaOs-2 cells seeded on the scaffold after IR lamp treatment for 5 minutes. (a) Cells nuclei marked in blue with Hoechst, (b) Live cells cytoplasm marked in green with Calcein, (c) Dead cells nuclei marked in red with Propidium. 10x magnification, scale bar 200 µm.

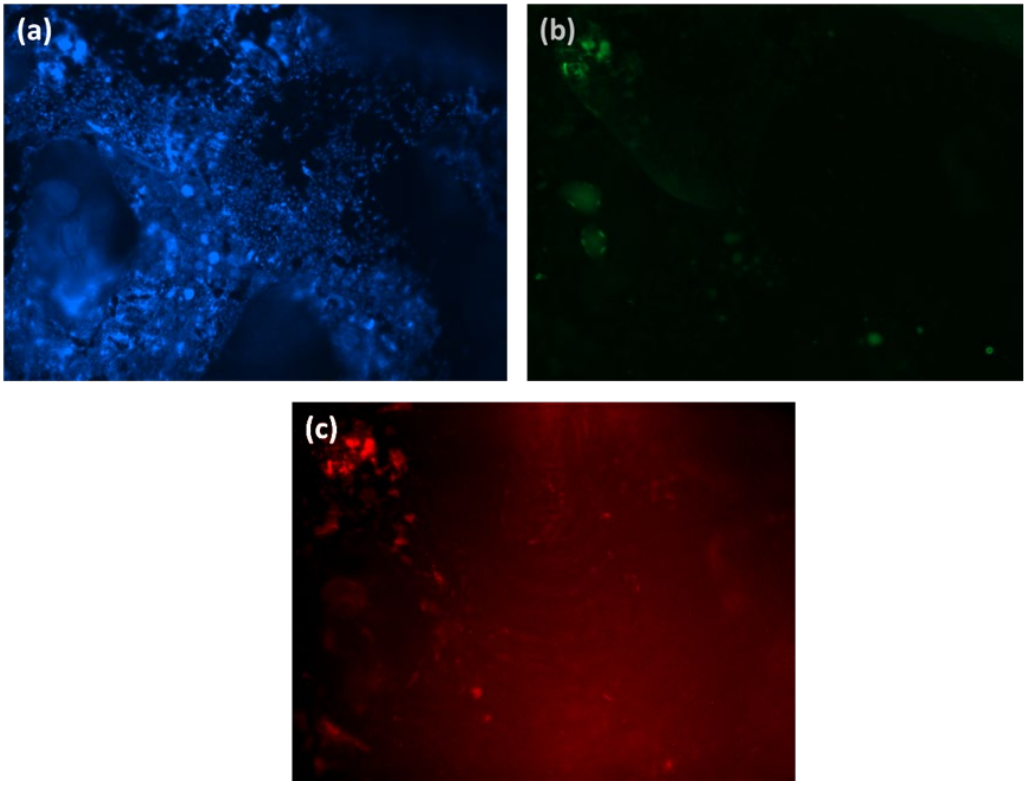

F**igure 3.28.** Results of Live&Dead assay for SaOs-2 cells seeded on the scaffold after IR lamp treatment for 10 minutes. (a) Cells nuclei marked in blue with Hoechst, (b) Live cells cytoplasm marked in green with Calcein, (c) Dead cells nuclei marked in red with Propidium. 4x magnification, scale bar 1000 µm.

The figures indicate that the number of dead cells increased with treatment time ranging from 30 seconds to 10 minutes. Specifically, the number of cells marked in green with Calcein decreased with increasing treatment time, as observed from Figures 3.23 to Figure 3.28. Calcein staining was preferred over Propidium staining, which can

sometimes be affected by autofluorescence, thus providing a more reliable measure of cell viability.

To demonstrate that the photothermal effect is strictly related to the pyrolytic carbon present in the scaffold's composition which, when irradiated with an IR lamp, heats up and causes cells death, a control test was analyzed. In these experiments, cell culture petri dishes were seeded with the tumor cell lines (approximately $2x10^5$ cells per dish) and left in culture for 14 days, similar to the scaffolds. The culture media was changed every two days to provide fresh nutrients. After the incubation period, the cell culture petri dishes were irradiated with the same IR lamp setup used for the scaffolds. After 24h of incubation, a Live&Dead test was carried out to analyze cells viability. In Figure 3.29 and Figure 3.30 are reported the results.

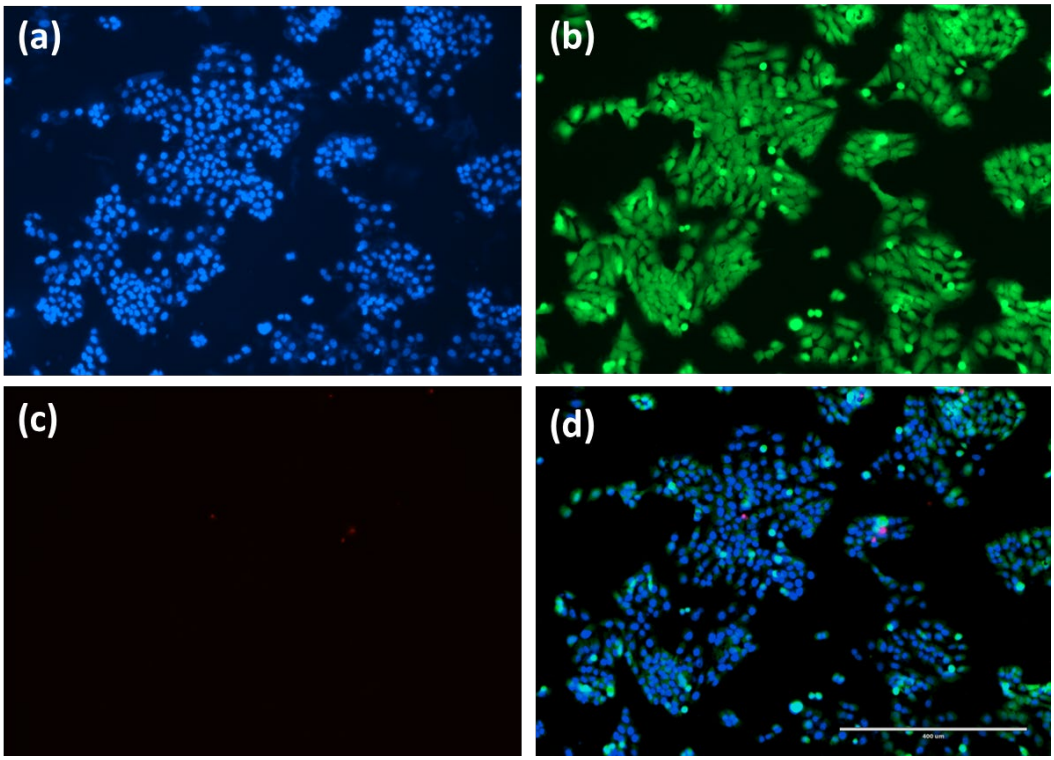

Figure 3.29. Results of Live&Dead assay for SK-N-AS cells seeded in dish after IR lamp treatment for 10 minutes. (a) Cells nuclei marked in blue with Hoechst, (b) Live cells cytoplasm marked in green with Calcein, (c) Dead cells nuclei marked in red with Propidium, (d) Merge. 10x magnification, scale bar 200 µm.

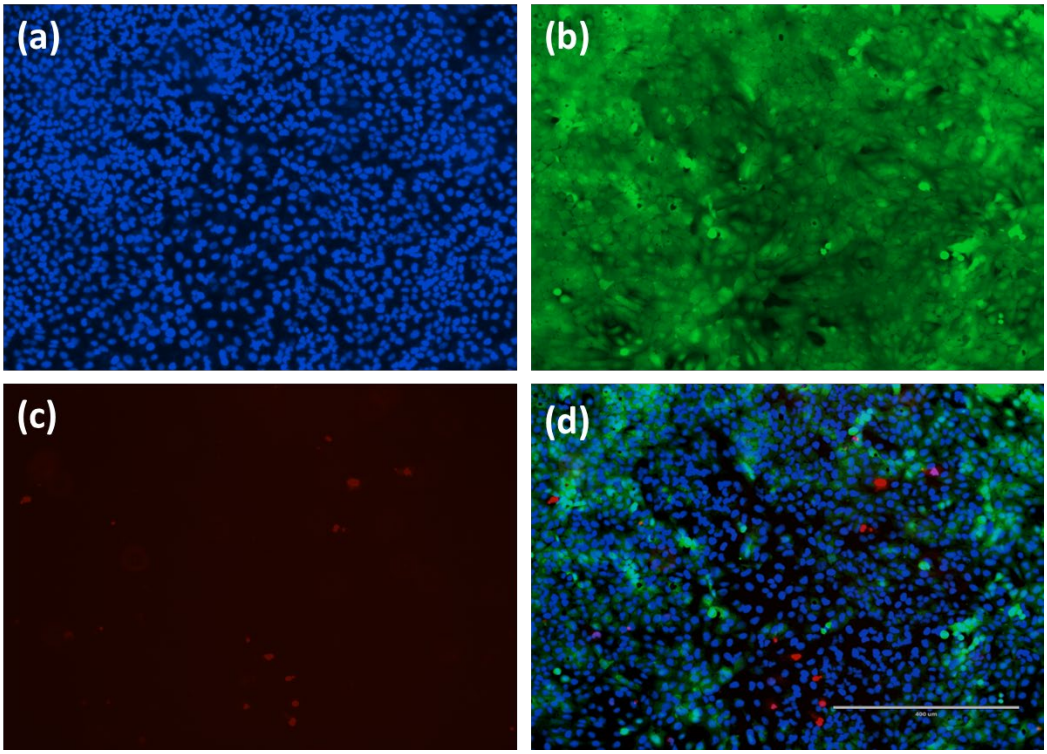

Figure 3.30. Results of Live&Dead assay for SaOs-2 cells seeded in dish after IR lamp treatment for 10 minutes. (a) Cells nuclei marked in blue with Hoechst, (b) Live cells cytoplasm marked in green with Calcein, (c) Dead cells nuclei marked in red with Propidium, (d) Merge. 10x magnification, scale bar 200 μm.

As shown in the figures, most cancer cells appeared to be alive at the time of the staining test, and only a few cells were dead, probably due to the high confluence on the surface of the petri or other physiological reasons. However, this result demonstrates that cells death is caused by the increase in scaffolds temperature over the 50°C and that this heating is attributable to the photothermal effect. This is supported by the control situation where irradiation alone did not result in cell death, demonstrating the importance of the scaffold's pyrolytic carbon composition for the photothermal effect.

3.6.2 MTT results

The MTT assay is a commonly used method for estimating the metabolic activity of living cells, which can provide insights into cell behavior after seeding on bio-glass scaffold and treated with the IR lamp. Both SK-N-AS and SaOs-2 cells were used as models for this cell viability analysis, which helps to confirm the results founded with

the Live&Dead assay. Typically, the longer the treatment time with the IR lamp, the lower the cells viability.

Cell viability on the bio-glass scaffolds was investigated by comparing to a blank control (bio-glass samples without cells) and a control consisting in the seeded bio-glass scaffolds without IR treatment. The results showed that the considered bio-ceramic scaffold has no inhibitory effect on cell proliferation and is biocompatible and cytocompatible, as the viability of cells seeded on the scaffold without treatment is high and close to 100%. Compared with the controls, the absorbance slightly decreased with increasing treatment time for both the cell lines considered for this test.

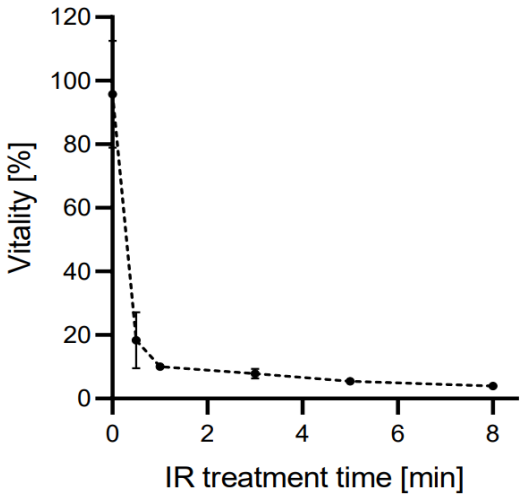

Figure 3.31. MTT assay results for SK-N-AS cells seeded on the scaffold after different time of IR treatment.

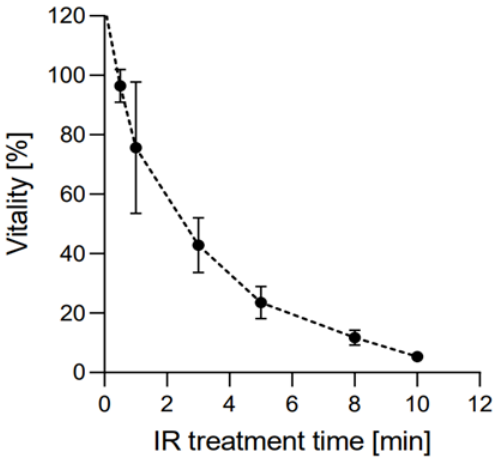

Figure 3.32. MTT assay results for SaOs-2 cells seeded on the scaffold after different time of IR treatment.

Analysis of the obtained graphs indicates that increasing the IR treatment time results in an exponential decrease in the cell viability. In particular, after 30 sec of treatment, the cells viability on the scaffolds seeded with SK-N-AS cells dropped to less than 20%, confirming the photothermal effect of the 70S30C bio-glass scaffold. Even a short treatment time resulted in an increase in scaffold temperature above 50°C, causing cells death. It should be noted that the decrease in cells viability is cell line-dependent, as the viability of SaOs-2 cells after 30sec of IR remained high, around 80%. However, as the treatment time increased, the cells viability decreased exponentially, reaching around 0% after probably 15 minutes of treatment.

Conclusions and Future Perspectives

The work carried out in this thesis involves the biological validation of two composition of a 3D bio-ceramic scaffold, 70S30C. The aim is to demonstrate the biocompatibility and cytocompatibility of the material. Additionally, the study investigates the photothermal effect of the material by using an IR lamp to irradiate the samples. The objective is to determine whether the increase in temperature resulting from the irradiation and possible due to the material composition of the scaffold would induce cancer cells death.

Biological assays were performed using different cancer cell lines (SK-N-AS and SaOs-2) and healthy cell lines (hMSC and BJ) to confirm the biocompatibility and the cytocompatibility of both scaffold compositions. The biological validation demonstrates good cellular adhesion and low cell death rates for all cell lines over time. The Live&Dead assay, performed using specific fluorescent markers, allowed us to confirm cellular adhesion over a period of several weeks. The assay demonstrates that the bio-glass scaffolds are suitable as cellular supports and are therefore cytocompatible. Immunofluorescence and SEM experiments were conducted to observe the morphology of cells after adhesion. The results showed that both hMSCs and BJ cells maintained their elongated morphology after adhesion to the scaffolds, while the SaOs-2 and SK-N-AS cells had a round shape, as expected.
A future study could involve biological validation with osteocytes to determine the suitability of both scaffold compositions for bone cells. Additionally, a more in-depth study of cellular proliferation over time could be conducted. At the same time, to confirm that the scaffolds release ions when placed in a biological environment, which allow for Hydroxyapatite formation, it is necessary to evaluate the nature of the ions released. Specifically, it is important to confirm that the released ions are SiO^{4-} and Ca^{2+}. Ion chromatography (IC) can be used to separate and quantify ions in a sample, and is therefore a suitable method for this analysis.

To evaluate the photothermal effect of the scaffolds, various experiments were

performed using cancers cell lines. Different treatment times with the IR lamp were considered to first demonstrate the efficacy of the treatment and to evaluate the time required to induce the cancer cell death. This is because the temperature of the scaffold would increase over the 50°C. A test with a thermal imager was carried out to measure the temperature variations in the samples while Live&Dead and MTT assays were performed on the cells seeded onto the scaffolds after 24 hours from IR irradiation. The results demonstrate that temperatures surpass 50°C after 30 seconds of irradiation. Additionally, increasing the IR treatment time resulted in a progressive decrease in cell viability due to the high temperature. This is because cancer cells are more sensitive to heat than healthy cells. To prove the efficiency of the treatment, the IR lamp irradiation was performed on culture petri seeded with the cancer cell lines (negative control), demonstrating that the photothermal effect is related to the scaffold.

A future study could involve irradiating scaffolds treated with air since pyrolytic carbon, which is responsible of the heat increase, is a product of the heat treatment with N_2. By using these methods, it could be possible to demonstrate that without the production of the pyrolytic carbon, the scaffold heating would not cause cells death since the temperature would not reach over the 50°C when irradiated with the lamp. Furthermore, in the future, it may be appropriate to perform irradiation experiments using an IR laser. There are several advantages of using an IR laser over a lamp for irradiation experiments. These include:

- Precision: an IR laser can be focused to a specific location, allowing for precise irradiation of a specific area or group of cells;
- Control: the power and duration of an IR laser can be easily controlled, allowing for more accurate and reproducible experiments;
- Efficiency: An IR laser can deliver more energy to a smaller area, making it more efficient than a lamp for certain types of experiments.
- Safety: IR lasers are typically safer than lamps, as they emit a focused beam of light that is less likely to cause damage to surrounding tissues or cells.

In conclusion, both compositions of the 70S30C bio-glass are biocompatible and cytocompatible, making them suitable for creating a support for cellular adhesion and

proliferation. At the same time, the photothermal effect of the material could be considered a new strategy in cancer treatment.

Bibliografy

1. Betts, J. Gordon, et al. (2017). *Anatomy and Physiology*. OpenStax, Rice University.
2. Drake, Vagi & Mitchell. (2014). *Grey's Anatomy for students.* Third Edition. Churchill Livingstone, Elsevier.
3. Chummy S. Sinnatamby. (2011). *Last's anatomy*. Twelfth Edition. Elsevier Ltd.
4. Susan Standring. (2016). *Grey's anatomy*. Forty-first Edition. Elsevier.
5. Robbins & Cotran. (2015). *Pathologic Basis of Disease*. Ninth Edition. Elsevier.
6. Arthur S. Schneider, Philip A. Szanto, Anne M. Mills, Sandra I. Kim, Todd A. Swanson. (2001). *Pathology*. Fifth Edition.
7. Ramin Oftadeh, Miguel Perez-Viloria, Juan C. Villa-Camacho, Ashkan Vaziri, Ara Nazarian. (2015). Biomechanics and Mechanobiology of Trabecular Bone: A Review. *Journal of Biomechanical Engineering*, **137**.
8. Elise F. Morgan, Ginu U. Unnikrisnan, and Amira I. Hussein. (2018). Bone Mechanical Properties in Healthy and Diseased States. *Annual Review of Biomedical Engineering*, **20**,119-143.
9. Jonathon DJ. Black, Baha John Tadros. Bone structure: from cortical to calcium. *Orthopaedics and Trauma*, **34(3)**, 113-119.
10. Arul Prakash Francis, Akshaya Rani Augustus, Sathyapriya Chandramohan, Suhail Ahmad Bhat, Veeraraghavan Vishnu Priya, Rukkumani Rajagopalan. (2022). A review on biomaterials-based scaffold: An emerging tool for bone tissue engineering. *Materials today Communications*, **34**.
11. Ana Paula Moreno Madrid, Sonia Mariel Vrech, María Alejandra Sanchez, Andrea Paola Rodriguez. (2019) Advances in additive manufacturing for bone tissue engineering scaffolds. *Materials Science and Engineering C*., **100**, 631-644.
12. Susmita Bose, Mangal Roy, Amit Bandyopadhyay. (2012). Recent advances in bone tissue engineering scaffolds. *Trends in Biotechnology*, **30(10)**, 546-554
13. Toktam Ghassemi, Azadeh Shahroodi, Mohammad H. Ebrahimzadeh, Alireza Mousavian, Jebraeel Movaffagh, and Ali Moradi. (2018). Current Concepts in Scaffolding for Bone Tissue Engineering. *The archives of Bone and Joint Surgery*, **6(2)**, 90-99.
14. Yu Wen, Sun Xun, Meng Haoye, Sun Baichuan, Chen Peng, Liu Xuejian, Zhang Kaihong, Yang Xuan, Peng Jiang and Lu Shibi. (2017). 3D printed porous ceramic scaffolds for bone tissue engineering: a review. *Biomater. Sci.*, **5**, 1690-1698.
15. Xiaoyu Du, Shengyang Fu and Yufang Zhu. (2018). 3D printing of ceramic-based scaffolds for bone tissue engineering: an overview. *Journal of Materials Chemistry B*., **6**, 4397.
16. Petra Chocholata, Vlastimil Kulda and Vaclav Babuska. (2019). Fabrication of Scaffolds for Bone-Tissue Regeneration. *Materials*, **12(4)**, 568.

17. Nikhil Kamboj, Antonia Ressler and Irina Hussainova. (2021). Bioactive Ceramic Scaffolds for Bone Tissue Engineering by Powder Bed Selective Laser Processing: A Review. *Materials*, **14(18)**, 5338.

18. Marco A. Velasco, Carlos A. Narváez-Tovar and Diego A. Garzón-Alvarado. (2015). Design, Materials, and Mechanobiology of Biodegradable Scaffolds for Bone Tissue Engineering. *BioMed Research International*.

19. Susheem Kanwar, Sanjairaj Vijayavenkataraman. (2021). Design of 3D printed scaffolds for bone tissue engineering: A review. *Bioprinting*, **24**.

20. Yasaman Niki and Alireza Seifzadeh. (2021). Characterization and comparison of hyper-viscoelastic properties of normal and osteoporotic bone using stress-relaxation experiment. *Journal of the Mechanical Behavior of Biomedical Materials*, **123**.

21. Hongshi Ma, Chun Feng, Jiang Chang, Chengtie. (2018). Wu 3D-printed bioceramic scaffolds: From bone tissue engineering to tumor therapy. *Acta Biomater.*, **79**, 37-59.

22. Renata Guimarães Ribas, Vanessa Modelski Schatkoski, Thaís Larissa do Amaral Montanheiro, et al. (2019). Current advances in bone tissue engineering concerning ceramic and bioglass scaffolds: A review. *Ceramics International*., **45(A)**, 21051-21061.

23. Elisa Fiume, Jacopo Barberi, Enrica Verné and Francesco Baino. (2018). Bioactive Glasses: From Parent 45S5 Composition to Scaffold-Assisted Tissue-Healing Therapies. *J. Funct. Biomater*., **9(1)**, 24.

24. Qiang Fu, Eduardo Saiz, Mohamed N. Rahaman, Antoni P. Tomsia. (2011). Bioactive glass scaffolds for bone tissue engineering: state of the art and future perspectives. *Materials Science and Engineering: C*., **31**, 1245-1256.

25. Gareth Turnbull, Jon Clarke, Frédéric Picard, Philip Riches, Luanluan Jia, Fengxuan Han, Bin Li, Wenmiao Shu. (2018). 3D bioactive composite scaffolds for bone tissue engineering. *Bioactive Materials*., **3**, 278-314.

26. Julian R Jones, Peter D Lee and Larry L Hench. (2006). Hierarchical porous materials for tissue engineering. *Philosophical transactions of the royal society A. Mathematical, Physical and Engineering Science.,* **364**.

27. Elena Tagliabue. (2022). Sintesi e stampa 3d di scaffolds a base di biovetro 70S30C supportate da emulsioni in polimero preceramico. Tesi di Laurea Magistrale, DEI, Università degli Studi di Padova.

28. Paulina Ożóg, Hamada Elsayed, Luca Grigolato, Gianpaolo Savio, Jozef Kraxner, Dušan Galusek, Enrico Bernardo. (2022). Engineering of silicone-based blends for the masked stereolithography of biosilicate/carbon composite scaffolds. *Journal of the European Ceramic Society*., **42**.

29. Christoph Pautke, Matthias Schieker, Thomas Tischer, et al. (2004). Characterization of Osteosarcoma Cell Lines MG-63, Saos-2 and U-2 OS in comparison to human osteoblasts. *Anticancer Res.*, **24(6)**, 3743-3748.

30. Jiao Gao, Xin-Long Yan, Ren Li, et al. (2010). Characterization of OP9 as authentic mesenchymal stem cell line. *Journal of Genetics and Genomics*, **37(7)**, 475-482.

31. Thomaz Oliveira, Ilana Costa, Victor Marinho, Valécia Carvalho, Karla Uchôa, Carla Ayres, Silmar Teixeira and Daniel F P Vasconcelos. (2018). Human foreskin fibroblasts: from waste bag to important biomedical applications. *Journal of Clinical Urology*, **11(6)**, 385–394.

32. Kyuseok Im, Sergey Mareninov, M. Fernando Palma Diaz, William H. Yong (2019). An introduction to Performing Immunofluorescence Staining. *Methods in Molecular Biol*., **1897**, 299-311.

33. Vancells JC. Direct vs indirect immunofluorescence. Available at: http://www.abcam.com/secondary-antibodies/direct-vs-indirectimmunofluorescence

34. Carpenter B. Secondary antibody selection guide. Available at: http://www.abcam.com/secondary-antibodies/secondary-antibody-selection-guide

35. Abcam. A comparison between polyclonal and monoclonal. Available at: http://www.abcam.com/protocols/acomparison-between-polyclonal-and-monoclonal

36. Abcam (2008) Fixation and permeabilisation tips for IHC and ICC. Available at: http://www.abcam.com/ps/pdf/protocols/fixation_permeabilization.pdf

37. Thermo Fisher Scientific Inc. (2016). Blocking Strategies for IHC. Available at: https://www.thermofisher.com/us/en/home/life-science/protein-biology/proteinbiology-learning-center/protein-biology-resource-library/pierceprotein-methods/blocking-strategies-ihc.html

38. Thermo Fisher Scietific Inc. (2011). Rhodamine Phalloidin. Available at: https://www.thermofisher.com/order/catalog/product/R415

39. Lorna J. Gibson. (2005). Biomechanics of cellular solids. *Journal of Biomechanics*, **38**, 377-399.

40. Ariane Parisien, Mostafa S.A. ElSayed, Hanspeter Frei. (2022). Mechanoregulation modelling of stretching versus bending dominated periodic cellular solids. *Materials today Communications*, **33**.

41. Elizabeth R Fischer, Bryan T Hansen, Vinod Nair, Forrest H Hoyt, David W Dorward. (2012). Scanning Electron Microscopy. *Curr Protoc Microbiol*., Chapter 2.

42. Jie Li, Wei Zhang, Wenhui Ji, Jiqing Wang, Nanxiang Wang, Wanxia Wu, Qiong Wu, Xiyan Hou, Wenbo Hu and Lin Li. (2021). Near infrared photothermal conversion materials: mechanism, preparation, and photothermal cancer therapy applications. *Journal of Mater. Chem. B*, **9**, 7909.

43. Cell proliferation and viability assay protocol with MTT. Available at: https://www.sigmaaldrich.com/IT/it/technical-documents/protocol/cell-culture-and-cell-culture-analysis/cell-counting-and-health-analysis/cell-proliferation-kit-i-mtt

44. Franco M. Stabile, Alessia Famengo, Danilo Pedron, Hamada Elsayed, Enrico Bernardo. Functional Carbon-based Bioglass Nanocomposite Scaffolds from Vat Photopolymerization of a Novel Preceramic Polymer-based Nanoemulsion. Manuscript in preparation.

45. Swati Midha, Taek Bo Kim, Wouter van den Bergh, Peter D. Lee, Julian R. Jones, Christopher A. Mitchell. (2013). Preconditioned 70S30C bioactive glass foams promote osteogenesis in vivo. *Acta Biomaterialia*, **9**, 9169–9182.